3D-ENGINEERED MUSCLE TISSUE AS A WIRELESS SENSOR

by

Çağla Karabulut

B.S., Electrical and Electronics Engineering, Istanbul Bilgi University, 2020

Submitted to the Institute for Graduate Studies in
Science and Engineering in partial fulfillment of
the requirements for the degree of
Master of Science

Graduate Program in Electrical and Electronics Engineering
Boğaziçi University

2023

3D-ENGINEERED MUSCLE TISSUE AS A WIRELESS SENSOR

APPROVED BY:

Assoc. Prof. Sema Dumanlı Oktar (Thesis Supervisor)	.....
Prof. Arda Deniz Yalçınkaya	.....
Assoc. Prof. Urartu Özgür Şafak Şeker	.....

DATE OF APPROVAL: 27.10.2023

ACKNOWLEDGEMENTS

The scientist describes what is; the engineer creates what never was.

-Theodore von Karman

Foremost, I would like to express my deepest gratitude to my thesis advisor, Assoc. Prof. Sema Dumanlı Oktar, without her endless support, guidance, and patience this work would not have been possible. She has been a constant source of inspiration throughout this academic journey, encouraging me to explore new ideas, providing insightful feedback, and fostering an environment of intellectual and personal growth.

I would also like thank each member of the BOUNTENNA research group. This experience would not have been nearly as enjoyable without the energy and the vibrance of this group of young individuals, under the guidance of Prof. Dumanlı. In particular, I want to thank Dr. M. Emre Laçin and Ahmet Bilir, with whom I spent many hours working side by side. It is my good fortune to have had the chance to work with them.

Lastly, I would like to thank my parents, Hatice and Hasan Karabulut. None of this would be possible without their endless love and support.

I would like to dedicate this thesis to the memory of my late grandfather Hasan Karabulut. His presence, though absent, has been a silent guide throughout these years. In addition, I dedicate this thesis to my beloved aunt, Filiz Çağla Karabulut, who has always cheered me on through this academic journey. Carrying her name is the greatest honor of my life and the void left by her untimely departure is deeply felt in this celebratory moment.

May their legacies continue to illuminate my path, reminding me that everlasting love and resilience are forces that can never be contained by the confines of space or time.

LIST OF PUBLICATIONS

This work was supported in part by Boğaziçi University Scientific Research Fund under project number BAP-M 19081 and by Council of Higher Education under project number YOK-ADP 19741. The resulting scientific publications are detailed below. Figures produced in these publications, for which the copyright was transferred to the respective publisher, have been reused in this thesis in accordance with the publisher's editorial policy on the reuse of author-produced text and graphics.

- **Karabulut, C.**, A. Bilir, M. E. Lacin and S. Dumanli, "3D Enigneered Muscle Tissue as a Wireless Sensor: Antennalive", IEEE Antennas Propagation Magazine, Vol. 65, No. 6, pp. 28–36, 2023.

- **Karabulut, C.**, A. Bilir, M. E. Lacin, A. Deniz Yalcinkaya and S. Dumanli, "Skeletal Muscle-Actuated Bio-Hybrid Implant and Wearable Reader Antenna System", 2022 3rd URSI Atlantic and Asia Pacific Radio Science Meeting (AT-AP-RASC), pp. 1–4, IEEE, Gran Canaria, Spain, 2022.

- Erden, O. K., A. Bilir, **C. Karabulut**, U. O. Safak Seker and S. Dumanli, "Antennas Reconfigured by Living Cells: AntennAlive," 2022 IEEE International Symposium on Antennas and Propagation and USNC-URSI Radio Science Meeting (AP-S/URSI), Denver, CO, USA, 2022, pp. 882-883.

- **Karabulut, C.**, A. Bilir, M. E. Lacin and S. Dumanli, "Implant Antenna Reconfigured by Engineered Skeletal Muscle Tissue," 2023 17th European Conference on Antennas and Propagation (EuCAP), Florence, Italy, 2023, pp. 1-5.

- **Karabulut, C.**, A. Bilir, S. Dumanli, "Tasarlanmış İskelet Kası Tabanlı Beden-İçi Algılayıcı," URSI Turkey Scientific Congress and National General Assembly, September 2023.

ABSTRACT

3D-ENGINEERED MUSCLE TISSUE AS A WIRELESS SENSOR

Implantable and wearable biomedical devices are advancing with new sensor technologies, holding great potential for early disease detection through continuous, real-time monitoring of physiological parameters. However, the majority of existing biomedical devices have limited lifetimes due to their power requirements and often focus on monitoring physical parameters rather than specific molecules relevant to specific diseases. The work detailed in this thesis proposes a wireless sensing and communication platform that can achieve in-vivo, real-time sensing at a molecular level by utilizing engineered mammalian cells. The proposed platform consists of a cell-based bio-hybrid implant device and a dual-port, wide-band on-body antenna. The molecular sensing is achieved by the bio-hybrid implant that is composed of three main components: a flexible scaffold, an in-body passive implant antenna, and 3D-engineered muscle tissue. The genetic circuitry of the cells that make up the 3D-engineered muscle tissue can be manipulated. This manipulation makes the tissue responsive to specific target molecules and the presence of these molecules triggers a contraction in the tissue. The tissue contraction and relaxation are used to reconfigure the resonance frequency of the implant antenna that is located on the flexible scaffold. To monitor the changes in resonance reconfiguration, the on-body reader antenna is positioned outside of the human body. The implant antenna's resonance variations are observed in response to the presence of the molecule of interest. In this thesis, the bio-hybrid implant and the on-body reader antenna were designed and fabricated. The sensing system is mechanically and electromagnetically simulated. Based on the simulations, electromagnetic measurements were taken inside tissue-mimicking phantoms to track implant antenna reconfiguration.

ÖZET

3B TASARIMLANMIŞ İSKELET KASI DOKUSU İLE KABLOSUZ ALGILAMA

İmplant edilebilir ve giyilebilir biyomedikal cihazlar, sensör teknolojilerindeki ilerlemeler ile hızla gelişmektedir. Bu tür cihazlardaki gelişmeler hastalıkların erken tespiti açısından büyük bir potansiyele sahiptir. Bu cihazlar, fizyolojik parametrelerin sürekli ve gerçek zamanlı izlenmesine olanak tanır. Ancak mevcut biyomedikal sensörlerin çoğunun güç gereksinimleri nedeniyle sınırlı ömürleri vardır ve genellikle hastalıklarla ilgili belirli moleküllerin algılanması yerine beden içindeki genel fiziksel parametrelerin izlenmesine odaklanırlar. Bu tezde, tasarımlanmış memeli hücreler kullanarak moleküler düzeyde in-vivo, gerçek zamanlı algılama yapabilen yeni bir algılama ve kablosuz iletişim platformu önerilmektedir. Önerilen platform, hücre tabanlı bir biyo-hibrit implant cihaz ve geniş bantlı çift portlu beden üstü antenden oluşmaktadır. Sistemin moleküler algılama yeteneği biyo-hibrit implant ile elde edilmektedir. Biyo-hibrit implant, esnek iskele, beden içi pasif implant anten ve 3B tasarımlanmış kas dokusu olmak üzere üç ana bileşenden oluşur. 3B tasarımlanmış kas dokusunu oluşturan hücreler genetik olarak manipüle edilebilir. Bu manipülasyon, dokunun belirli hedef moleküllere duyarlı hale gelmesini sağlar ve bu moleküllerin varlığı dokuda bir kasılmaya sebep olur. Doku kasılması ve doku gevşemesi, esnek iskele üzerinde bulunan implant anteninin rezonans frekansını yeniden yapılandırmak için kullanılır. Rezonansın yeniden yapılandırılmasını izlemek için beden dışı okuyucu anten, insan bedeninin üstüne yerleştirilir. Rezonanstaki bu değişiklikler, hedef molekülün varlığına tepki olarak gözlemlenir. Bu tezde, biyo-hibrit implant ve beden dışı okuyucu anten tasarlanmış ve üretilmiştir. Algılama sistemi mekanik ve elektromanyetik olarak simüle edilmiştir. Bu simülasyonlara dayanarak, doku benzeri fantomlar üretilerek implant anteninin yeniden yapılandırılmasını izlemek üzere elektromanyetik ölçümler alınmıştır.

TABLE OF CONTENTS

LIST OF FIGURES

LIST OF TABLES

LIST OF SYMBOLS

Å	Angstrom
C	Capacitance
E	Elasticity modulus
f	Frequency in Hertz
F	Force in Newtons
L	Inductance
Z	Impedance in Ohms
ε	Strain
ε_{eff}	Effective permittivity
ε_r	Relative permittivity
σ	Stress

LIST OF ACRONYMS/ABBREVIATIONS

2D	Two Dimensional
3D	Three Dimensional
ACh	Acetylcholine
ATP	Adenosine Triphosphate
C2C12	Skeletal Myoblast Cell Line
ChR2	Channelrhodopsin-2
DAK	Dielectric Assessment Kit
DM	Differentiation Medium
ECM	Extracellular Matrix
FBS	Fetal Bovine Serum
GM	Growth Medium
HFSS	High-Frequency Structure Simulator
MCU	Microcontroller Unit
PBS	Phosphate-Buffered Saline
PCB	Printed Circuit Board
PEC	Perfect Electric Conductor
PHC	Perfect Magnetic Conductor
PDMS	Polydimethylsiloxane
RPM	Round Per Minute
SLA	Stereolithography
VNA	Vector Network Analyzer

1. INTRODUCTION

Advancements in medical diagnosis technologies have been revolutionizing the way we understand human diseases. Breakthroughs in this field have opened up new techniques for diagnosing, monitoring and treating a range of medical conditions while providing insightful knowledge of human physiology. In the recent decades, the size of such medical diagnosis and monitoring equipment has significantly decreased as a result of remarkable recent advancements, particularly in microelectronics [1]. Not so long ago, it required an army of healthcare professionals and technicians to operate and maintain bulky and complicated medical monitoring and diagnosis equipment. However, nowadays, the same tasks are undertaken by intelligent implants and portable wearable devices. These compact and user-friendly technologies have reshaped healthcare delivery, giving individuals immediate access to tools for monitoring their health. Furthermore, the continuous monitoring capability of implant and wearable devices has provided a complete picture of a patient's medical state for healthcare professionals and researchers [2]. An illustration is given in Figure 1.1 for the landscape of implant and wearable devices carried in various body parts.

Implant and wearable biomedical devices are composed of various components that work together in harmony to provide functionality and performance. One can think of these components as the pieces of a puzzle. Often, these pieces are brought together to meet specific medical needs for specific use cases. However, typically at the core of these devices are sophisticated sensors designed to detect and monitor a wide range of physiological parameters and vital signs including heart rate, blood pressure, glucose levels, body temperature, and others [3]. These sensors serve as the device's principal interface with the human body, transforming physiological information into electrical or digital representations that may be further evaluated by outside readers. Furthermore, the proximity of these sensors to the disease-causing molecules can play a great role in preventive healthcare. Diseases frequently initiate at the molecular level, well before any obvious symptoms appear. Biomarkers and certain molecules act as

early warning signals of health issues. Thus, early detection at a molecular level not only allows for immediate treatment but also offers the chance to slow or stop disease progression before irreversible damage is done. By taking advantage of their location, if the implant sensors could be made to sense specific disease molecules, they could become powerful tools to fight serious medical conditions at very early stages.

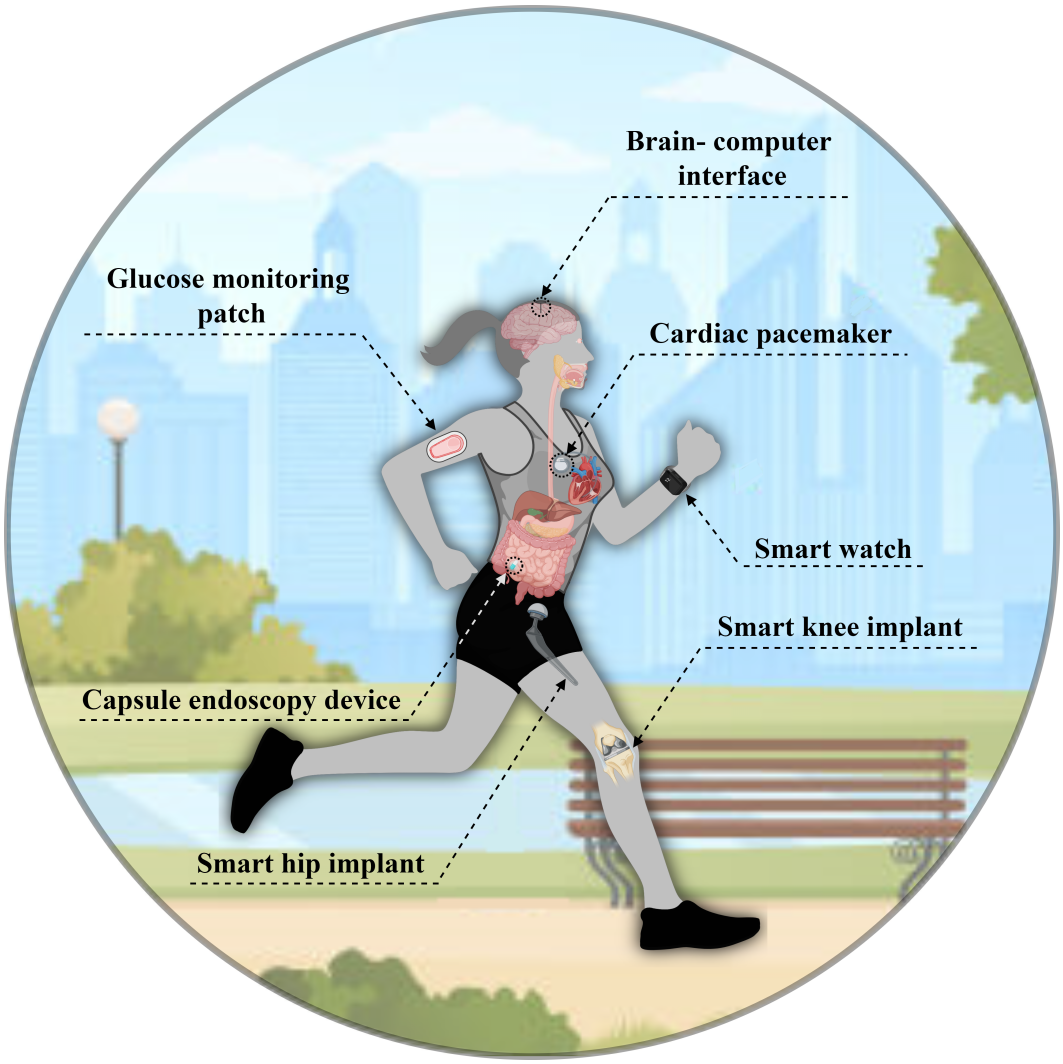

Figure 1.1. Implant and wearable devices worn on various body parts.

Wireless communication is another crucial aspect of biomedical implants and wearable devices. These devices are typically equipped with enhanced wireless communication units to allow continuous data transmission and communication. Antennas are the centerpieces of such wireless units and antenna design is particularly significant in biomedical applications due to the unique challenges posed by the human body. And

the need for reliable, efficient communication is ever-present in biomedical monitoring devices. Thus, utilizing their enhanced antenna capabilities, biomedical devices connect to external readers or healthcare platforms via technologies such as Bluetooth, Wi-Fi, or other radio frequency means. As a result, real-time data transfer, remote monitoring, and continuous integration with healthcare platforms and experts become possible.

Microcontroller units (MCU) act as the device's brain, running complicated algorithms, analyzing sensor input, and coordinating numerous activities and processes. They are also responsible for managing the data collected by sensors. These processing units enable real-time decision-making, and device behavior customization to meet particular requirements.

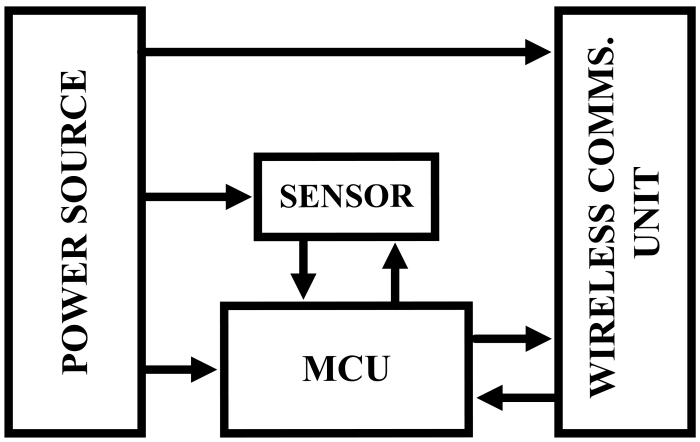

Figure 1.2. Components of a conventional biomedical device.

The power source is the final piece of the biomedical device puzzle. An illustration depicting the components of a conventional biomedical device is shown in Figure 1.2. Power sources such as batteries or energy harvesting techniques, provide the energy required to keep these devices in operation. These power systems are engineered to assure device longevity and efficiency, allowing for lengthy durations of continuous monitoring. However, in biomedical implants, the integration of external power sources such as batteries necessitates further surgical procedures, which increase invasiveness. Surgical procedures for battery replacement involve risks, skilled medical personnel, and

resources. Thus, over time, the upkeep and replacement of these power sources burden the healthcare system and the patients. The viability of traditional batteries being implanted in certain parts of the body may also be constrained by their size and weight. Due to these concerns about traditional batteries, there is a demand to eliminate or minimize the need for batteries in biomedical implant devices by incorporating energy harvesting techniques.

Energy harvesting techniques, when properly optimized, can provide consistent and reliable power to the implant device and they have the potential to leverage the body's natural processes to generate power, making implants more efficient. Investigating alternatives such as using adenosine triphosphate (ATP) as the energy source appears as an attractive route to pursue. As the basic energy unit in living creatures, ATP is in abundance inside the human body and it holds the potential for a biologically harmonious power solution for implant devices [4]. This strategy is consistent with the goal of improving biocompatibility, eliminating the need for invasive operations, and maintaining long-term device functionality. Using ATP as an energy source, however, poses challenges such as the need for efficient enzymatic systems to convert ATP into usable energy. While promising, ATP-based energy harvesting within implant devices requires careful consideration of biological systems, safety, and the sophisticated design required to integrate this natural energy source into medical technology.

1.1. Objectives and Significance

As impressive as the advancements in conventional implant and wearable medical device technologies, there is an evident need for a new revolution that will leverage sensing capacities to new heights. This next stage of development necessitates the inclusion of artificial smart living sensors, by making use of the enormous potential of synthetic biology [5]. A new generation of intelligent living cell-based sensors capable of actively sensing and responding to a wide range of molecular signals can be a game changer for understanding how diseases initiate and evolve inside the human body.

Cells have a natural ability to recognize and respond to various molecular stimuli in their surrounding mediums. This natural reaction serves as the foundation for their prospective use in sensing systems. Nowadays, synthetic biology allows us to effectively manipulate the genetic circuitry of cells. This innovative approach enables the development of transgenic sensors that are specifically engineered to respond to specific target molecules. With newly emerging tissue engineering techniques, these engineered cells can be harnessed to construct tissue structures that could amplify a single cell's reaction. These bioengineered tissues, equipped with the ability to identify certain molecular targets, can be integrated into sophisticated implant devices. Then, these tissues' reactions to the presence of target molecules can be amplified and manipulated, transforming molecular interactions into tangible signals that can be perceived by external systems. Herein, lies the fundamental challenge: in order to use living cells for molecular sensing in practice, the cell's reaction to detection needs to be converted into a readout signal that humans can identify. One of the most commonly used readout signals in the literature is optical, within the visible light spectrum, so that the detection is observable to the human eye [6]. The propagation depth of visible light in the human body, however, is incredibly low, which shows that the typically utilized optical response is not reliable. Hence, it remains an open question to link cellular responses to outside readers reliably.

In this thesis, a generic biomedical monitoring platform based on engineered living cells is presented [7–9]. The proposed method employs microwaves to connect a cell's reaction to the external world, enabling the use of a cell-based molecular sensor as an implant with wireless connectivity. One significant obstacle in using microwaves to sense changes on a cellular level is that such changes often occur within the angstrom (Å) range, a scale too small for microwaves to detect. Since these changes occur at such a minor scale, high-frequency electromagnetic radiation is usually required for detection. Using high-frequency electromagnetic waves, such as X-Rays, for continuous sensing or monitoring inside the body is not only impractical but also could lead to health problems due to continuous radiation exposure. To overcome this limitation, a conversion process is necessary, where the cellular reaction is translated into a change

that microwaves can detect. This conversion is accomplished in the proposed system by reconfiguring a passive implant antenna by 3D-engineered skeletal muscle tissue.

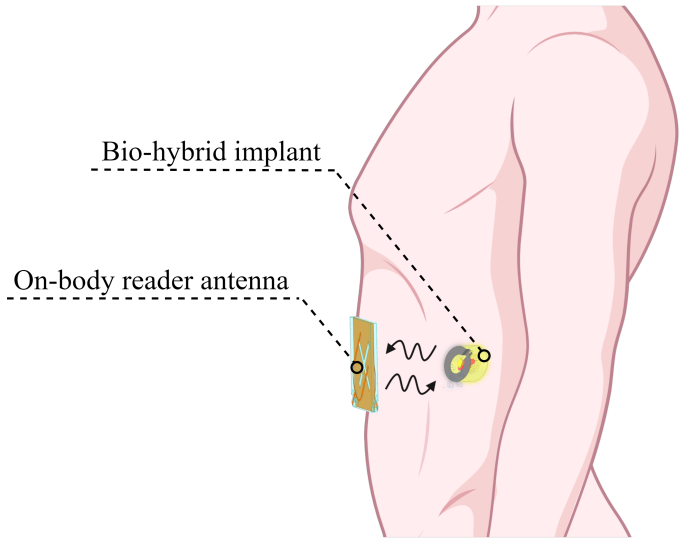

(a)

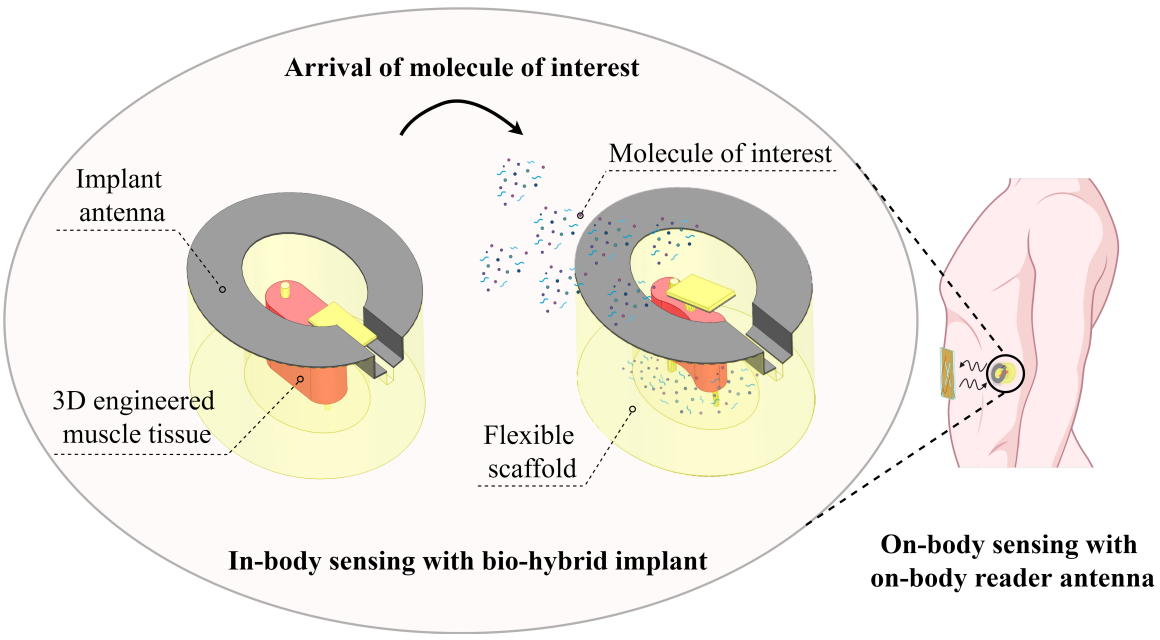

(b)

Figure 1.3. Proposed sensing and communication system. (a) A general view of the sensing and communication system components. (b) Exploded view of the sensing in action.

In essence, the proposed sensing and communication system is made up of a bio-hybrid implant and an on-body reader antenna. In Figure 1.3(a), the components of the proposed system are shown. The bio-hybrid implant consists of a flexible scaffold, in-body passive implant antenna, and 3D-engineered muscle tissue as shown in Figure 1.3(b). In theory, the genetic circuitry of the cells that form the 3D-engineered muscle tissue can be manipulated and the tissue can become sensitive to the specific molecules of interest. The presence of these molecules triggers a contraction in the tissue that is located inside the scaffold. The mechanical contraction and tissue relaxation movements are employed to reconfigure the resonance frequency of the passive implant antenna which is located on the flexible scaffold. To monitor these variations in resonance reconfiguration, an on-body reader antenna is placed outside the human body. Since the resonance variations occur in response to the presence of the molecule of interest, the resonance variation data can be further analyzed to track the molecule of interest.

This thesis presents the four work packages that are required the test the proposed sensing and communication concept. In the first work package, the flexible scaffold was designed and mechanically analyzed to simulate the scaffold's response to the hypothetical contraction forces applied by the muscle tissue. Optimized scaffold models were fabricated in an stereolithography (SLA) 3D printer. In the second work package, a biological protocol was established to grow 3D-engineered skeletal muscles, and the 3D-engineered muscle tissues were fabricated inside previously designed scaffolds. In the third work package, a wide-band dual port cross-slot antenna was designed and optimized as the on-body reader antenna. The optimized design was fabricated using high-permittivity dielectric material. Lastly, a phantom to electrically mimic the human tissue is fabricated and all the work packages were brought together in a measurement setup. This thesis is a proof of concept that if the 3D-engineered muscle tissue can be genetically manipulated to generate sufficient force in the presence of a molecule of interest, the implant antenna gets reconfigured. Based on the measurements that are taken inside the human tissue phantom, the reconfiguration can be tracked with the designed on-body reader antenna.

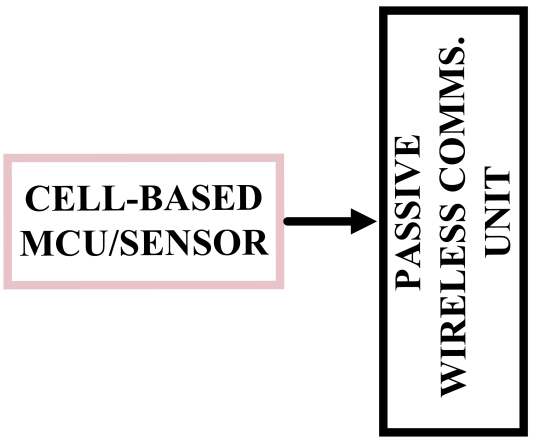

Figure 1.4. Components of the proposed sensing and communication system.

The proposed sensing and communication platform is a significant improvement to conventional biomedical sensing systems. Conventionally, all four of the components described in Figure 1.2, are physically present in most implant sensors of today. Chemical batteries often power these devices, and the sensing and processing units are typically built with electronic components. However, the introduction of a new kind of implant sensor represents a remarkable departure from traditional designs. In the proposed sensing platform, the separate power unit is entirely eliminated, transforming the very essence of how implant sensors are constructed and function. The processing and sensing units are merged into a single multi-functioning cell-based unit. This not only simplifies the design but also reduces the dependence on traditional energy sources, leading to a more sustainable and potentially more efficient solution. The components of the proposed sensing and communication system are shown in Figure 1.4.

A fundamental paradigm shift is introduced here, in which the sensory tasks are pushed to living cells rather than relying on conventional electronic sensor devices. This paradigm shift has the potential to transform medical diagnostics by providing improved and tailored methods for diagnosis, monitoring, and therapy at the smallest scale possible. We have the chance to set the path for a future in which smart living sensors seamlessly interact with the human body, offering real-time molecular-level insights into the patient's health.

1.2. Organization of Thesis

Throughout this thesis, the bio-hybrid implant, the on-body antenna, and the measurement setup that mimics the human body were fabricated, and electromagnetic measurements were taken as proof of concept of the presented idea.

In Chapter 1, the concept is revealed and the objectives of the proposed system are outlined. In Chapter 2 an extensive literature review was given for this multi-disciplinary work and the novelty of the proposed system is discussed. In Chapter 3, design considerations and fabrication methods for the bio-hybrid implant and the on-body implant antenna were discussed in detail. Chapter 4 presents the numerical models of the proposed sensing system. The system is analyzed mechanically and electromagnetically in this chapter. In Chapter 5, a measurement setup was created with human tissue-mimicking phantoms, and measurements were taken based on the numerical models that were formed in the previous chapter. The results of these measurements are discussed in this chapter. Chapter 6 concludes the work.

2. LITERATURE REVIEW AND CONTRIBUTION OF THE THESIS

2.1. Literature Review

This thesis investigates the idea of an implant sensor that utilizes engineered skeletal muscle tissue as its sensor unit. The presented work represents a multi-layered approach integrating three major fields of work: engineered muscle tissues, biomedical implants, and living cell-based sensors. As a result, the relevant literature will be divided into three parts, with each section dedicated to the examination of these interconnected areas.

2.1.1. Engineered Muscle Tissue-Based Biomachines

Synthetic biology and tissue engineering hold great potential for advancing regenerative medicine and creating bioengineered solutions for a variety of health issues. Combining these disciplines leads to innovation and pushes the boundaries of biological engineering, creating new paths for enhancing the quality of life. They are paving the way for the development of synthetic functional organs for transplantation and the creation of artificial biomachines that are engineered to accomplish specific tasks.

The term "biomachines" refers to a device or system that uses biological components or principles together with engineering methods to carry out certain jobs or functions [10]. These functions are often mechanical, and examples of biomachines include bioactuators and bio-inspired robots [11–14]. Recent advances in tissue engineering have led to the development of innovative biomachines by allowing the direct integration of living cells and tissues with artificial components. This integration utilizes the efficiency of biological actuation within artificial devices combining the best features of biological and manufactured systems. In biomachine applications, muscle cells appear as the ideal cell source for powering devices, primarily because of their

natural ability to produce mechanical work [15]. Myocytes, the scientific name for muscle cells, have special contractile abilities that enable them to transform chemical energy into mechanical force and motion [15].

In the literature, the most frequently used muscle cells for biomachine applications have been mammalian skeletal muscle cells and heart muscle cells, also known as cardiomyocytes. Endeavors of building biomachines using muscle cells started as early as the mid-2000s. [16] was the first study to assemble individual cardiomyocyte cells into 2D muscle films to actuate bio-hybrid devices. In this work, a silicon-based cantilever beam was fabricated using MEMS techniques. The entire microstructure was covered with a thermally responsive polymer and this polymer was selectively etched to create a micro-patterned surface for cell assembly. The application of this polymer layer is critical for guiding the growth and direction of the muscle cells. With this technique, cells grow and self-assemble into muscle bundles by aligning on the patterned areas. Once the cantilever is released and an electrical stimulus is applied, the beating of the muscle bundles moves the microstructure by 38 µm/s. A similar micro pattern approach was taken in [17], where the authors fabricated a polydimethylsiloxane (PDMS) thin film substrate in the shape of a jellyfish. The substrate was micro-patterned to guide the organization of cardiomyocyte cells. The cardiomyocytes were then seeded on the substrate and left to self-assemble into cardiac tissue. The overall structure mimics the muscle tissue organization observed in jellyfish. With the applied electrical stimulation, the device was able to produce a maximum speed of 2.4 mm/s.

The collaboration of synthetic biology and tissue engineering started to produce one of its first fruits in [18]. In this work, the authors created a bio-hybrid device by patterning cardiomyocytes onto a four-layer elastomeric/metal substrate. Most crucially, cardiac cells used in this work were optogenetically engineered to express channelrhodopsin-2 (ChR2), a light-sensitive ion channel. This made the cells sensitive to blue light at powers of 10 mW. The cardiac cells on the substrate could propel the device and the speed and direction were controlled by modulating the frequency of light stimuli.

As the cell-seeded substrate fabrication processes advanced, biorobots with more accurate control and stability began to appear in the literature. [19] describes the development of a fin-driven swimming robot. The substrate is made up of two composite polymers with tunable densities and a PDMS cantilever with a cardiomyocyte fusion layer. Without outside assistance, the robot can maintain its diving depth, pitch, and rolling by configuring the substrate mass density. This meant great stability, however, the device could not produce much speed compared to its predecessor swimming biorobots. It could only produce a top speed of 142 µm/s.

The authors of [20] developed a swimming robot that imitates the body of a stingray fish. The cardiomyocytes used to power the robot were optogenetically engineered to be light-sensitive, similar to the approach taken by [18]. Optical stimulation caused sequential waves to flow from the front to the back axis, resulting in forward movement due to the oscillation of the fins. Applying the light signal on both fins synchronously resulted in straight movement. However, applying an asynchronous light signal resulted in the fins spinning due to asymmetric motion. For the first time in literature, a swimmer biorobot was direction controlled [20].

So far, the biomachines examined previously were 2D thin film cardiomyocyte-based structures. To generate larger actuation forces, 3D structures have started to appear in the literature allowing biomachines with more advanced capabilities such as gripping, walking, and performing larger robot deformations. To accomplish this, the authors of [18] have further developed their devices in [21], and built a string ray fish-like robot with a layered skeleton. In this work, cardiomyocytes were introduced to a multi-layer extracellular matrix (ECM) based hydrogel skeleton. The usage of ECM-based hydrogels allowed for improved 3D cell organization on the substrate as well as greater deformation of robots. For the first time in literature, cardiomyocytes were combined with ECM to form a solid muscle strip in 3D.

Building biological actuators using cardiomyocytes appears as a more straightforward process due to their natural ability to produce spontaneous beating without

the need for external stimulation. Nevertheless, due to this very factor, controlling the timing and magnitude of the contraction poses a considerable challenge. Therefore, using skeletal muscle cells emerges as a more appealing option for gaining better control of the device and its functions.

Recent advancements in tissue engineering have enabled the design and construction of 3D skeletal muscle biomachines that surpass previous cardiomyocyte-driven devices in terms of force output and modularity [11]. The work presented in [22] pioneered the development of 3D skeletal muscle microtissues connected to structures resembling tendons, such as micropillars. This innovative approach utilized the widely popular C2C12 cell line, a type of skeletal muscle cells derived from mouse myoblasts [23]. Notably, this study also achieved a significant milestone by optogenetically engineering the C2C12 cell line to respond to light stimulation. 3D-engineered skeletal muscle microtissues were connected between rigid micropillars and the bioactuator produced a passive tension force of 10.8 µN and an active contraction force of 1.41 µN in response to external optical stimulation [22].

Since then, 3D skeletal muscle structures have grown to a much larger millimeter size, providing substantially larger passive and active tension forces [11]. Authors of [24] designed a 3D-printed a flexible hydrogel skeleton, consisting of two rigid pillars, joined by a compliant beam to simulate articulating joints. Skeletal muscle generated from the C2C12 myoblast cell line was engineered around the rigid pillars using an injection molding procedure. Electrically triggered muscle contraction propelled soft biorobot deflection, producing up to 1 mN passive tension force and 200 µN active tension force [24]. A similar 3D-printed pillar and beam structure was used in [25], however, this time optogenetic cells powered the biorobot. A light-emitting diode was utilized to regulate direction of the biorobot motion. Light stimuli was also used to mechanically train muscle bioactuators during differentiation. With this technique, skeletal muscle bioactuators were trained to generate up to 2 mN passive tension force and 300 µN active tension force.

Imitating nature's own work has proved to be one of the most fruitful strategies for developing a reliable biomachine. By getting inspiration from the antagonistic muscle pair found in human body, the authors of [26] developed a biorobot with outstanding gripping capabilities. The biorobot was made out of a skeleton with anchors and a rotating joint. Myoblast-laden hydrogel sheets were placed on the skeleton anchors to generate 3D skeletal muscle tissues, which eventually rotated the joint 90 degrees when electrical stimulation was applied. The robot successfully controlled the object by conducting pick and drop operations using selective muscle contraction [26]. In this study, primary mouse myoblasts were used which means there is a need for regular animal sacrifices to get fresh primary cells.

[27] introduced a circular distributed multi electrodes (CEs) approach, which was used to create a myoblast-driven crawling robot. In this study, it was demonstrated that the CEs approach may increase C2C12 cell differentiation and regulate the movement speed of the crawling robot. This technique provides a possible tool for the construction and control of biosynthetic robots as early as the differentiation period.

A practical approach was taken in [28] to utilize the C1C12 skeletal muscles as micro-pumps. In this study, C2C12 cells were cultured on a PDMS mold to create a muscle ring, which was then mounted on a hydrogel tube to create a pump-robot in. In this configuration, under electrical stimulation, the entire muscle ring contracted. The asymmetrical location of the muscle ring and the joining of a hose and a rigid pipe enabled the pump's one-way net flow to be achieved. In this study, skeletal muscle cells were used as micro-pumps for the first time [28].

In 2019, the thin film micro-patterning technique that was utilized in cardiomyocyte-driven devices was adapted to C2C12 cell line and 2D skeletal muscle-driven biorobots were developed on a thin film membrane. Under 1 Hz and 40V electrical stimulation, the maximum displacement of the thin film biorobot was observed to be 276 $\pm$ 55 µm [29].

To push the limits of the biorobots even further, the same research group that developed the gripper biorobot in [26], has further improved their idea by constructing biorobot capable of moving in the air without the need for a liquid nutritional medium. For the first time in the literature, a biorobot capable of operating in the air was fabricated. The designed robot wraps skeletal muscle tissue and flexible substrate material in a small collagen structure. The results demonstrated that the robot retains high cell activity and contractility in the air and can bend when electrical stimulation is applied [30]. This study also shown that C2C12 tissue can survive on minimal nutrients, provided by a small collagen. structure.

In these studies, tissue engineering's enormous potential in creating soft robotics was highlighted. Although this work is focused on using engineered muscles as biosensors, these studies provide insightful parallels and learning opportunities for the research at hand. All the studies examined show that there is tremendous potential in tissue engineering and synthetic biology.

2.1.2. Biomedical Implant Devices

The field of biomedical implant devices has evolved significantly over the last few decades, transforming into a robust and critical industry. With the mass production of countless devices, these sensors have become an integral part of many people's daily lives [31]. Their widespread use is a testament to how innovation can effortlessly integrate into our daily lives. Notable examples of commonly used biomedical devices include cardiac implants such as cardiac pacemakers that monitor and regulate abnormal heart rhythms. Since 2009, around 700,000 pacemakers are implanted worldwide every year [32]. Implantable cardioverter-defibrillators are also in great demand due to an increase in cardiac arrhythmia-related complications. These defibrillators are designed to sense irregularities in the heart's rhythm and restore it to normal levels by applying controlled electric shocks [33].

Capsule endoscopy devices offer a non-invasive solution for visualizing the gastrointestinal tract, providing quality images and videos. The data collected by these capsules give healthcare providers crucial insights into conditions that were previously difficult to visualize non-invasively, such as gastrointestinal bleeding, polyps, and ulcers [34].

Deep brain implants are surgically inserted into the brain tissue to record electrical activity and, in some cases, to send controlled electrical impulses for therapeutic purposes. These implants continuously monitor brain rhythms and patterns that are important in neurological research [35]. They are also used to reduce or manage symptoms associated with some neurological and psychiatric illnesses, such as Parkinson's disease, epilepsy, and obsessive-compulsive disorder. [36]. Deep brain stimulation is especially in high demand due to its effectiveness against neurological conditions that are resistant to traditional pharmaceutical treatments.

Smart orthopedic implants make up a smaller but significant portion of the widely used implant devices of today. They are an innovative combination of traditional joint replacements with modern sensor technology. These implants, which are used in joints such as the knee, hip, and spine, can assess stress, pressure, alignment, and temperature data, detecting early signs of mechanical wear in the joint implants [37] [38]. Smart knee implants with adaptive cushioning [39], hip implants that can measure the applied forces and moments [40], and spinal implants that may release medication gradually [41] are a few examples.

Electrochemical implant sensors with molecular sensing capabilities offer ways to monitor and analyze physiological parameters inside the body. Such molecular sensing have been practised ex-vivo settings [42, 43] with pH [44] and various protein sensing applications [45, 46]. To make such sensors available for implantation is a promising research subject in the implant sensors landscape. The purpose of these sensors is to be implanted in specific tissues or organs, allowing for continuous and real-time monitoring of different biological signals and molecular markers. These devices have

numerous benefits, such as their high sensitivity, accuracy, and capability to deliver precise measurements for long durations. Moreover, these sensors have the potential to enable early detection of diseases, provide personalized treatment options, and optimize therapeutic interventions. Electrochemical implant sensors have the capability to detect a wide range of phenomena. Some examples of what these sensors can sense include pH [47] and glucose molecules [48].

Perhaps, continuous glucose-monitoring devices are the devices most similar to the one investigated in the current study because of their capacity to predict the existence of glucose molecules. Glucose monitoring devices offer a continuous stream of blood glucose data to help the management of diabetes [49]. Unlike traditional glucose monitoring technologies that involve finger pricking, these sensors are often implanted or inserted beneath the skin and record glucose levels in the interstitial fluid continuously. In the literature, implant sensors that can sense glucose molecules are limited to electromagnetic sensors [50–54]. However, these devices often monitor the secondary effects of glucose molecules rather than detecting the glucose molecules themselves. When it comes to molecular monitoring, the secondary effects such as an increase in tissue permittivity could be misleading as they could be caused by various other factors.

2.1.3. Living-Cell Based Sensors

Living-cell sensors are a promising new frontier in the field of biosensors, with important implications for medical, environmental, and industrial applications. These sensors detect specific substances or changes in the surrounding environment by utilizing living cells, either whole cells or biological components [5, 55].

While they provide unique solutions and have enormous potential, their development and implementation are packed with difficulties. The topic is a combination of biology, engineering, ethics, and technology, and ongoing research is expected to deliver more sophisticated and accessible tools in the future years. Although few,

there are some examples of the engineered cell-based biosensors in the literature including environmental bacterial biosensors for detecting heavy organic pollutants in environment. Such biosensors offer high sensitivity and specificity, allowing them to accurately identify contaminants. Additionally, they have the capability to provide real-time monitoring, enabling quick responses to changes in contaminant levels. They provide affordable solutions for continuous monitoring, capable of detecting a wide range of pollutants such as heavy metals, pesticides, and industrial chemicals in water, soil, and air [6, 56, 57]. The integration of IoT and data analytics enhances their potential for comprehensive environmental monitoring, which can contribute to environmental protection and the preservation of public health.

The applications of engineered cell-based biosenors are not limited to environmental monitoring. In the recent years such biosensors have been developed to detect inflammatory agents in the human body [58–60]. These biosensors provide several advantages, including early disease detection, high specificity, and sensitivity. They allow for the monitoring of inflammation in real-time, which helps in creating personalized treatment plans and advancing the development of targeted therapies. In addition, these biosensors play a significant role in advancing research in immunology and drug development for a wide range of inflammatory conditions. Cell-based biosensors have also been studied for drug testing [61].

While the majority of these sensors are used in-vitro, recent studies has shown some remarkable studies investigating the integration of cell-based biosensors for in-vivo applications [62,63]. These novel studies show a growing interest in the development of biosensors that may function within living organisms, indicating a possible shift toward cell-based and real-time monitoring of biological system.

2.2. Contribution of the Thesis

Facilitating electromagnetic molecule sensing inside the human body is a major difficulty that has not been extensively discussed in the literature prior to this proposal. The major concern has been the scale difference between the molecular links and to electromagnetic links. Because molecular linkages function at such a small scale, high-frequency electromagnetic readers are required in order to successfully record their outputs. The difficulty of this task has thus far prevented thorough investigation, leaving a unclosed gap in the literature regarding the smooth integration of molecular connections inside the human body with external electromagnetic readers.

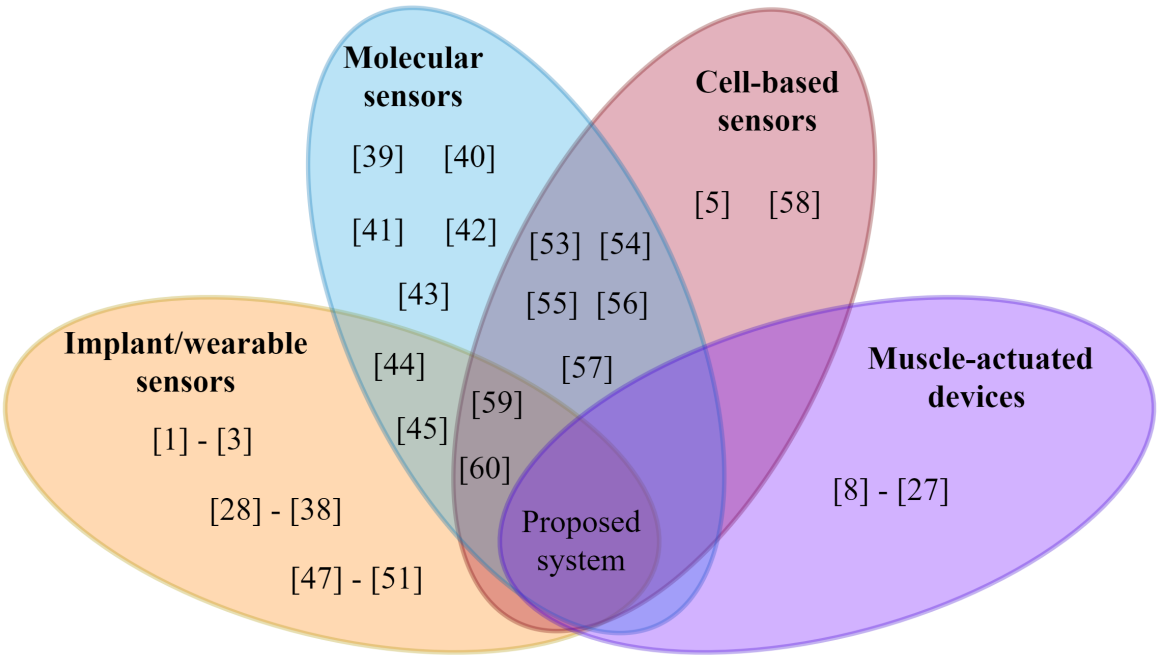

Figure 2.1. An overview of the state of the art.

By allowing the integration of external electromagnetic readers and molecular linkages, the proposed project seeks to close this gap and enable accurate molecular readings inside the human body. The study focuses on the creative application of engineered living cells in order to achieve this challenging goal. Although engineered living cells have been utilized as bio sensors in in-vitro environments, the use of these cells as

in-vitro implant biosensors have not yet been extensively investigated. Interestingly, no prior research has taken advantage of the potential of synthetic skeletal muscle tissue as a biological sensor capable of detecting and responding molecular signals in the surrounding medium. This study is unique in its use of skeletal muscle as a sensor and represents the first instance of skeletal muscle being used as an implant. Furthermore, the achievement of molecular in-vivo sensing through mammalian cell-based biosensors has yet to be realized. A comparison between this study and the current state of the art is presented using a lotus graph in Figure 2.1.

3. METHODOLOGY

3.1. Bio-hybrid Implant Design

In the proposed system, the sensing process is primarily achieved by the bio-hybrid implant device. The device consists of an implant antenna that undergoes reconfiguration through the utilization of 3D-engineered skeletal muscle tissue. Additionally, a 3D-printed flexible scaffold is employed to provide support for both the implant antenna and the 3D development of the skeletal muscle tissue.

In the bio-hybrid device, the skeletal tissue is enclosed within the flexible scaffold and reports the presence of the trigger molecule by its contractile output. The flexible scaffold is made up of a micro-well with two thin pillars attached to the bottom. One of the pillars includes a conductive bridge that extends toward the implant antenna. The bridge essentially functions as an electrical switch. When a target molecule is present in the medium, the muscle contracts and deforms the pillars. The conductive bridge is then pulled and the short circuit connection between the bridge and the implant antenna is broken. Thus the switch is toggled, and the resonance of the implant antenna switches from one state to another, The working principle of the bio-hybrid implant device is depicted in detail in Figure 3.1. This chapter investigates the components of the bio-hybrid device, starting from the innermost element, the 3D-engineered skeletal muscle tissue, and extending to the outermost element, the implant antenna.

3.1.1. 3D Engineering of Skeletal Muscle Tissue

3D muscle engineering is the process of creating functioning muscle tissues in vitro utilizing artificial 3D scaffolds and extracellular matrices (ECM). While the artificial 3D scaffolds provide the tissue with the required mechanical support by mimicking the bones and tendons, the artificial ECM provides structural and biochemical support by mimicking the natural micro environment of cells.

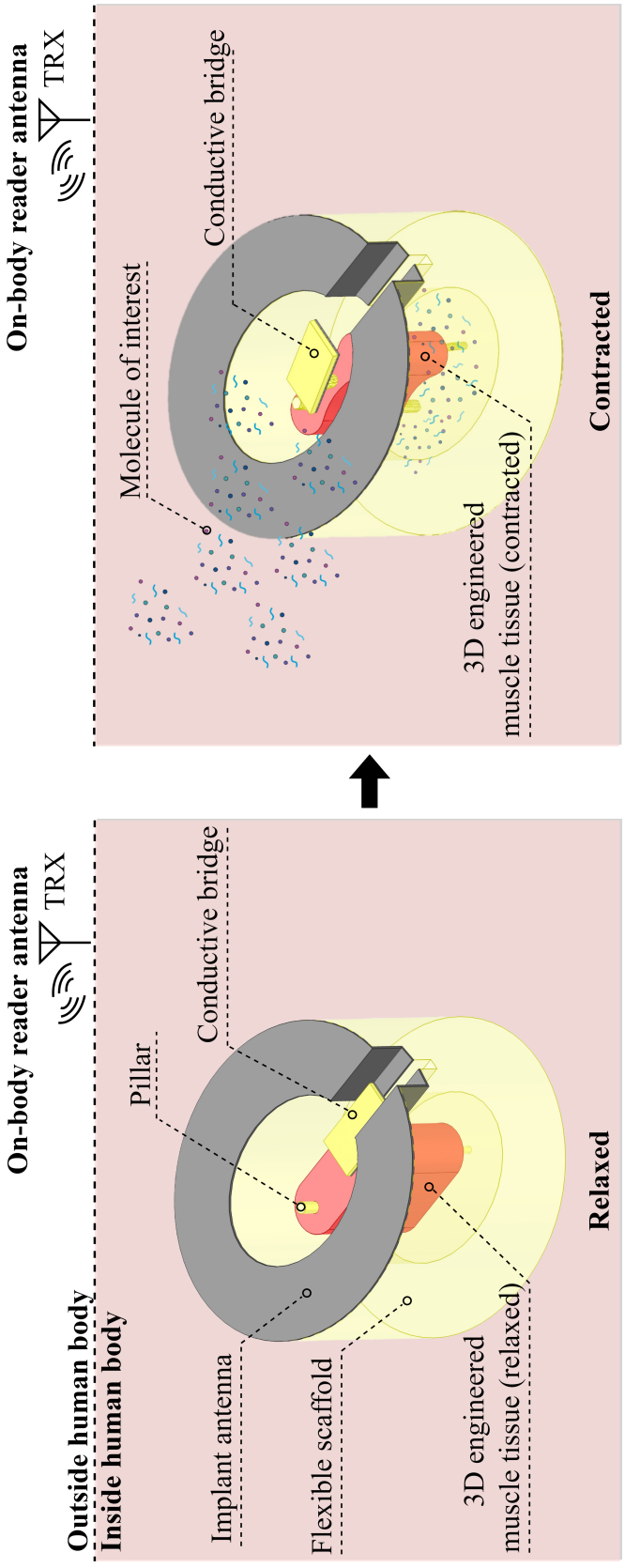

Figure 3.1. Working principle of the bio-hybrid implant and the on-body reader antenna.

The ECM is a complex network of proteins that surrounds and supports the cells biochemically to form tissues and organs [64]. ECM is utilized to direct the precise formation of tissues by providing both structural support and essential cell signaling for growth direction. It is present in all of the organs and tissues of the human body and plays an essential part in determining the physical medium that the cells live in.

The ECM's role in tissue engineering is very crucial. It significantly improves cell survival and function by providing a supportive and biochemically active environment, resulting in the successful development of tissues. By changing the composition, structure, and characteristics of ECM or ECM-derived materials, it is possible to develop environments that are precisely customized to specific use cases of tissues. Therefore imitating ECM is one of the key elements in creating 3D engineered muscle structures. The most commonly used ECM proteins in skeletal tissue engineering applications are collagen, fibronectin and lamminin [65]. For this project, collagen type IV was chosen and an ECM-cell mixture recipe based on [66] was developed and optimized. The ingredients of the optimized recipe are seen in Table 3.1.

Table 3.1. The ingredients of the ECM-cell mixture used for generating 3D engineered skeletal muscle tissues.

Ingredient	**Percent**
Collagen type IV	65%
10X phosphate-buffered saline (PBS)	10%
Matrigel	20%
C2C12	5%

The skeletal muscle tissue generation process is illustrated in Figure 3.2. The procedure to be followed for this process is detailed as follows:

(i) Flexible scaffold preparation and sterilization: This initial step involves the flexible scaffold preparations that need to be completed before the process can start. Prior to the loading day of the scaffold, the flexible scaffold is placed inside a 6-well plate and firmly anchored to the base of the plate using a biocompatible adhesive. This anchoring is crucial to ensure cell dormancy during the growth and differentiation periods, allowing for steady cell expansion and attachment to both each other and the extracellular matrix. Following the scaffold anchoring, the well undergoes sterilization with filtered water and alcohol, followed by exposure to UV light for a duration of 15 minutes. Subsequent to the sterilization process, the micro-well of the flexible scaffold is coated with a collagen stock, prepared earlier, at a concentration of 0.02 %. Collagen coating improves the biocompatibility of synthetic materials when employed as a coating, making them more suited for interacting with cells and tissues. Furthermore, it provides an optimal surface for cell adhesion and expansion and interacts with the cells, boosting cell attachment and assisting the cells to spread and grow on the surface. Collagen-coated scaffolds are placed in the incubator and left at least overnight.

(ii) Culturing C2C12 myoblasts: C2C12 myoblast cells are cultured in growth medium (GM) composed of Dulbecco's Modified Eagle Medium (DMEM, with high glucose, Sigma-Aldrich) supplemented with 10% fetal bovine serum (FBS, heat inactivated, Sigma-Aldrich), 100 IU/mL penicillin and 100ug/mL streptomycin (Sigma-Aldrich) and L-Glutamine (200 mM, Capricorn Scientific) maintained at 37°C in a saturated humidity atmosphere containing 5% CO2. Once the cells reach 60-80% confluency, they are subcultured with 0.25% Trypsin-0.01% EDTA (Sigma Aldrich) solution. C2C12 cells used in this project were a gift from Assoc. Prof. Urartu Özgür Şafak Şeker at Bilkent University, UNAM. The cells were in P15 when they were delivered.

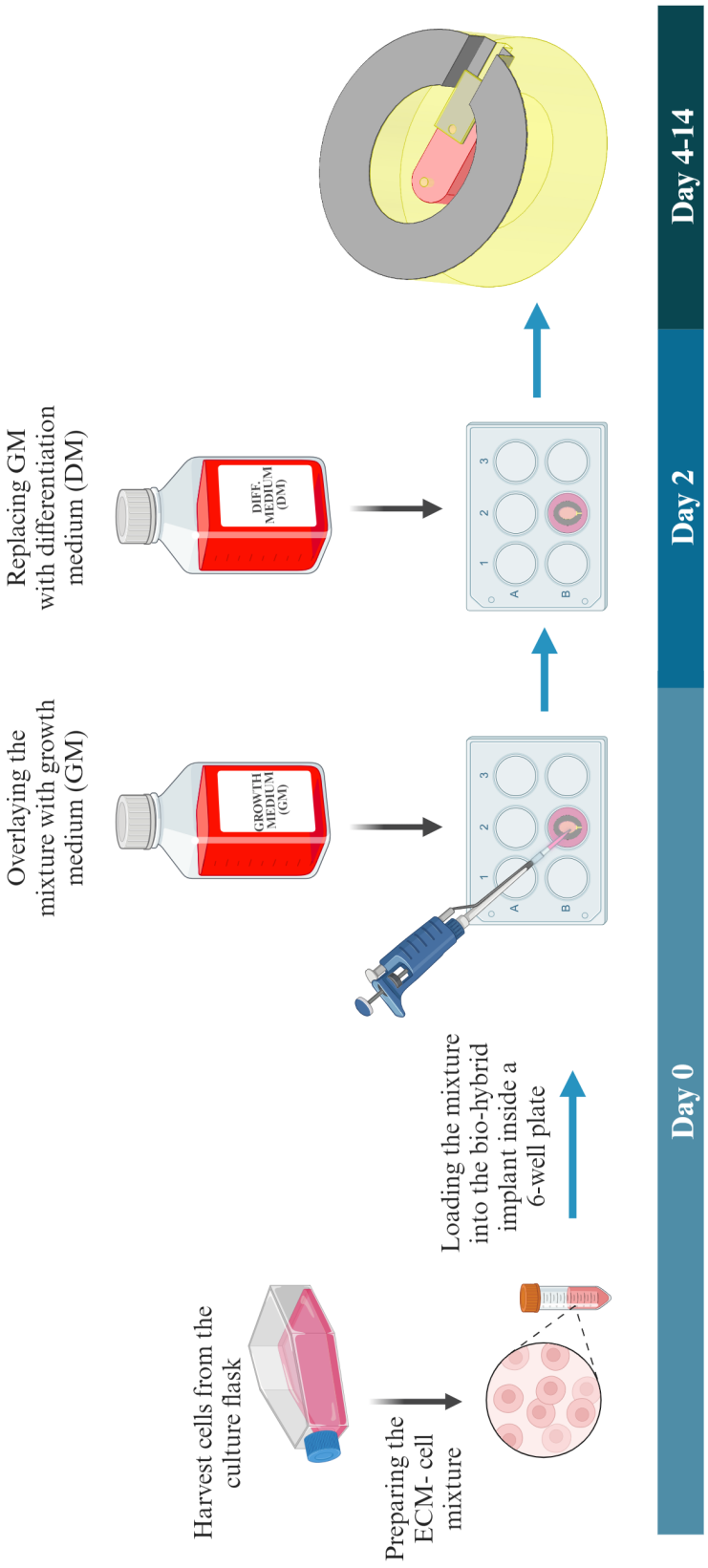

Figure 3.2. Procedure for generating 3D engineered C2C12 skeletal muscle tissues.

(iii) ECM preparation: In this step the ECM composed of collagen type IV, 10X PBS (Sigma-Adrich) and matrigel (Corning) are mixed with C2C12 cells to form the ECM-cell mixture. First, the matrigel solution in the freezer is thawed and subsequently placed in an ice bucket to prevent premature gelation. While matrigel solution is thawing, collagen is dissolved to a concentration of 3.2mg/mL in sterile 0.02% acetic acid to obtain the collagen stock solution. Collagen stock solution pH can be adjusted by adding 0.5M NaOH until a light pink color is obtained indicating a neutral pH of 7.5. Collagen stock is placed in the ice bucket to prevent gelation. Then, ice-cold matrigel solution is added to the ice-cold collagen. Finally, 10X PBS solution and growth medium are added to the collagen-matrigel mixture. This final mixture is referred to as the ECM, and it is carefully stored in the ice bucket to prevent gelation until the cells are harvested.

(iv) C2C12 myoblast harvesting: The cells will be observed under a microscope to verify their confluency and general health. GM will be removed from the culture flask and the flask will be rinse with PBS to remove any residual medium. 3-5 mL of trypsin-EDTA solution will be added to the cell flask to detach the cells from the surface and the flask will be incubated at 37°C atmosphere containing 5% CO2 for 3 minutes. Once the cells are detached, 15- 20 mL of GM will be added to neutralize the trypsin. The amount of GM depends on the culture flask that is used. Then the cell suspension will be transferred to centrifuge tube and centrifuged for 5 minutes at a speed of 5000 rounds per minute (RPM). The cell pellet will gently re-suspended in 1 mL fresh GM and an aliquot will be taken of the resuspended cells for cell counting. After many optimizations, the ideal cell number for this project is determined as 10 - 15 $\times$ 10^6 cells/cm^3. The desired number of cells will be centrifuged again at 5000 RPM for 5 minutes and the supernatant will be gently removed.

(v) Flexible scaffold loading and tissue differentiation: On the scaffold loading day, the flexible scaffold will be taken out of the incubator and loaded with the cell-gel mixture. First, the mixture will be applied to the space between the pillars and

then to the remaining area within the scaffold. 5-10 min after loading the cell-gel mixture, the mixture is inspected by gentle tapping to confirm gelation. When the gel is rigid, it is transferred to the incubator. After 1-2hr incubation, the gel within the micro-well is overlaid with warm GM. Every two days, half of the old GM inside the 6-well plate is discarded and replaced with fresh GM. On the fourth day, the entire GM is replaced by differentiation medium (DM). Every two days, half of the existing DM inside the 6-well plate is discarded and replaced with fresh DM. After 10-12 days of differentiation, skeletal tissues are matured.

For optimization purposes, the recipe was tried inside various different test substrates. Samples of the fabricated matured skeletal tissues inside the test substrates and inside the designed flexible scaffold are shown in Figure 3.3(a) and in Figure 3.3(b), respectively.

To validate the functionality of the fabricated tissues, acetylcholine (ACh) test was conducted to the matured skeletal tissues at the end of the 14 day differentiation period. ACh is a neurotransmitter that is essential in the process of skeletal muscle contraction. Its primary function is at the neuromuscular junction, where motor neurons interact with muscle fibers [67]. The ACh test setup is illustrated in Figure 3.4. The test configuration involves the use of three syringe pumps, two for fluid flow into the 6-well plate and one for fluid flow out of the 6-well plate. One of the inlets delivers ACh, while the other delivers PBS at a rate of 500 μL/min. Importantly, the two inlets do not operate simultaneously; when the ACh pump is active, the PBS pump is inactive, and vice versa. The setup is designed to observe the skeletal tissue contraction upon the activation of ACh flow and tissue relaxation upon the deactivation of ACh flow and activation of the PBS flow. Lastly, the outlet syringe pump operates continuously to control the ACh and PBS within the test medium. During the controlled administration of ACh and PBS, the skeletal tissue is observed under an inverted microscope.

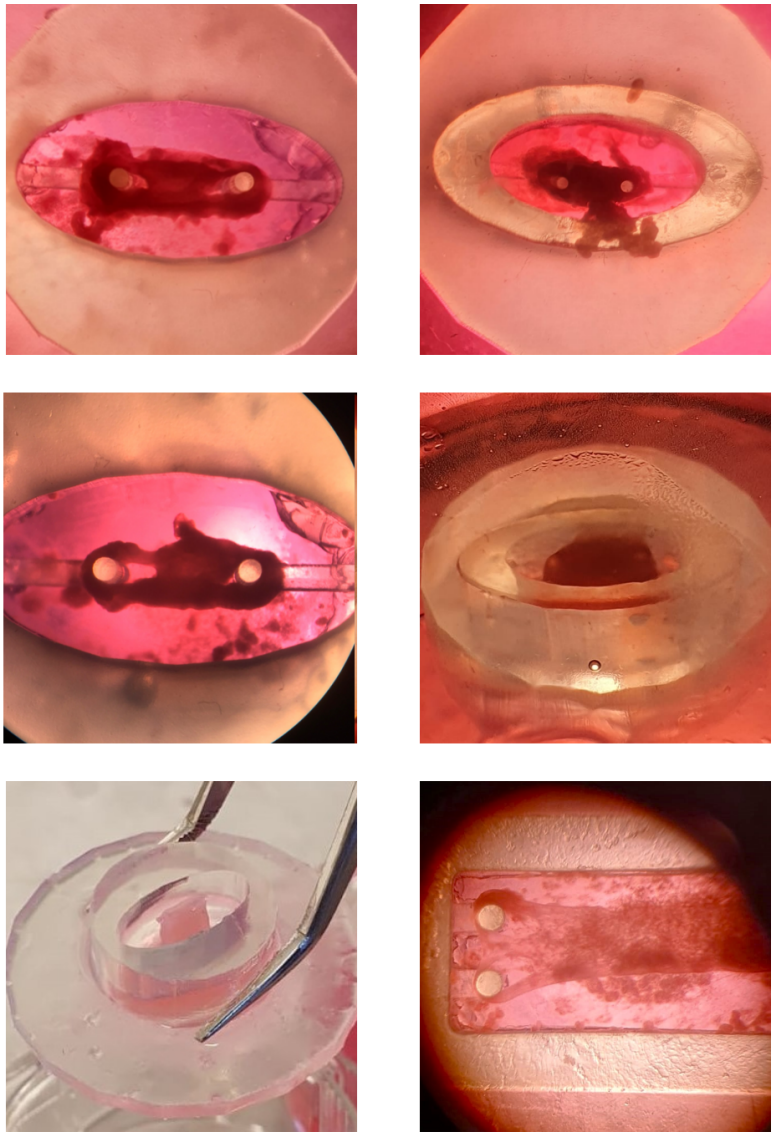

(a)

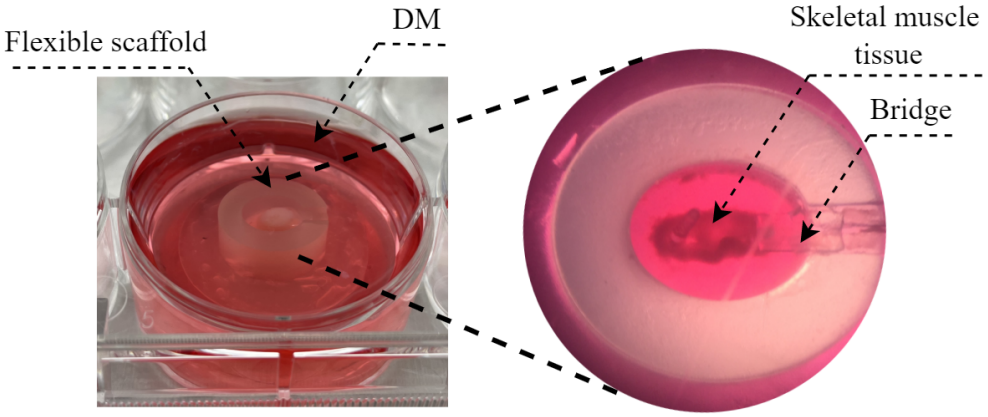

(b)

Figure 3.3. Samples of fabricated tissues grown inside (a) various test substrates. (b) designed flexible scaffold.

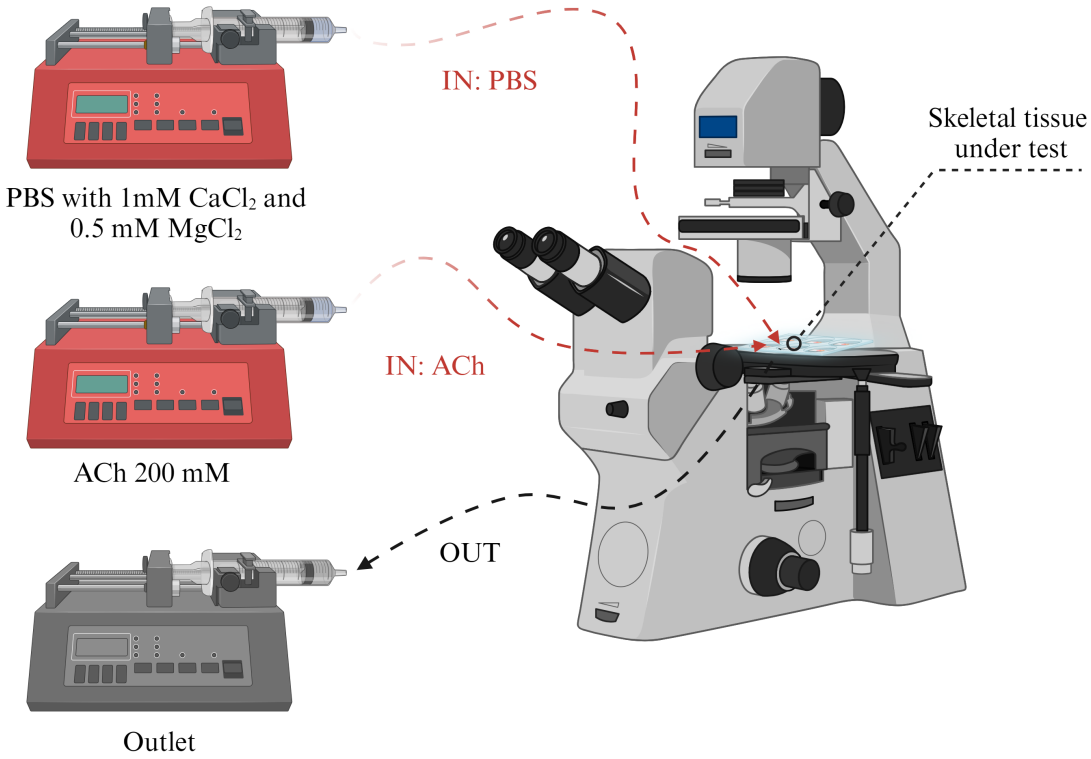

Figure 3.4. The ACh test setup.

During the testing phase, C2C12 cells are stimulated sequentially with 200 mM ACh for 2 minutes. Following, the medium is cleaned with PBS for 5 minutes in between ACh pulses to allow the tissue to relax. The PBS is supplemented with $MgCl_2$ and $CaCl_2$. Calcium encourages muscular contraction since it is produced when a signal is received by the muscle, letting proteins to interact and create a pulling force that causes muscular contraction [68]. The contraction of the tissue is tracked using a digital microscope camera mounted on the inverted microscope. ImageJ software [69] is used to determine the contraction in arbitrary units by quantifying and comparing the visible area of the tissue while it is relaxed and contracted, as shown in Figure 3.5. The fluid flow time table for the test is given in Table 3.2. During the test, two ACh pulses were applied to the tissue and in between the ACh pulses 3 PBS washes were done. The first ACh pulse caused a distinct contraction in the tissue, however the second ACh pulse's effect was not very obvious as only a fraction of the contraction was observed. This might be due to tissue's desynthesization aganist multiple ACh pulses. It should be noted that the tissue contractions observed during the ACh test

were not sufficient to cause deflection in the flexible scaffold pillars. Therefore, the skeletal tissues could not be used for the measurements of this thesis. Instead, the electromagnetic measurements were taken with mock deflected models which are 3D-printed versions of the mechanical simulation outputs. Mechanical simulations and electromagnetic measurements are detailed in Section 4.1 and Section 5.2, respectively.

Table 3.2. Fluid flow timetable for the ACh test.

Duration (minutes)	**PBS**	**ACh**	**Outlet**
0 - 1	ON	OFF	ON
1 - 3	OFF	ON	ON
3 - 8	ON	OFF	ON
8 - 10	OFF	ON	ON
10 - 12	ON	OFF	ON

3.1.2. Flexible Scaffold

Artificial scaffolds play a crucial role in tissue engineering, serving to replicate the ECM seen in natural tissue. These scaffolds act as a supportive structure that allow cells to connect, grow, and differentiate. One of the most significant advantages of these scaffolds is their controlled architecture. By adjusting their size, shape, and porosity, it is possible to create scaffolds that precisely mimic the particular features of many tissues, from bone to cartilage.

Optimally, a scaffold encourages the engineered tissue's smooth integration with the surrounding artificial structure, resulting in a unified, functioning body of bio-hybrid structure. Furthermore, it guides tissue development in a more regulated manner by managing the alignment of the cells in the differentiation period. During the

early stages of differentiation, C2C12 myoblasts begin to produce fiber-like structures in two dimensions. In the absence of external structural support, tissue fibers cannot align vertically and remain flat. To offer the necessary structural support to the two-dimensional tissue fibers, a tendon-like flexible scaffold is created. This scaffold imitates the native musculoskeletal system's tendon and bone structures. In this study, the proposed scaffold not only provides structural support to the skeletal muscle tissue but it also facilitates the implant antenna and the resonance reconfiguration action that is required to realize molecular sensing. The implant antenna and the resonance reconfiguration will be detailed in Section 3.1.3.

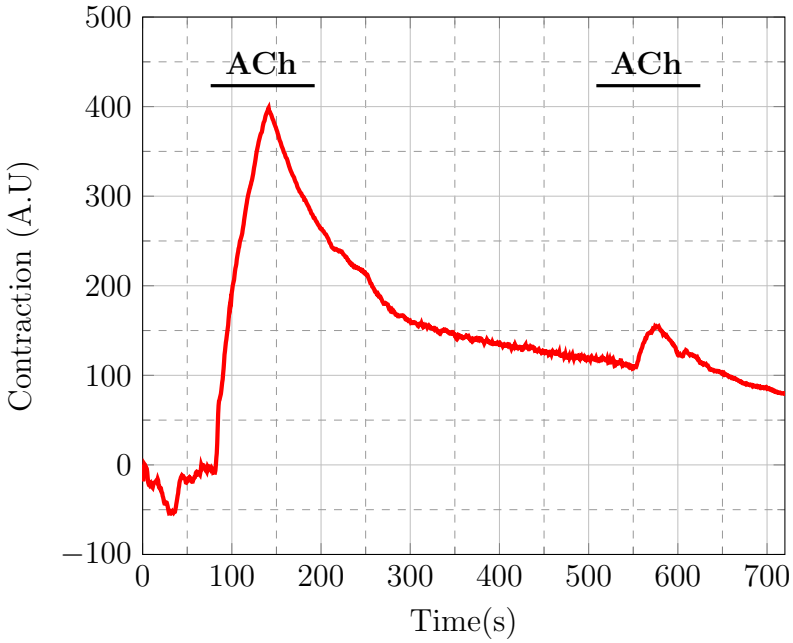

Figure 3.5. Contraction versus time in the ACh test.

The dimensions of the designed scaffold are given in Figure 3.6. The elliptical scaffold has a major diameter of 14 mm and a minor diameter of 12 mm, which is approximately the size of a large vitamin pill. The elliptical shape of the scaffold is selected in order to avoid sharp edges. The pillar diameters are set at 0.5 mm and the lower body diameter of the conductive bridge-carrying pillar is reduced to 0.3 mm, with the specific intention to enhance deformation. The bridge is situated on this pillar and it has a width, length and thickness of 1.9 mm, 3.5 mm and 0.2 mm, respectively. The pillar and bridge sizes are chosen to achieve maximum deflection against the limited

external contraction forces created by the muscle tissue.

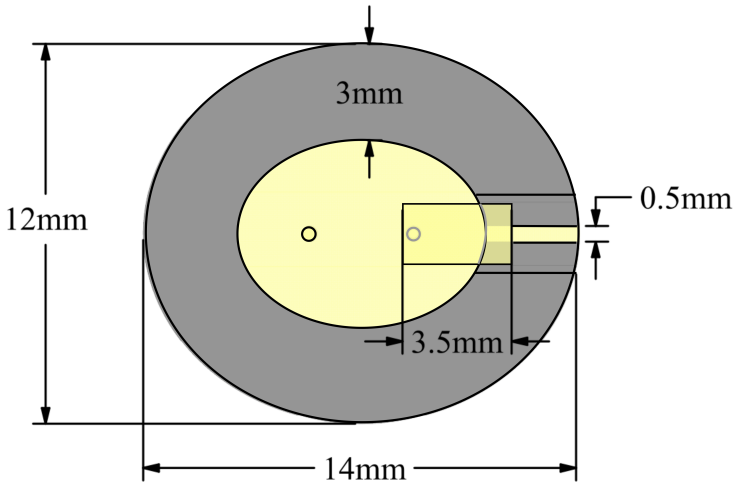

(a)

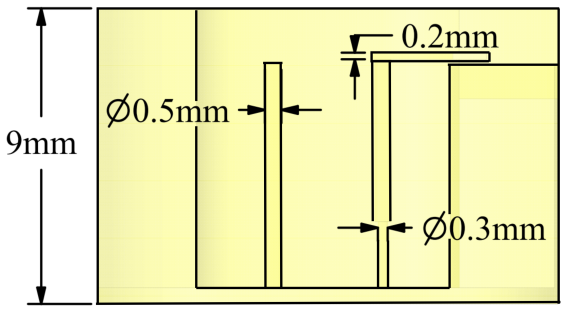

(b)

Figure 3.6. The bio-hybrid implant dimensions (a) top view. (b) side view with lower outer wall.

Considering the complex geometry and the minimal dimensions of the pillars and the bridge, it is clear that high resolution and precision fabrication are essential to fabricate such a 3D structure. Achieving complex shapes with high resolution is a challenging task using conventional assembly production and methods. As a solution, stereolithography (SLA) 3D printing can be employed to quickly and precisely fabricate a scaffold or a system that has controllable geometric and mechanical properties. One advantage pf SLA printing is its ability to polymerize a wide range of materials with different levels of flexibility. This printing technology cures liquid resin into hardened plastic objects with the specified stiffness using a light source such as a laser or a pro-

jector. SLA-manufactured components have higher resolution and precision, sharper details, and smoother finishes compared to other 3D printing techniques. This is due to the pinpoint accuracy of the laser which allows for extremely fine detail in micrometer ranges. The precision of the SLA printed flexible scaffolds are photographed under an non-inverted microscope as seen in Figure 3.7.

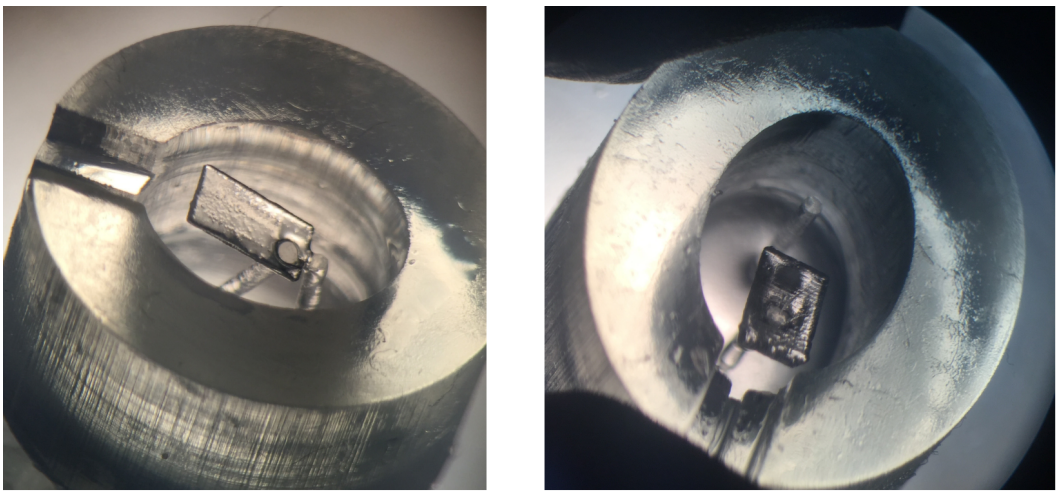

Figure 3.7. Microscope view of the flexible scaffolds printed with SLA printing technique.

The selection of the most suitable SLA resin is crucial for this project due to the limited contractile capabilities of the tissue, necessitating the utilization of a flexible SLA 3D-printed scaffolds. Our research laboratory BOUNTENNA is equipped with an SLA 3D printer manufactured by Formlabs, which is widely recognized for its selection of custom-formulated resins that are optimized for use in precise printing with SLA printers. The resins offered by Formlabs demonstrate a range of characteristics, including flexibility, elasticity, and biocompatibility.

After conducting a thorough evaluation of the resins offered by Formlabs, two candidates have emerged as highly suitable for this project: the biocompatible IBT resin and the Flexible 80A resin. In order to conduct a thorough comparison of these two resins, it was necessary to gather data on their tensile properties, especially on their elasticity modulus. Elasticity modulus, is a measure of a material's stiffness.

It measures a material's ability to endure deformation when subjected to an external force. It specifically characterizes the stress-to-strain ratio (force exerted per unit area) in a material under tension or compression. Elasticity modulus is represented by the symbol E and has the unit of pascals (Pa) or megapascals (MPa) and is calculated using the formula

$$E = \frac{\sigma}{\varepsilon} = \frac{F/A}{\Delta L/L}, \tag{3.1}$$

where σ is stress, which represents the amount of force exerted on a material per unit area, and ε is the strain, which represents the resulting elongation of the material in the direction of the applied force, in relation to its original length. In practical terms, a higher elasticity modulus indicates that a material is stiffer and less likely to deform when subjected to stress. On the other hand, a lower elasticity modulus suggests that the material is more flexible and can be deformed more easily. Materials that have higher elasticity modulus are typically classified as rigid, whereas materials with lower values are generally regarded as more flexible. Elasticity modulus is a fundamental parameter and it is crucial to understand how materials react to different external forces.

While Formlabs provided the elasticity modulus and other tensile properties for the IBT resin, such data was unavailable for the Flexible 80A resin. Consequently, a ASTM638 tensile test on the Flexible 80A resin was carried out at Yeditepe University's Materials Science & Nanotechnology Engineering Department using the Instron 6800 Series Universal Testing machine. The dog-bone shaped test specimen used for the ASTM638 test is shown in Figure 3.8(a).

After conducting tensile tests at three different pulling speeds, the force versus elongation graph was obtained, which is shown in the Figure 3.8. Elasticity modulus was calculated using this graph, by taking the average of the three pulling speed results. Comparison of the tensile properties of the candidate resins has been summarized in Table 3.3. Following a detailed evaluation of the tensile properties, the Flexible

80A resin emerges as the more flexible option, making it the ideal choice for this project. However, Formlabs delivers a more detailed characterization of the IBT resin's tensile characteristics which provides more comprehensive understanding of the resin capabilities. Thus, the mechanical system can be more properly recreated in mechanical simulations utilizing the IBT resin's properties. Using the better characterized resin assures that the mechanical models accurately depict the actual deflections experienced in real-life circumstances.

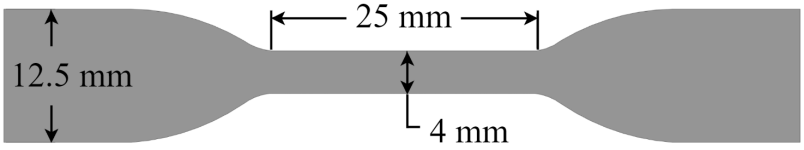

(a)

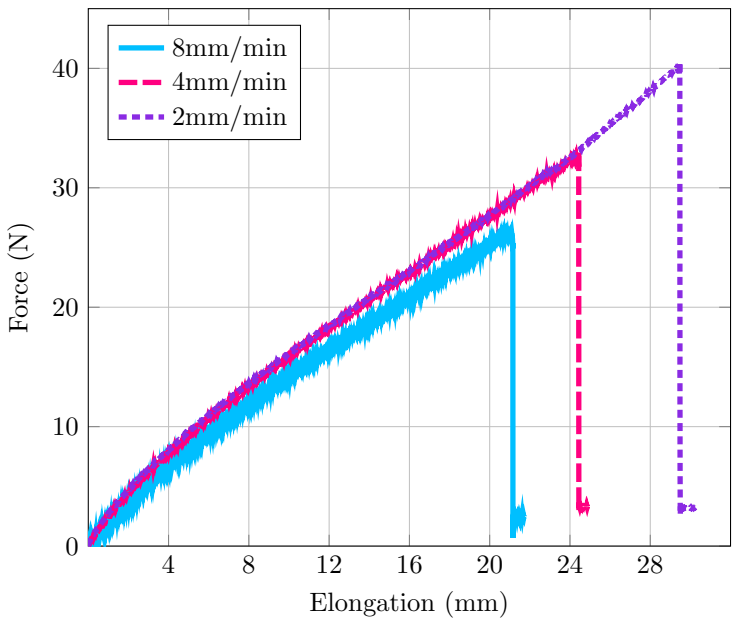

(b)

Figure 3.8. (a) The dog-bone specimen used for the ASTM638 tensile test. (b) Force versus elongation curve for three pulling speeds.

In addition, this modeling strategy takes into consideration a worse-case scenario. If the deflection of the bio-hybrid implant, simulated with the IBT resin, is found to be insufficient in practical use, there is always the option to switch back to the more flexible 80A resin during production. Thus, the IBT resin is advantageous due to its comprehensive tensile property data and also due to its biocompatibility. This is especially beneficial during the initial phases of the project, when a biocompatible and flexible scaffold could be helpful to fine-tune the 3D engineering process of the skeletal tissue.

Table 3.3. Comparison of the candidate SLA resins.

Property	**IBT**	**Flexible 80A**
Ultimate Tensile Strength	$\geq$ 5 MPa	8.9 MPa
Elasticity Modulus	$>$ 16 MPa	4.1 MPa
Biocompatibility	Yes	No

3.1.3. Implant Antenna

The implant antenna is the central binding element of the proposed system, acting as the intermediary component that connects the molecular links to the electromagnetic links. In the proposed configuration the tangible outcome of the molecular sensing is contraction of the engineered tissue. However, external electromagnetic readers do not have direct access to this molecular sensing output. Consequently, a translation process is required to make this biological response accessible to external electromagnetic readers. In the proposed system, the implant antenna serves as a translator. This chapter will detail the translation process of the implant antenna.

The translation is initiated with the muscle contraction. Upon detecting the presence of the target chemical, the skeletal tissue contracts, causing a deflection in

the surrounding pillars. Subsequently, the pillar that carries the conductive bridge is displaced from its original position. In its default state, the bridge is positioned over the implant antenna gap, effectively shorting the arms of the implant antenna. When the conductive bridge undergoes displacement, a dynamic reconfiguration unfolds within the implant antenna, inducing a shift in its resonance from one frequency to another. This change in the electromagnetic resonance of the antenna essentially converts the biological response into an electromagnetic signal that can be picked up by external electromagnetic readers. As a result, the implant antenna not only harmonizes the biological and electromagnetic components, but also allows for monitoring and analysis of the system's molecular sensing outputs.

It should be noted that reconfiguration of the implant antennas is not a new concept. Previously, reconfigurable implantable antennas were proposed in the literature, using vias and pin diodes to reconfigure the implantable antenna's radiation pattern [70, 71], polarization [72], and resonant frequency [73]. To perform the reconfiguration task, such devices require a power unit. A significant advantage of the proposed system is its ability to eliminate the requirement for a physical power unit by shifting reconfiguration and sensing responsibilities to living cells.

Implant antenna dimensions are shown in Figure 3.9. In the proposed system, the conductive bridge shorts the implant antenna gap when the tissue is relaxed. This is the first configuration of the implant antenna. In this configuration, implant antenna is a loop antenna. As the tissue starts contracting, a critical reconfiguration occurs within the implant antenna. The conductive bridge that initially shorts the implant antenna gap is displaced, leading to the emergence of the 3D elliptical split ring resonator which is the second configuration of the implant antenna. Split ring resonators are well studied in the literature. In existing literature, the resonance frequencies of split ring resonators are often determined using the well-established formula

$$f_0 = \frac{1}{2\pi\sqrt{LC}}, \tag{3.2}$$

where C is the capacitance and L is the inductance related to the split ring resonator.

Notably, it's important to recognize that these equations were formulated for planar split ring resonators that are mounted on rectangular fully-covering substrates. In the current arrangement, the split ring resonator has a three-dimensional structure and it is situated on the upper walls of the flexible scaffold which partially covers the split ring resonator. This non-standard shape and substrate coverage significantly differs from the assumptions that is made in traditional resonance calculations. Furthermore, when the conductive bridge rises due to muscle contraction, capacitances form with its adjacent conductive surfaces. The dynamic generation of these capacitances is a multi-faceted phenomena that challenges simple representation in analytical computation setups, contributing to the system's non-ideal nature. In addition to the non-ideal aspects associated with the implant antenna, the uncertainties related to the effects of dielectric loading on human interstitial fluid further complicate analytic calculations.

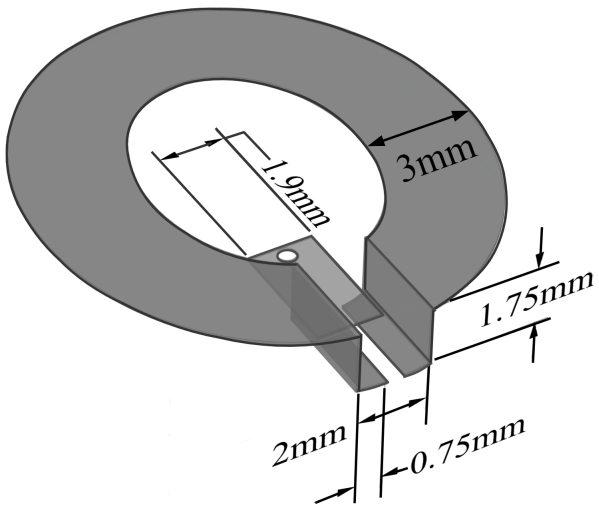

Figure 3.9. Dimensions of the implant antenna.

As a result of these non-idealities, calculating the resonance frequencies of the implant antenna's 3D split ring resonator case is a difficult problem. The complexities of the geometry, substrate coverage, dynamic capacitance generation and the dielectric loading of the human body challenge normal analytical approaches. Consequently, precisely determining the resonance frequencies of the implant antenna configurations presents ambiguity from the perspective of analytical calculations.

To overcome these challenges, the use of waveguides appears as a practical solution. Waveguide simulations are often used to predict the resonance of resonators due to their ability to accurately model the behavior of electromagnetic waves within a confined structure. Furthermore, waveguide simulations help neutralizing the effects of reader antennas and which can produce reliable estimates for the implant antenna's resonance. Hence, to accurately predict the resonance frequency of the implant antenna configurations, the bio-hybrid implant which includes implant antenna and the flexible scaffold, is placed inside a waveguide loaded with DMEM serum. The dielectric properties of DMEM serum, which are shown in Figure 3.10, are measured with SPEAG Dielectric Assessment Kit (DAK) 3.5.

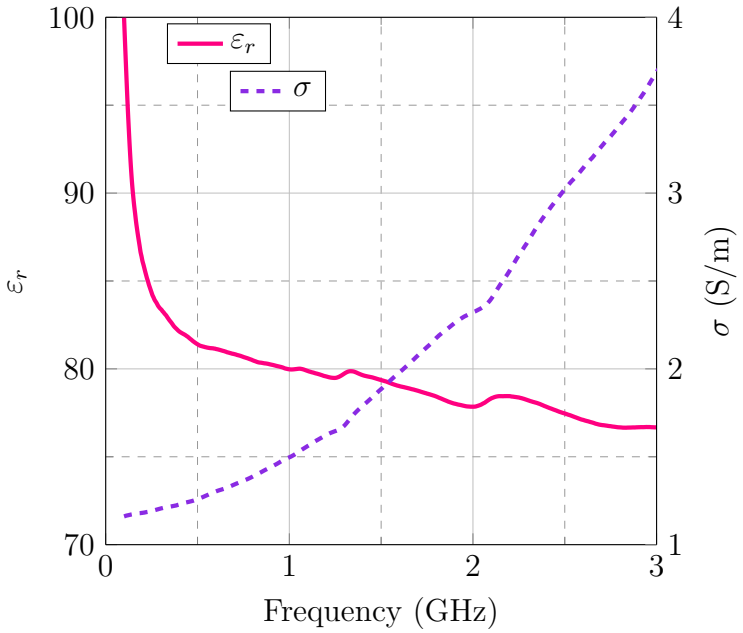

Figure 3.10. ε_r and σ of DMEM serum.

The waveguide simulations were conducted in ANSYS High Frequency Simulation Software (HFSS) and the dimensions of the waveguide setup is shown in Figure 3.11. The perfect electric conductor (PEC) boundary is applied to the outside faces of the vacuum box that lies on the x-axis and the perfect magnetic conductor (PHC) boundary is applied to the outside faces that lies on the y-axis. Two lumped ports were assigned between the PEC boundries. To realistically investigate the resonance of the implant antenna configurations, the outputs of the structural mechanical simulations were used

in the waveguide simulations. The mechanical simulations, which will be detailed in Section 4.1, involve applying three hypothetical force values to the pillars, namely 50 μN, 100 μN and 300 μN. The main goal of these mechanical simulations is to observe how the gradual increase of the contraction force affects the deflection of the pillars and the displacement of the conductive bridge. Consequently, integrating the mechanical simulations outputs into the waveguide simulations will enhance our understanding of the implant antenna configurations and the gradual transition occurring between these configurations.

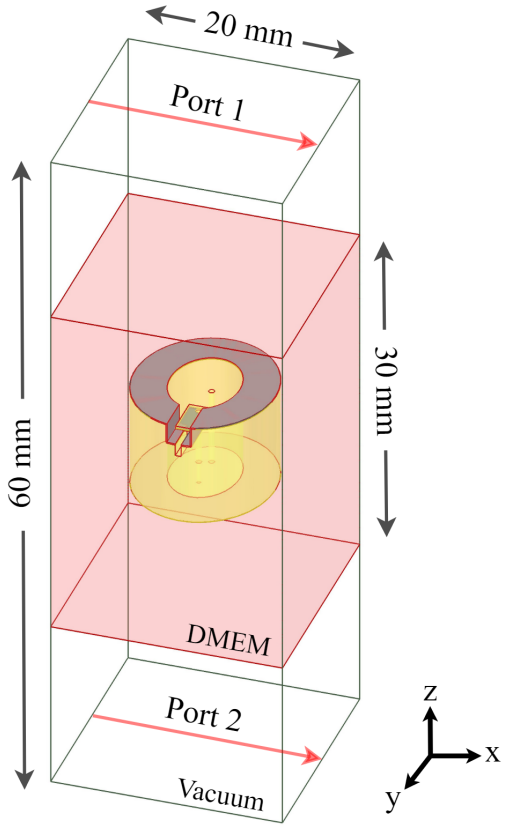

Figure 3.11. Waveguide simulation setup and dimensions.

The resonance characteristics of the implant antenna can be observed in the transmission coefficient between the two ports of the waveguide. Based on the waveguide analysis conducted, it is predicted that the implant antenna will exhibit a resonant frequency ranging from 1.46 GHz to 1.71 GHz as it undergoes reconfiguration from its initial loop configuration to 3D split ring resonator, as depicted in Figure 3.12. In this transmission coefficient graph, "Relaxed" case represents the loop configuration and

the “50 μN”, “100 μN”, “300 μN” cases represent the 3D split ring resonator case with varying degrees of deformation and the conductive bridge displacement. “Only scaffold” case represents the resonance characteristics of the flexible scaffold in the absence of the implant antenna. This case is studied to distinguish and isolate the influence of the implant antenna on the system’s overall resonance.

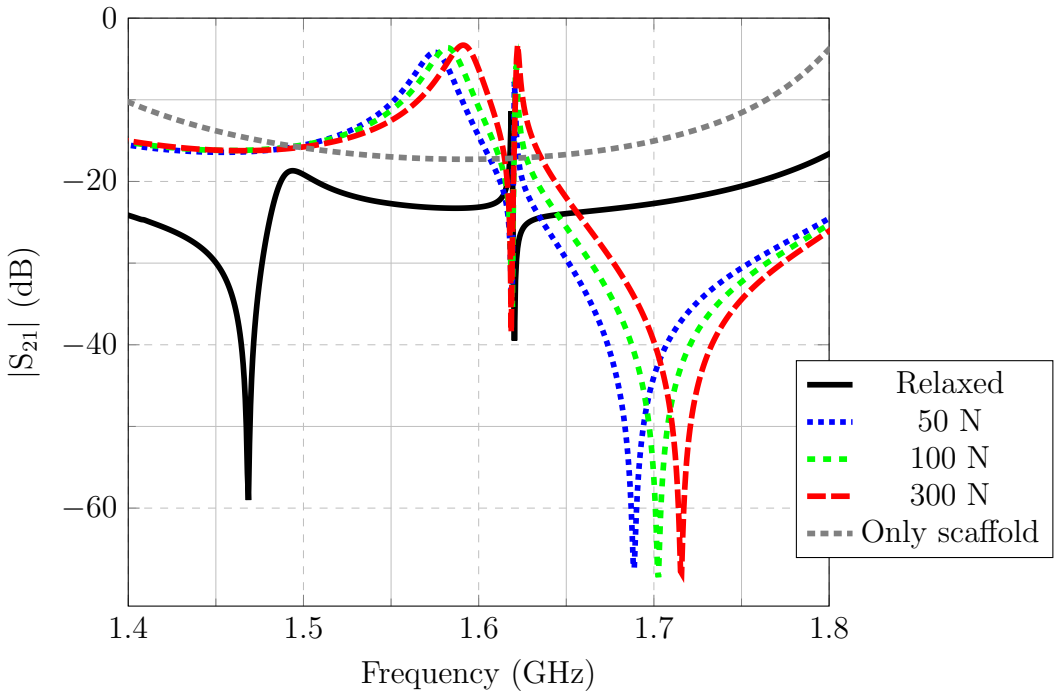

Figure 3.12. The transmission coefficient magnitude of the waveguide for different muscle contraction cases.

Examining the transmission coefficient versus frequency graph in Figure 3.12, it is observed that the loop antenna configuration of the implant antenna approximately resonates at 1.46 GHz. Once the tissue starts contracting and hypothetically applying 50 μN to the pillars, the loop antenna reconfigures to 3D split ring resonator. As a result of this reconfiguration, the resonance frequency shifts to 1.68 GHz. When the contraction increases to 100 μN and 300 μN, the resonance frequency shifts to 1.70 GHz and 1.72 GHz respectively, resulting in approximately 20 MHz difference in resonance frequency between the three contraction cases. The same resonance characteristics can be observed in the phase of the transmission coefficient as seen in Figure 3.13.

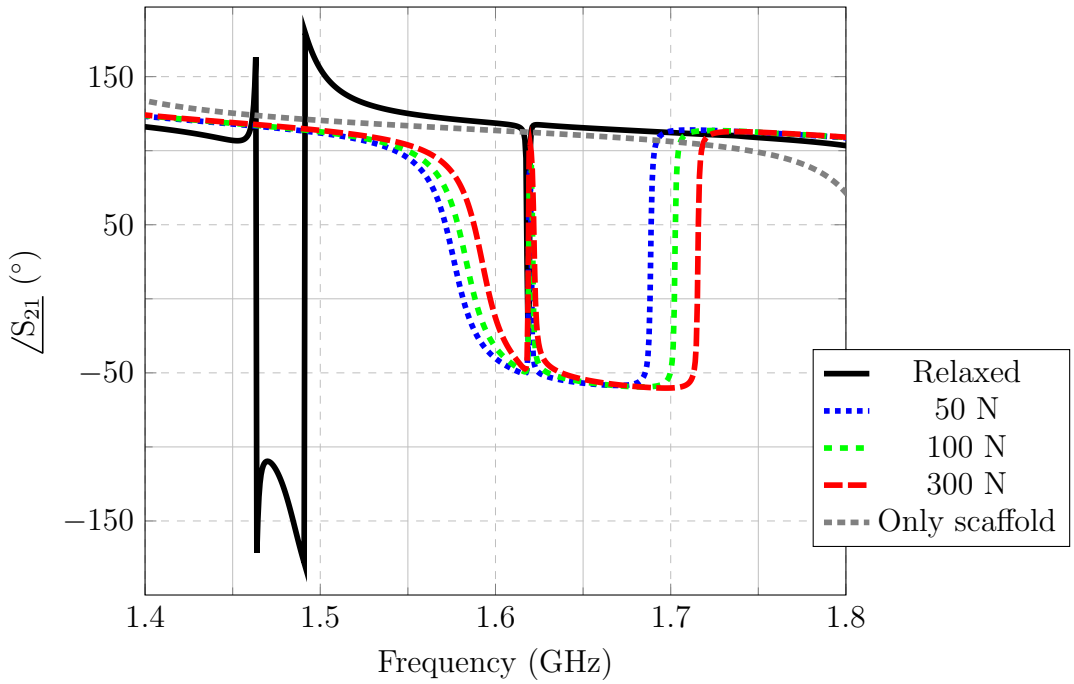

Figure 3.13. The transmission coefficient phase of the waveguide for different muscle contraction cases.

Also, the reconfiguration of the implant antenna is visible from the surface current density point of view, as shown in Figure 3.14.

In the light of the waveguide analysis, the implant antenna is printed on top of the 3D printed scaffold. The fabricated implant antenna prototype is shown in Figure 3.15. The printing process is manually conducted under a non-inverting microscope, by applying a conductive ink with thin paint brush. Adhetron EL-TECH 142 flexible silver paste is used as the conductive ink.

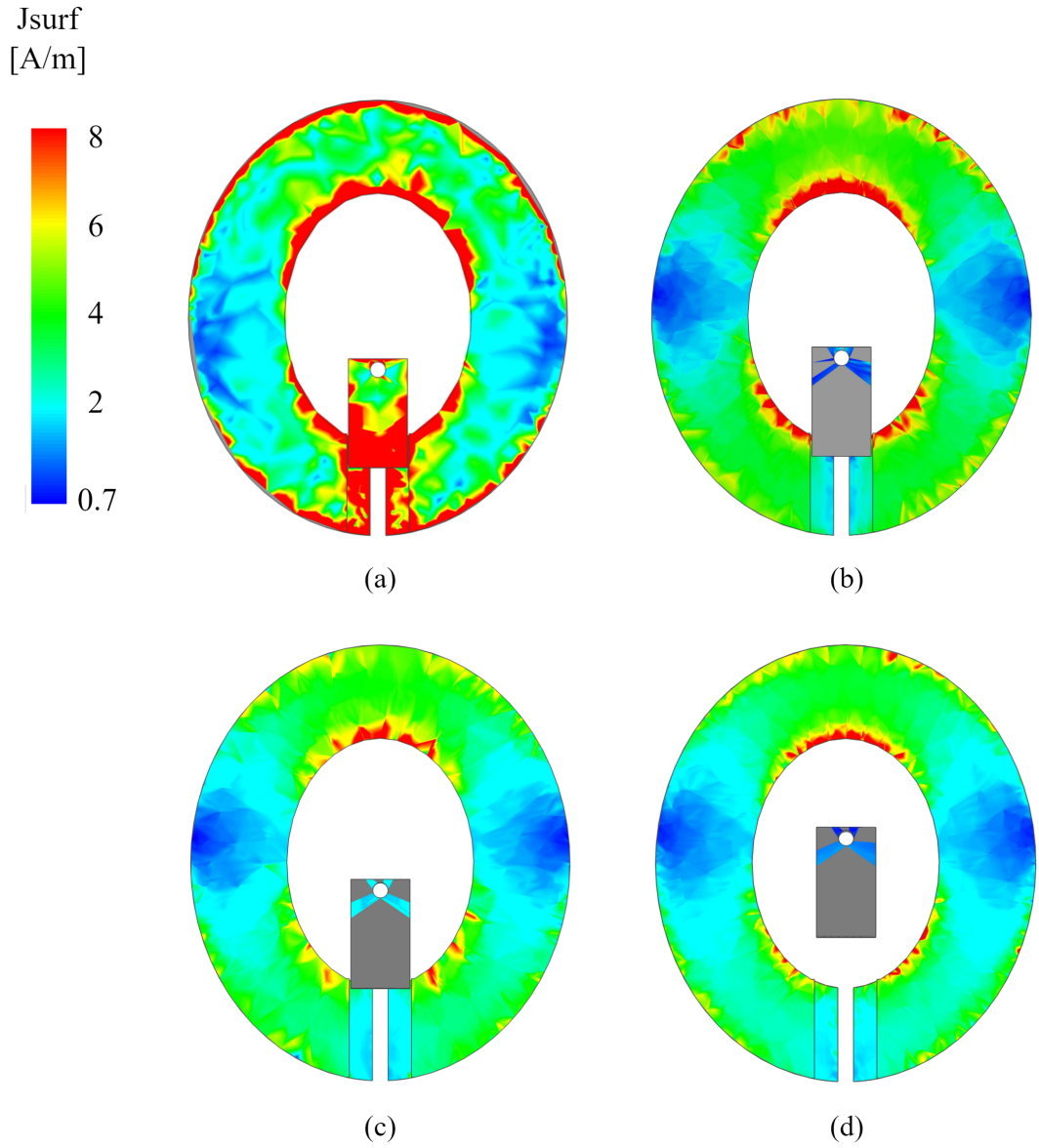

Figure 3.14. Surface current density for the (a) Relaxed case at 1.46 GHz. (b) 50μN at 1.68 GHz. (c) 100μN at 1.7 GHz. (d) 300μN case at 1.72 GHz.

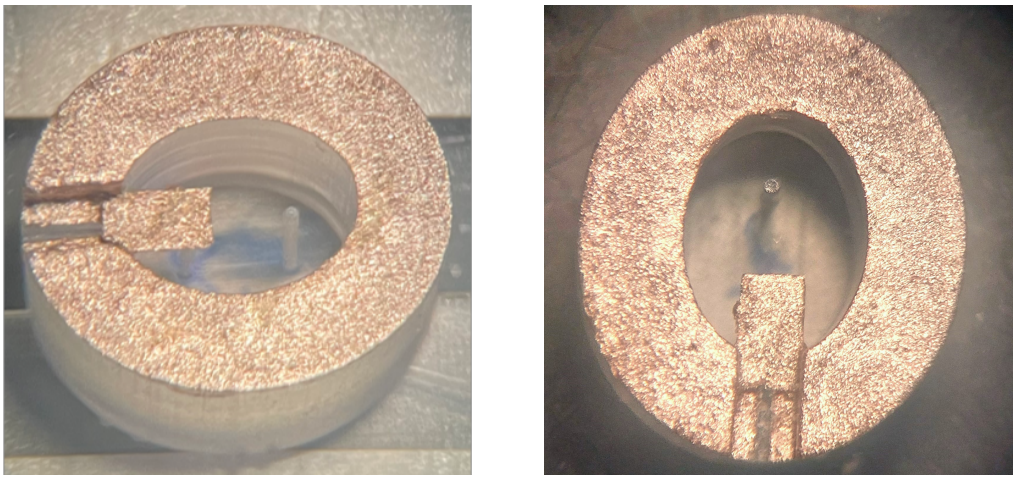

Figure 3.15. Fabricated implant antenna prototypes.

3.2. On-Body Reader Antenna

3.2.1. Design Considerations

On-body antennas are at the leading edge of the wearable and implantable technology revolution, allowing us to stay connected and seamlessly transfer data to the digital world. The design of the on-body antenna directly impacts a device's wireless connectivity, performance, and overall user experience. Therefore, on-body antenna design is crucial in the development of a on-body device and there are several points to consider when designing a on-body antenna. The first and foremost consideration here is the near-field effects of the human body on electromagnetic devices. Antennas are frequently placed on or close to the human body in wearable technologies in order to facilitate wireless communication between the implant device and other gadgets or networks. The human body is a lossy dielectric environment with high water content and on-body antennas experience loss and detuning effects from the human body when they are put close to or in direct contact with body. These influences may change the antenna's frequency response, decrease its radiation efficiency and distort its radiation pattern [74, 75]. Furthermore,the antenna of the implant device which the on-body antenna communicates may get detuned due to variations in orientation or due the

dynamism of the human body. Additionally, alterations in permittivity may occur as the composition of tissues changes from person to person.

A way to minimize these detuning effects is to choose an antenna with a wide-band operation. A wide bandwidth is a crucial feature for on-body antennas to ensure that the antenna can perform well in the presence of detuning effects generated by the human body. The antenna's wide bandwidth enables it to retain stable performance and dependable wireless communication and sensing capabilities.

Size compactness is also a key requirement for on-body antennas. Due to their close proximity to the human body, these antennas need to be small and lightweight. This allows for comfortable and unobtrusive integration into clothing or accessories, without hindering the wearer's mobility or comfort.

When it comes to choosing a suitable antenna type for on-body applications, it is essential to understand the interaction between antennas and the human body in order to develop efficient on-body communication systems. The recent studies highlight the advantages of using magnetic antennas in applications that require direct contact with the body [74, 76]. As reported in these studies, magnetic antennas have a distinct advantage in efficiently transmitting electromagnetic signals through the human body. The magnetic field generated by these antennas maintains its strength as it passes through the body, unlike electrical antennas. The reason behind this phenomenon is that human tissues do not experience magnetic losses. As a result, the high magnetic near fields are less likely to dissipate in the human body compared to electrical elements. Based on these insights, it is evident that the utilization of a magnetic slot antenna appears as a more promising choice for on-body applications.

3.2.2. Slot Antenna Basics

Slot antennas are a specific type of antennas that have a narrow and elongated aperture in a conductive surface, usually constructed from metal [77]. The slot is

typically created by cutting a metal plate and it is used as the radiating element for the antenna. The geometry of slot antennas is determined by various factors, such as the dimensions of the slot itself, including its length (L), width (W), and shape. The dimensions of the antenna have a direct impact on its operating frequency and radiation properties. A typical microstrip fed slot antenna model is shown in Figure 3.16.

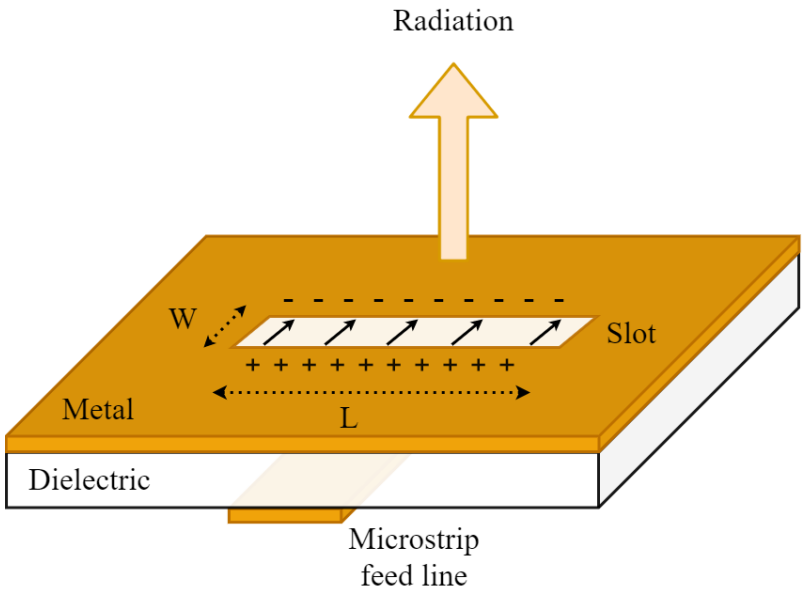

Figure 3.16. A microstrip fed slot antenna model.

The resonant frequency of the slot antenna is determined by the length of the slot, where longer slots correspond to lower frequencies and shorter slots correspond to higher frequencies. The width of the slot is an important factor in determining both the impedance and bandwidth of the antenna.

As outlined in the previous subsection, slot antennas are commonly recognized as magnetic antennas because their radiation mechanism is primarily associated with the magnetic field component. When an alternating current passes through a narrow slot, it creates a magnetic field that is oriented at a right angle to the slot's plane. The radiation of electromagnetic waves are associated to the magnetic field, which is why slot antennas are often referred to as magnetic antennas.

Slot antennas have a stronger magnetic field component and a comparatively weaker electric field component when compared to other types of antennas [77]. The dominance of their magnetic field adds to their efficient radiation capabilities, especially when they are close to non-zero conductivity surfaces like the human body. The human body does not experience magnetic losses primarily because it is made up of materials that are typically non-magnetic [74]. This implies that the body's tissues do not dissipate a significant amount of energy when exposed to magnetic fields. The reason why the human body does not experience magnetic losses is because it does not contain materials that possess significant magnetic properties. The behavior is further influenced by the non-complex and real nature of permeability. The fact that permeability is non-complex means that it does not exhibit significant frequency-dependent behavior or losses. The human body does not experience magnetic losses because it is made up of non-magnetic materials and its component tissues have real, permeability. Therefore, slot antennas are often the preferred choice for on-body applications and wireless communication systems in environments where the presence of human body can affect the performance of the antenna.

Up to this point, all the features of the traditional slot antenna align with the objectives of this project. However, slot antenna has one feature that is not suitable for the use case of this project which is its narrow bandwidth. Slot antennas are categorized as narrow-band antennas because to their unique geometry. Because their construction is a narrow, elongated opening in a metal sheet, the range of frequencies they can transmit or receive is naturally limited. The antenna's resonance frequency is directly related by the slot aperture's dimensions, which results in a limited operational bandwidth. These antennas work on the basis of resonance behavior. They have a single dominant resonance mode that limits the frequency response of the antenna to a specific range, which makes them useful for a restricted band of frequencies. Higher-order modes can allow many resonant modes, although they are typically associated with higher frequencies, which further reduces the bandwidth of the antenna. The operational bandwidth of slot antennas is expanded by researchers through different techniques like aperture tuning and novel feeding mechanisms. This enables slot an-

tennas to be more suitable for applications that need signal transmission across a large frequency range. Therefore, such operational bandwidth enhancements techniques for the slot antenna has been investigated for this project.

3.2.3. Optimized Model

To track the implant antenna reconfiguration realized by the engineered muscle, a cross-slot, dual-port on-body antenna based on [78] is designed at BOUNtenna research laboratory by my colleague A. Bilir. The antenna has two ports placed on the adjacent edges of the antenna substrate. These two ports feed the two fork strips that lay on the opposite sides on the antenna, perpendicular to each other. The cross slot is sandwiched between two perpendicular microstrip fork feeds. Each of these feeds excites the cross slot along one of its diagonals. As the diagonals are oriented orthogonally, the isolation between the ports is minimal. For the frequency range of operation, which is approximately from 900 MHz to 2.5 GHz, the coupling between the ports is less than -30 dB. The wide-band functionality is achieved through the utilization of wide slots and utilization of open-ended fork feeds [78]. Figure 3.17(a) shows the top view of the antenna, Figure 3.17(b) shows the side view of the antenna with the layers exposed.

The antenna's overall dimensions are 55 x 55 x 3.9 mm. The dimensions were set based on the through investigation of antenna parameters conducted in [78]. For miniaturization purposes, the antenna is designed with high-dielectric material of RO6010 ($\varepsilon_r = 10.2$) with a thickness of 1.91 mm. The antenna is feed with a microstripline which simply modeled in Figure 3.18. To match the standard 50 Ω transmission line, the dimensions of the microstrip feed line is calculated using the following microstrip line impedance formula [79]

$$\varepsilon_{eff} = \frac{\varepsilon_r + 1}{2} + \frac{\varepsilon_r + 1}{2} + \left[\frac{1}{\sqrt{1 + 12\left(\frac{W}{H}\right)}} + 0.04\left(1 - \left(\frac{W}{H}\right)\right)^2 \right] \tag{3.3}$$

$$Z_0 = \frac{60}{\sqrt{\varepsilon_{eff}}} \ln\left(8\left(\frac{H}{W}\right) + 0.25\left(\frac{W}{H}\right)\right), \tag{3.4}$$

where ε_{eff}, ε_r, W, H and Z_0 are effective permittivity, relative permittivity, width of the feed line, height of dielectric substrate and the characteristics impedance of the transmission line, respectively.

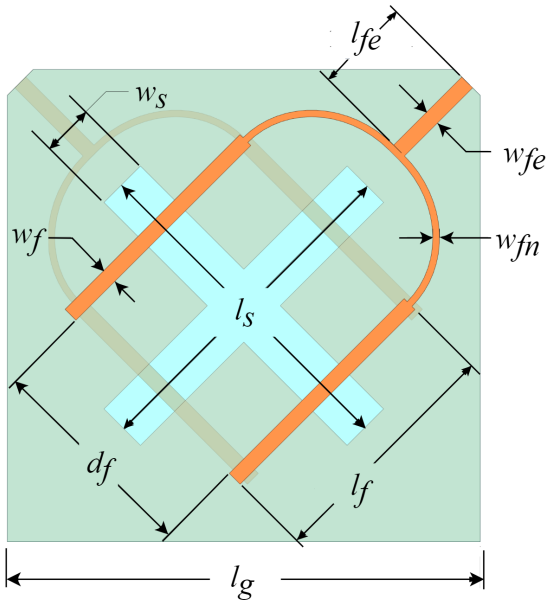

(a)

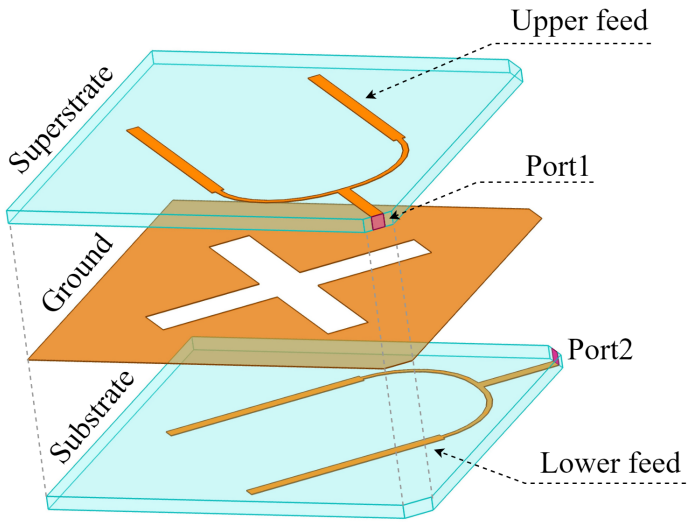

(b)

Figure 3.17. Optimized antenna model (a) top view. (b) side view with the layers exposed.

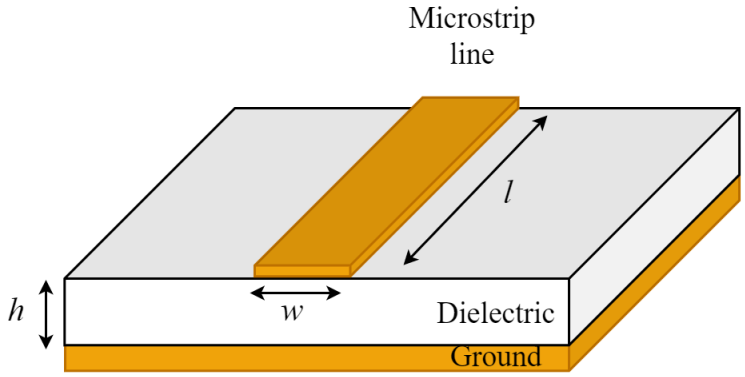

Figure 3.18. Microstrip feed line model.

The optimized dimensions of the antenna are given in Table 3.4. For tissues with a relative permittivity greater than 30, the antenna works satisfactorily within the necessary frequency range [78]. This is due to the radiator's placement between the microstrip feeds and a low-loss dielectric substrate, which makes the antenna detuning robust. Optimized antenna's simulated $|S_{11}|$ and $|S_{22}|$ magnitudes are shown in Figure 3.19. The antenna reliably operates approximately between 0.9 GHz and 2.5 GHz. Figure 3.20 shows the optimized antenna's $|S_{21}|$ magnitude. For the operating frequency the coupling between the two ports of the antenna is lower than -45 dB.

Table 3.4. The dimensions of the optimized antenna.

Parameters	**Optimized values (mm)**
l_s	40
w_s	4
l_f	27.75
d_f	25.2
w_f	1.8
w_{fn}	0.78
w_{fe}	1.8
l_{fe}	11.2

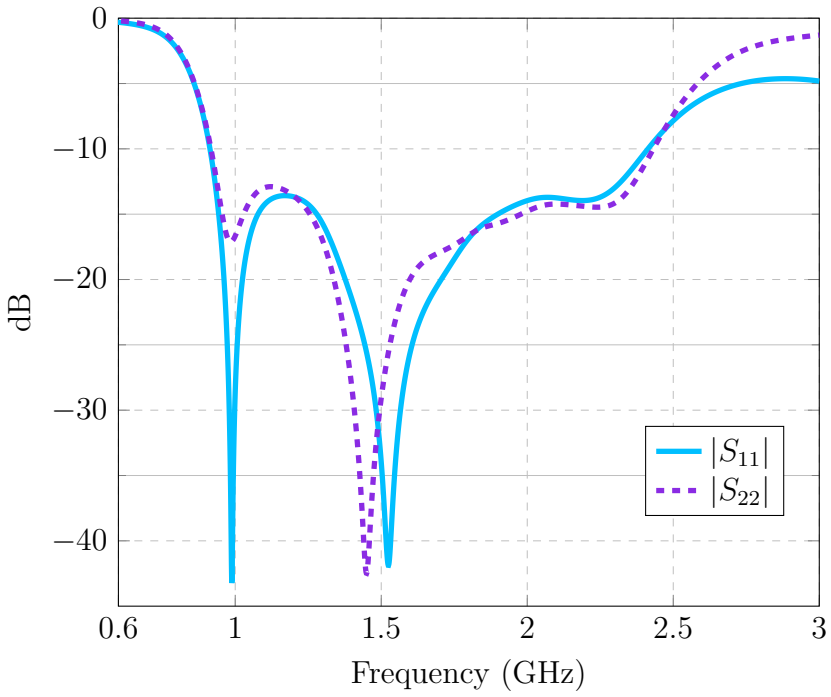

Figure 3.19. dB versus frequency graph for the $|S_{11}|$ and $|S_{22}|$ of the optimized antenna.

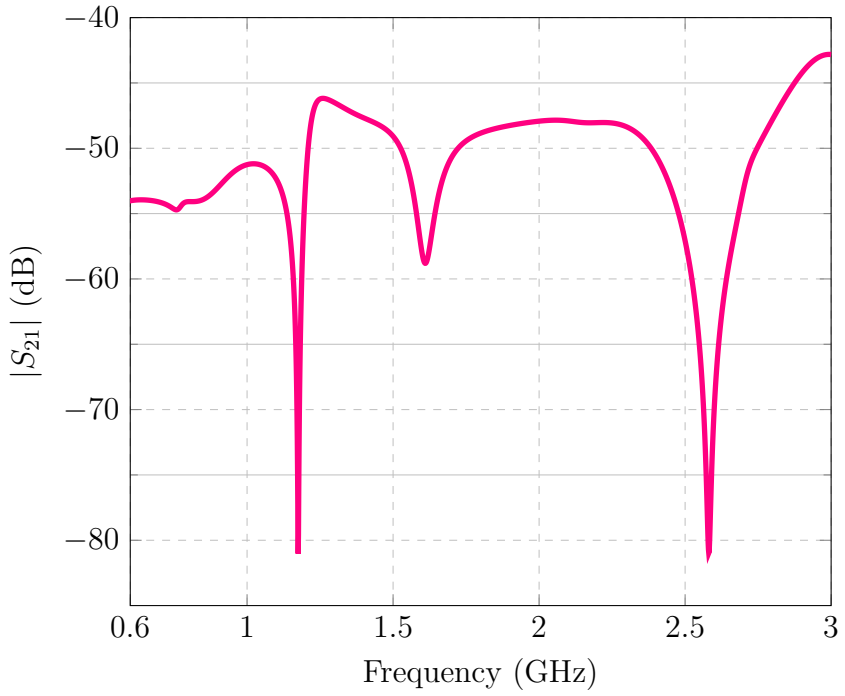

Figure 3.20. $|S_{21}|$ versus frequency graph of the optimized antenna.

The 3D radiation patterns of the optimized antenna across four different frequencies, namely 0.91 GHz, 0.98 GHz, 1.52 GHz and 2.42 GHz, are shown in Figure 3.21. The 2D radiation patterns at the same frequencies with $\phi = 0°$ and $\theta = 90°$ angles, are shown in Figure 3.22.

In the light of these results, the optimized antenna was fabricated in LPKF S103 printed circuit board (PCB) development machine with RO6010 dielectric substrate with a thickness of 1.91 mm as shown in Figure 3.23(a) and 3.23(b). The fabricated antenna's performance will be given in Section 5 on the measurement setup.

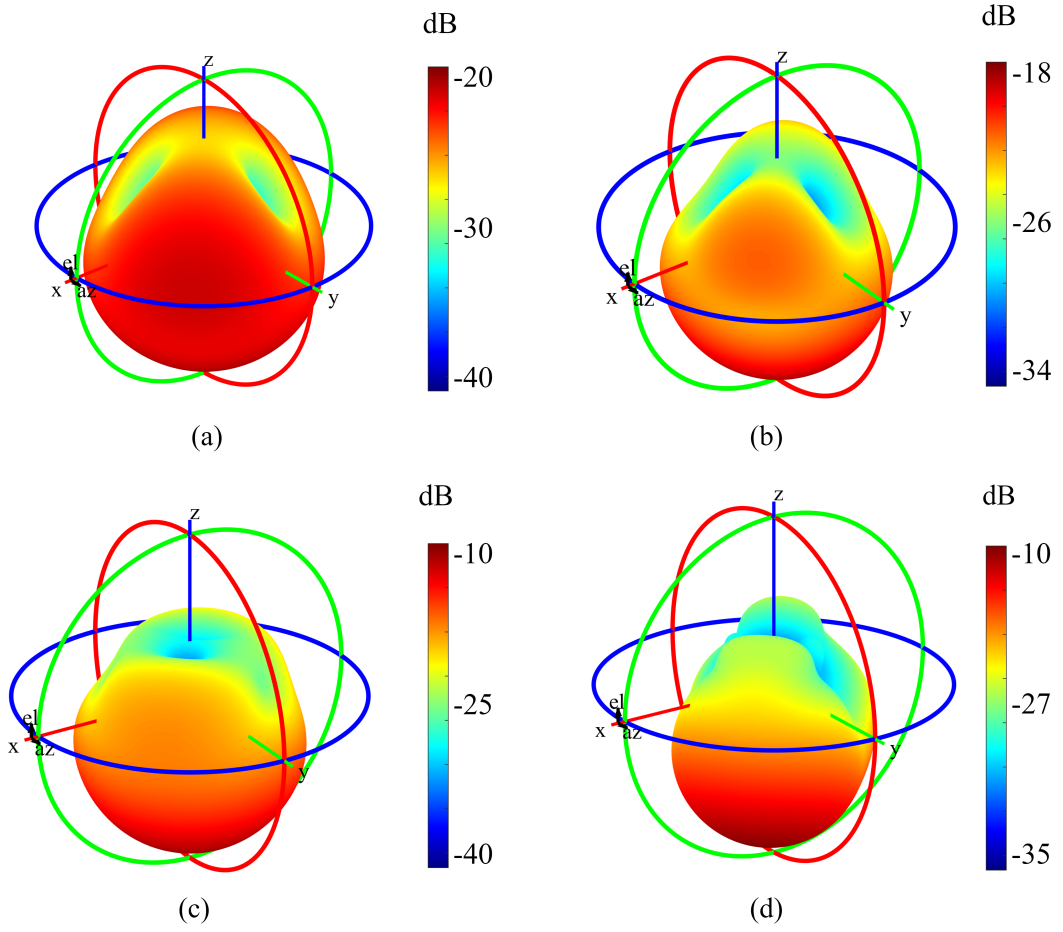

Figure 3.21. 3D Radiation pattern of the optimized antenna at (a) 0.91 GHz (b) 0.98 GHz (c) 1.52 GHz (d) 2.42 GHz.

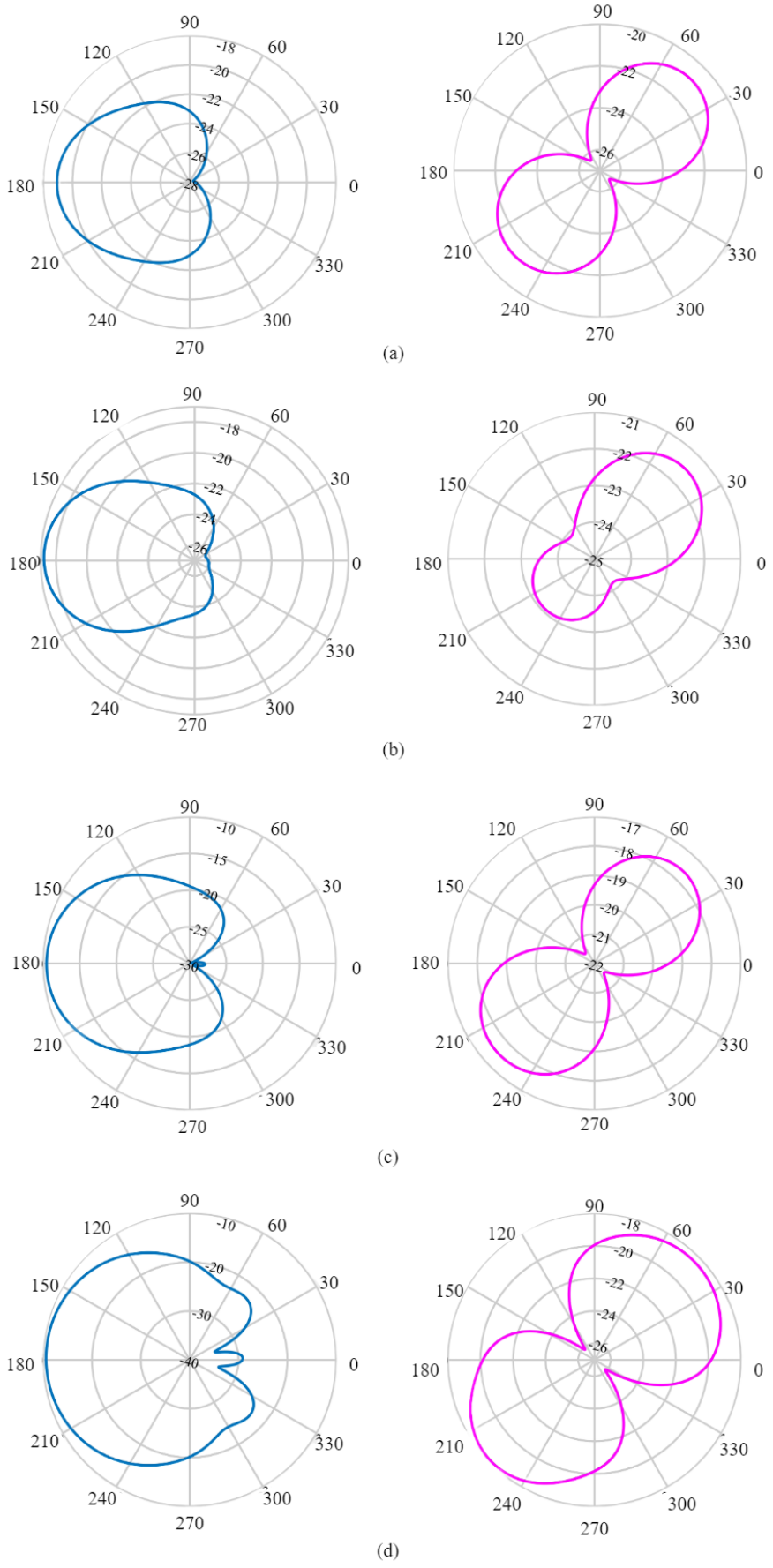

Figure 3.22. 2D radiation pattern of the optimized antenna at (Blue= $\phi = 0°$, Pink= $\theta = 90°$) (a) 0.91 GHz (b) 0.98 GHz (c) 1.52 GHz (d) 2.42 GHz.

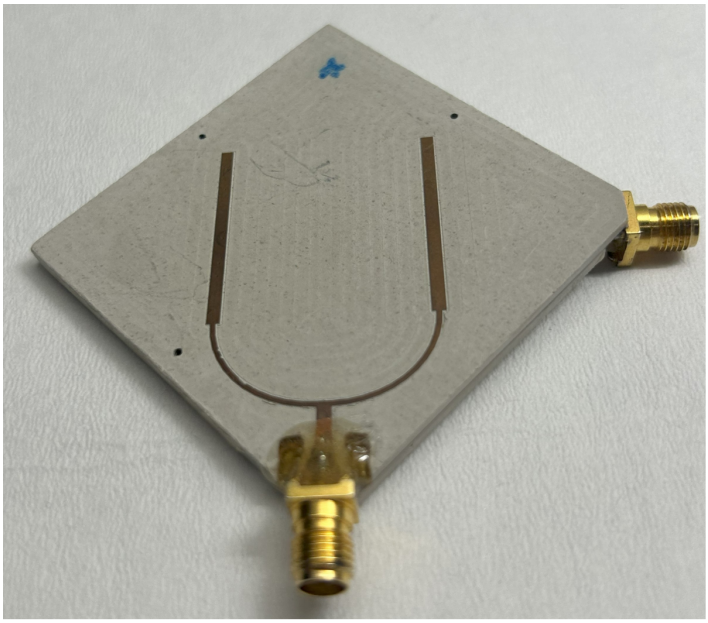

(a)

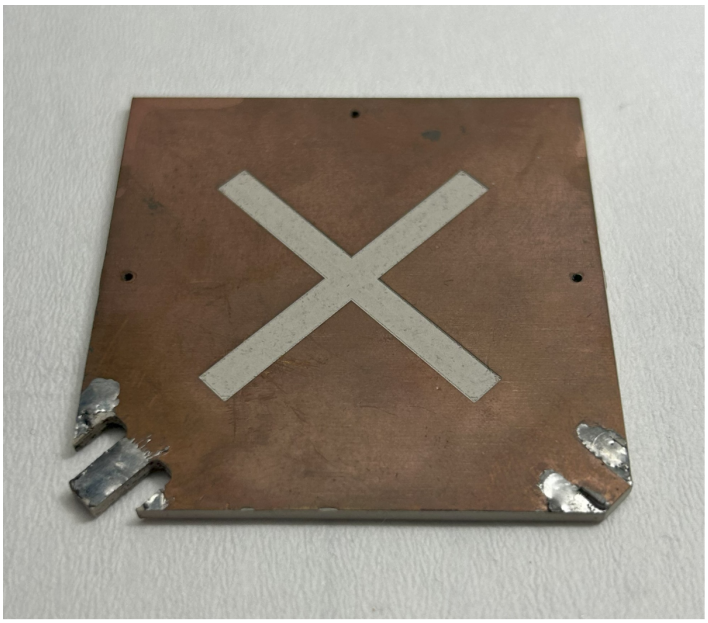

(b)

Figure 3.23. Fabricated optimized antenna (a) top view. (b) cross-slot layer.

4. NUMERICAL MODELS

4.1. Mechanical Models and Simulation Results

Mechanical simulations are used in the field of bio-hybrid device design to investigate the deflections of the artificial scaffolds when subjected to contractile forces generated by skeletal muscle tissue. These simulations take into account the properties of commercial Formlabs IBT resin, a polymer-based elastic resin known for its impressive tensile strength and elasticity modulus, exceeding 5 MPa and 16 MPa, respectively [80].

Previous research has indicated that 3D-engineered skeletal muscle tissues can produce contraction forces ranging between 10 µN and 2.5 mN [81]. In the given simulations, 300 µN are applied in both positive and negative x directions to the pillars. Exerted forces result in maximum deflections of the conducting bridge at 1889 µm and 965.9 µm in the negative x and z directions, as shown in Figure 4.1. Within these illustrations, part of the flexible scaffold's outer walls has been intentionally omitted to enhance clarity.

The mechanical analysis further examines the gradual variations in tissue contraction and bridge deflection by considering intermediate force values of 50 µN and 100 µN. At 50 µN of force, the bridge's maximum deflection reaches 245 µm and 121 µm in the negative x and z directions, while at 100 µN, it extends to 533 µm and 271 µm in the same directions. Subsequent electromagnetic simulations conducted in ANSYS HFSS are built on top of the outcome of these mechanical simulations which will be detailed in the next section.

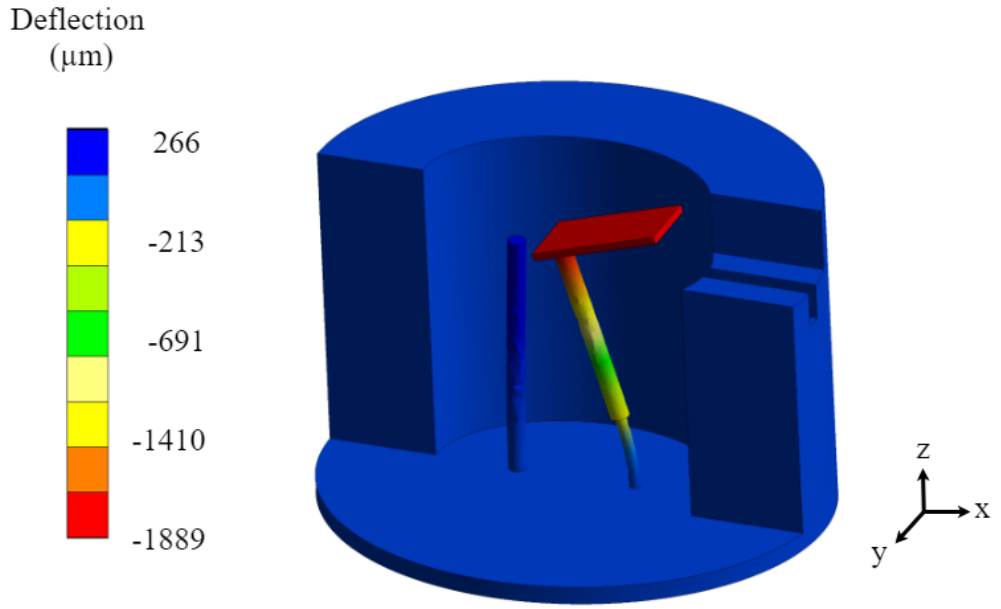

(a)

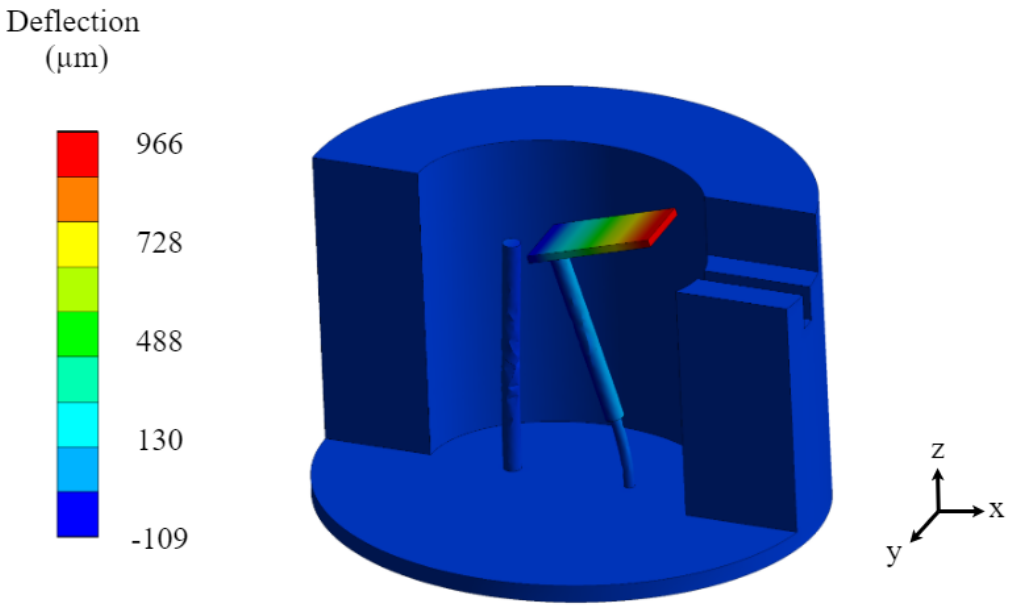

(b)

Figure 4.1. Mechanical deflection analysis of the flexible scaffold. (a) Deflection in x-direction. (b) Deflection in z-direction.

4.2. Electromagnetic Model and Simulation Results

The electromagnetic model's isometric view that is shown in Figure 4.2 is a visual representation of the sensing system and its various components. The simulation process involves replicating muscle contraction in a detailed numerical phantom. The numerical phantom consists of two separate layers: the human muscular tissue layer and human interstitial fluid layer. Each layer plays a role in the electromagnetic behavior that is being analyzed. The bio-hybrid implant is positioned in the interstitial fluid layer and the surrounding environment are covered with human muscle tissue layer. This configuration allows for a targeted study of how it interacts with the surrounding biological environment that is the human body. The simulation environment aims to replicate a real-world scenario where the implant is deployed inside the human body. It takes into account the complex interaction between human muscle tissue and interstitial fluid.

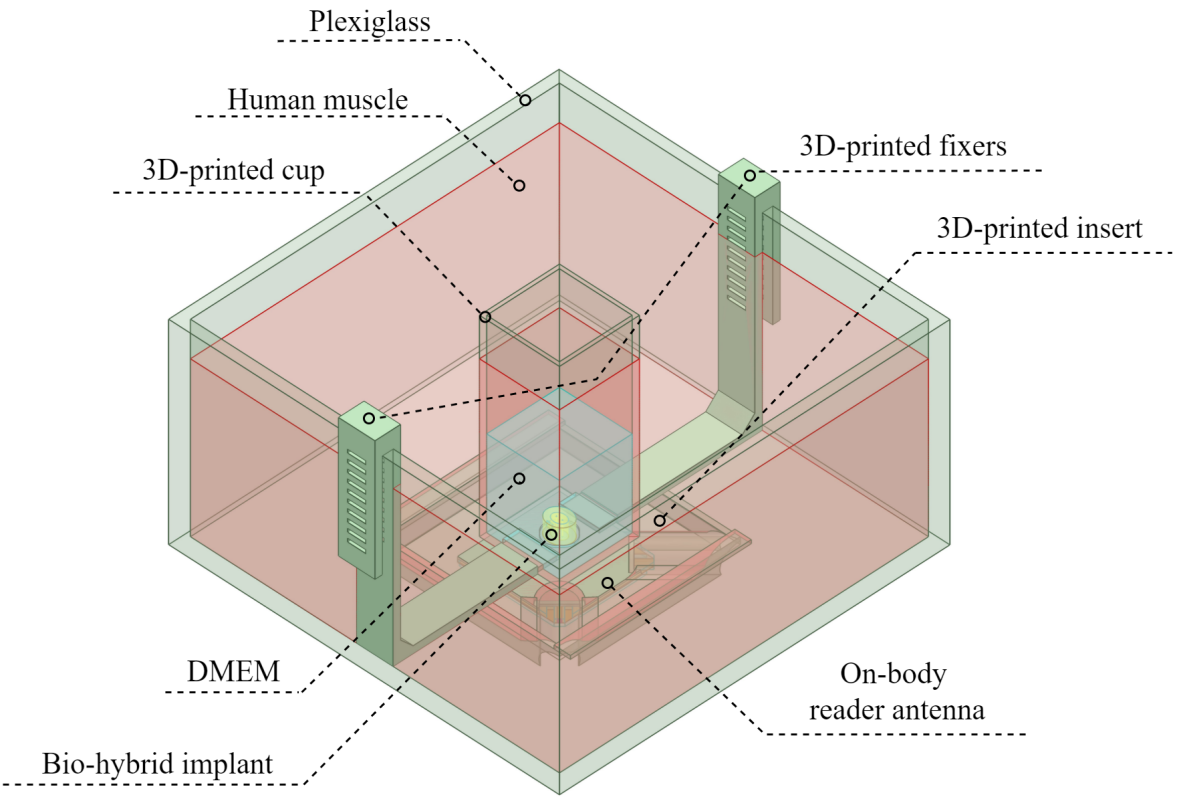

Figure 4.2. Isometric view of the numerical electromagnetic simulation model.

The system is designed to simulate the integration of the implant within the human body. In the simulation setup the ANSYS HFSS human muscle model is used to represent human muscle tissue layer, while the DMEM serum effectively represents the interstitial fluid as a nutritionally rich medium. Choosing DMEM as a substitute for interstitial fluid is a sensible decision for this project, given its similarity in terms of nutritional composition and ion characteristics to the actual interstitial fluid. In addition, DMEM is an optimal nutrient medium that supports the nourishment and vitality of skeletal tissue and cells, thereby ensuring the accuracy of the simulation setup.

The electromagnetic simulation setup consists of a sturdy plexiglass container with dimensions of 20 cm $\times$ 20 cm $\times$ 12 cm. Inside the container, there is a 3D-printed square prism cup measuring 4 cm $\times$ 4 cm $\times$ 10 cm, which is positioned at the center of the plexiglass container. The precise alignment of the cup is made possible by integrating 3D-printed fixers that control the height and the position. These fixers ensure that the cup is securely held at a specific depth of 90 mm within the plexiglass container. The 3D-printed cup is filled with DMEM. The space between the plexiglass container and the 3D-printed cup is filled with a human muscle phantom, which accurately mimics the characteristics of real muscle tissue. The bio-hybrid implant is placed at the bottom of the 3D-printed cup, exactly 10 mm away from the on-body reader antenna. The top and bottom view of the electromagnetic setup model is shown in Figure 4.3(a) and Figure 4.3(b), respectively.

The on-body antenna's performance when located on the electromagnetic simulation setup is shown in Figure 4.4. The antenna continues to reliably operate between 0.9 GHz and 2.5 GHz when positioned on the 3D printed insert of the electromagnetic simulation setup.

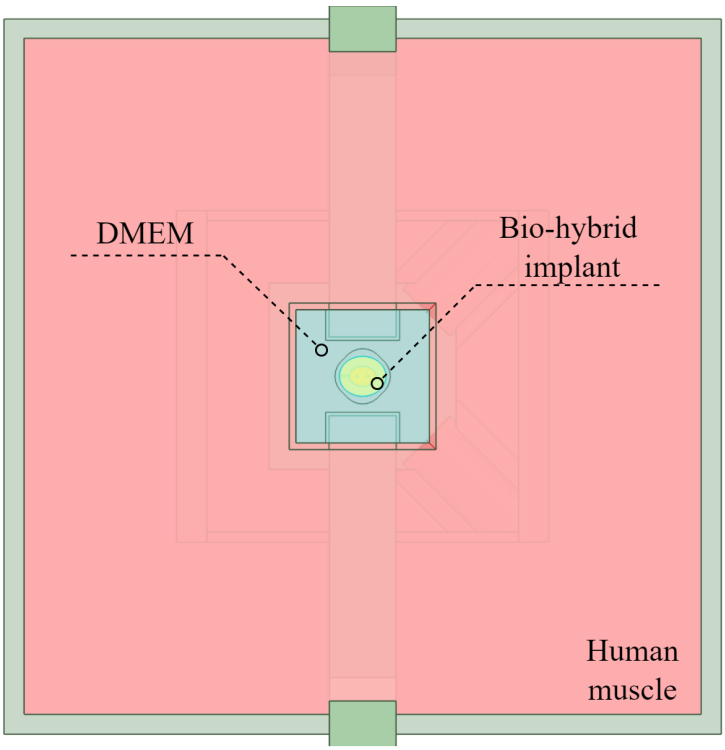

(a)

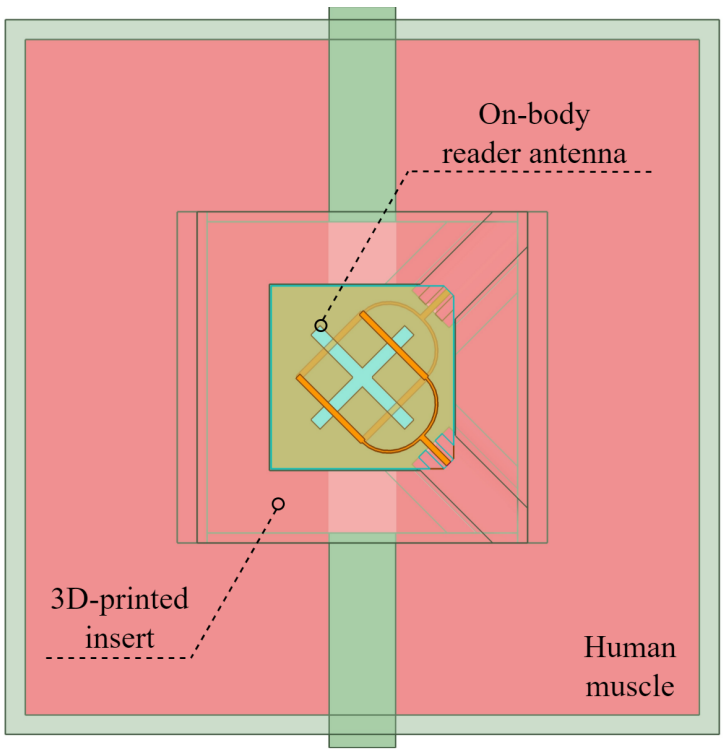

(b)

Figure 4.3. Numerical electromagnetic simulation model (a) top view. (b) bottom view.

For the most accurate representation of the gradual muscle contraction and the implant antenna reconfiguration, the outputs of the mechanical deflection simulations were used in the electromagnetic simulations. As outlined in the Section 4.1, the mechanical simulations were conducted with three hypothetical contraction forces of the skeletal tissue, namely, 50 μN, 100 μN and 300 μN. Gradual deflection models of the bio-hybrid implant are shown in Figure 4.5. These models are directly integrated with the electromagnetic simulations.

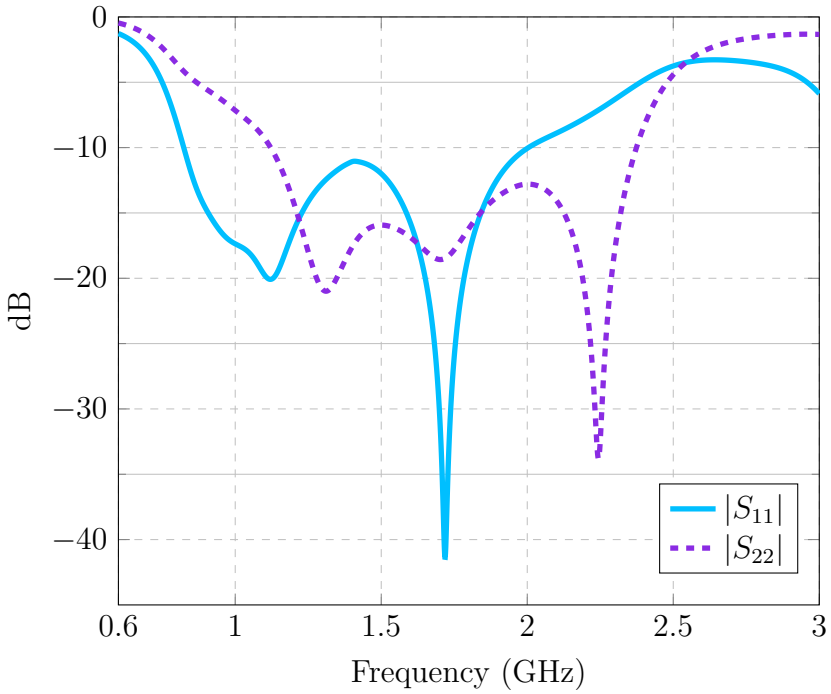

Figure 4.4. dB versus frequency graph for $|S_{11}|$ and $|S_{22}|$ of the optimized antenna located on the electromagnetic simulation setup.

Examining the simulation results in Figure 4.6, it is observed that the transmission coefficient between the ports of the on-body antenna changes as the implant antenna is reconfigured by the skeletal tissue contraction. The degree of deflection for 50 µN, 100 µN, 300 µN as well as the reconfiguration can be tracked. In relaxed case, $|S_{21}|$ of the on-body antenna has a distinct dip at 1.48 GHz. When the hypothetical contraction forces subsequently increase to 50 µN, 100 µN and 300 µN, the dip shifts to 1.57 GHz, 1.59 GHz and 1.62 GHz, respectively, indicating the resonance reconfiguration of the implant antenna . The reconfiguration of the implant antenna can also

be observed in the phase of $|S_{21}|$ plot as given in Figure 4.7. The electromagnetic setup simulation results are parallel with the results of the waveguide simulations that were detailed in Section 3.1.3. Figure 4.8 shows the surface current densities for the four implant antenna cases at the specific resonance frequencies they resonate. Reconfiguration of the implant antenna is also visible in the surface current densities for the different cases.

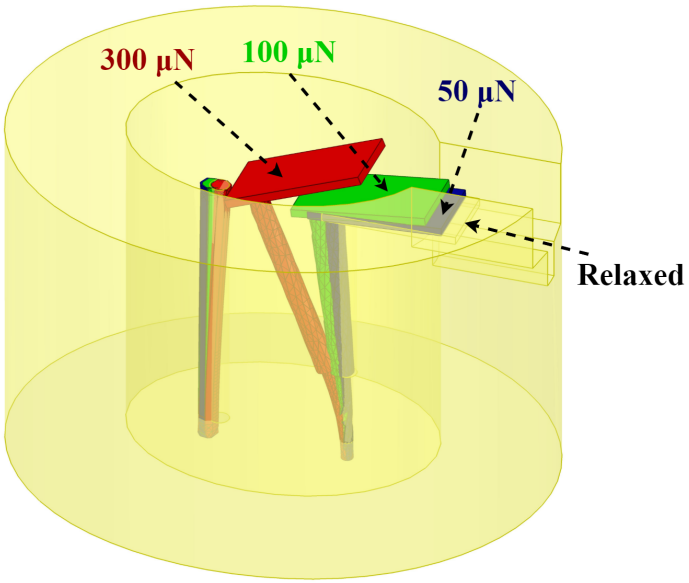

Figure 4.5. Gradual deflection of the bio-hybrid implant against hypothetical contraction forces.

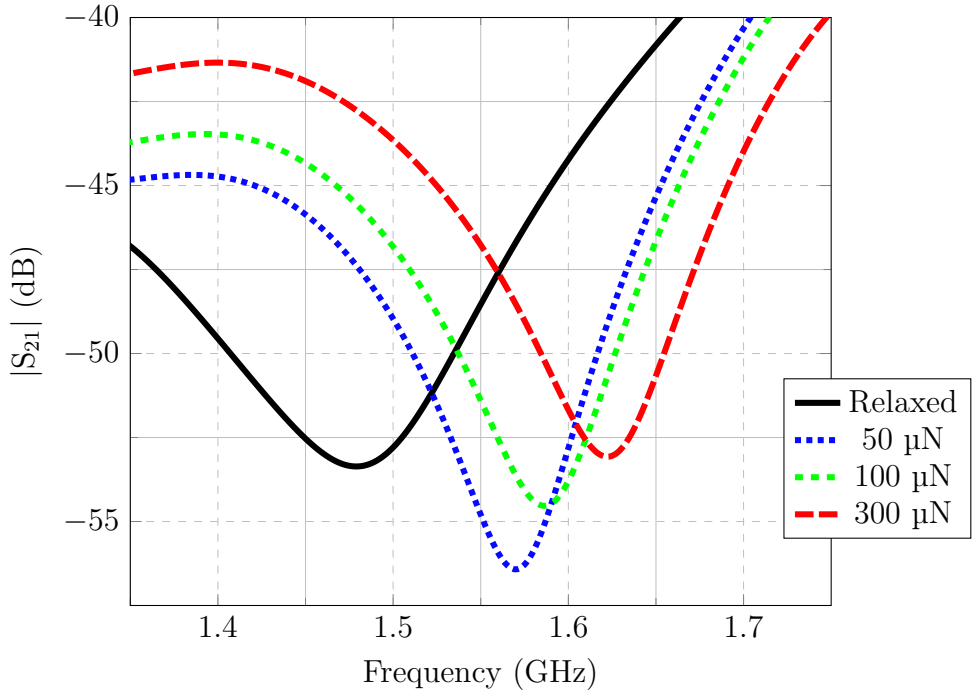

Figure 4.6. Simulation results for the change in $|S_{21}|$ magnitude against the gradual contraction of the tissue.

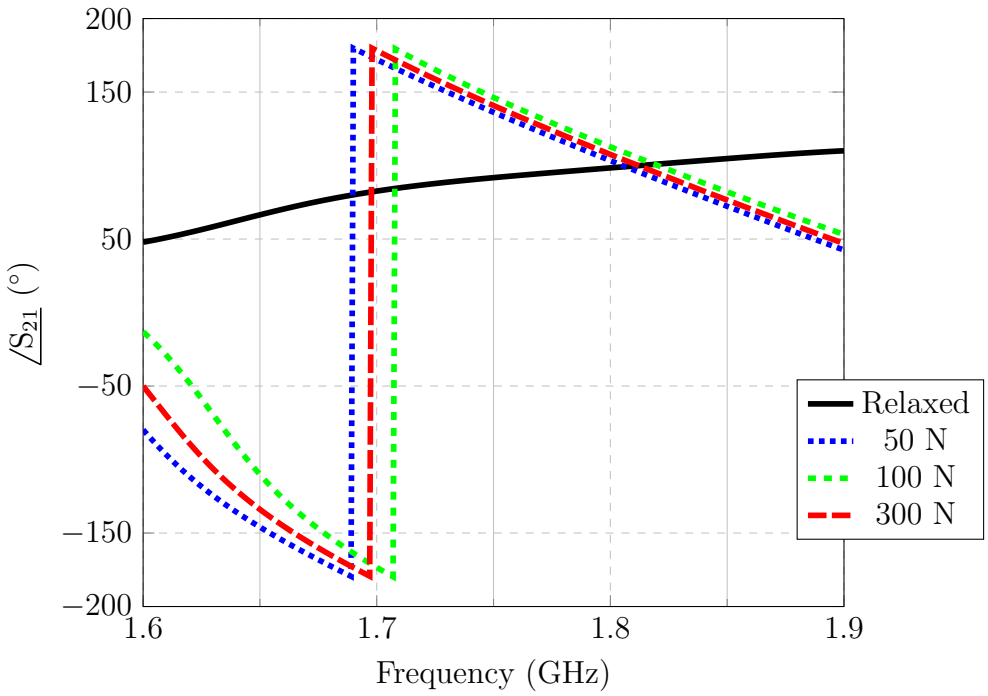

Figure 4.7. Simulation results for the change in $|S_{21}|$ phase against the gradual contraction of the tissue.

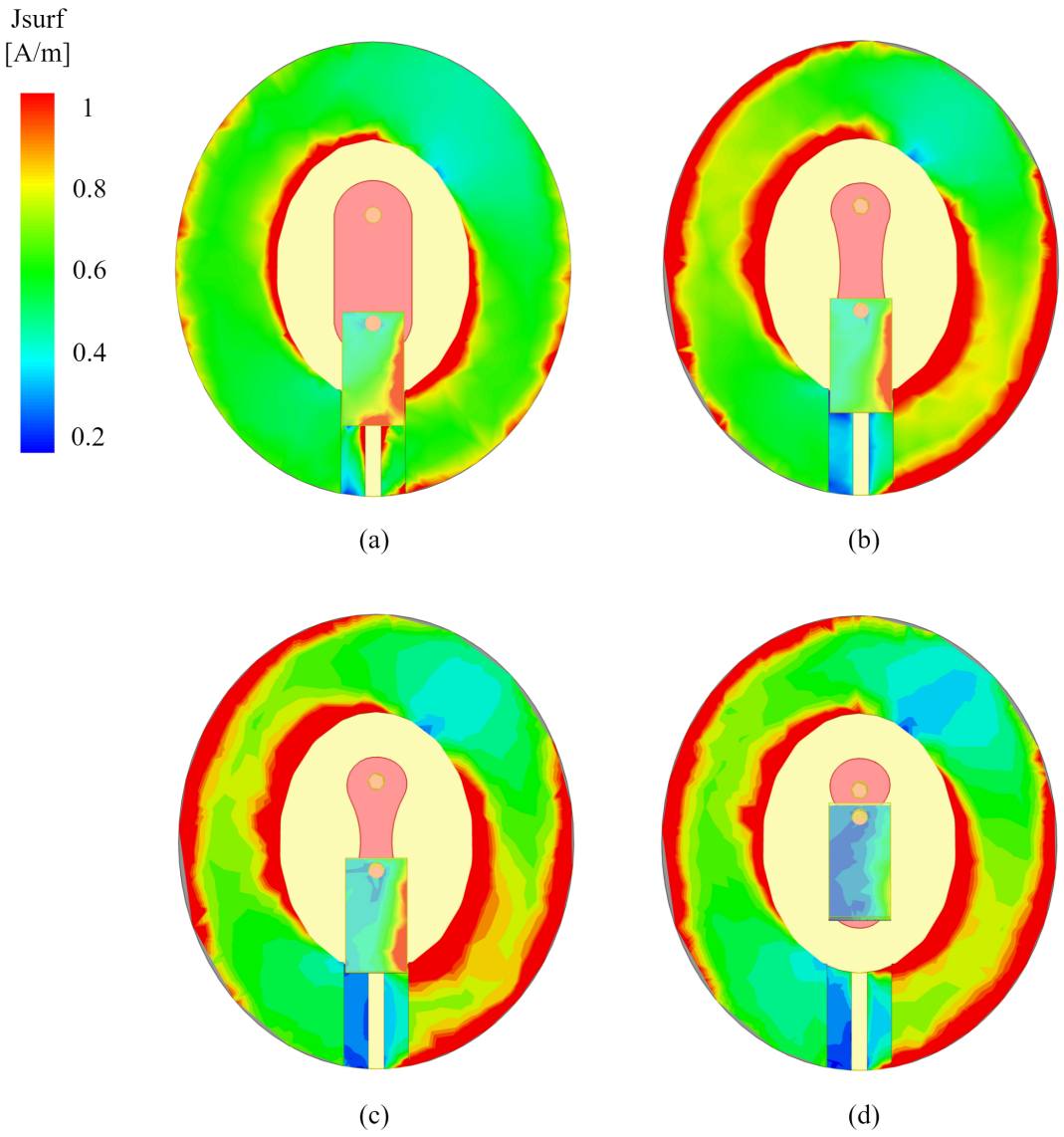

Figure 4.8. Surface current density for the (a) Relaxed case at 1.48 GHz (b) 50μN case at 1.57 GHz (c) 100μN at 1.59 GHz (d) 300μN case at 1.62 GHz.

5. MEASUREMENTS AND RESULTS

5.1. Phantom Development

Human tissue-mimicking electromagnetic phantoms refer to materials or structures specifically created to replicate the electrical and electromagnetic characteristics of human tissues [82]. They provide an accurate representation of how electromagnetic waves interact with the human body. Phantoms are utilized by researchers and engineers to effectively test and validate the performance of various devices, including antennas and imaging equipment. This is achieved by creating a controlled and consistent environment for conducting experiments.

Table 5.1. The ingredients used for the physical phantoms per unit volume.

Ingredient	**ANSYS Human Muscle**	**DMEM**
Distilled Water	100 mL	100 mL
Salt	0.2 g	0.8 g
Granulated sugar	60 g	-
Gelatin	9 g	-
Sodium azide	0.3 g	-
Food coloring gel	40 drops	-

The measurements for the proposed sensing system were carried out inside the fabricated tissue-mimicking phantoms that were used in the electromagnetic analysis. The human muscle tissue-mimicking phantom for ANSYS human muscle model was fabricated using water, granulated sugar, gelatin, sodium azide, and food coloring gel. The recommended ingredient proportions for the human muscle tissue-mimicking

phantom are given in Table 5.1 and the instructions to fabricate this phantom with are given are as follows:

(i) In a beaker, combine distilled water and granulated sugar and salt. Heat the mixture on a magnetic hot plate stirrer, stirring continuously until the granulated sugar dissolves completely. While granulated sugar is used to adjust the permittivity of the mixture, salt is used to adjust the conductivity.

(ii) Add the recommended amount of gelatin in small batches to avoid clumping in the mixture.

(iii) While the gelatin dissolves in the mixture, increase the heat to help dissolve faster and more smoothly. While the gelatin is dissolving and the heat is increasing, cover the beaker with plastic wrap to avoid excessive vaporization of water.

(iv) Once gelatin is dissolved and the the mixture appears homogeneous, add sodium azide and the food color. Sodium azide prolonges the lifetime of the phantom and the phantoms that contain sodium azide lasts longer without any bacterial molding. The food color is used to give the phantom a human tissue-like appearance and it is optional.

(v) Turn off the heat and constantly stir the mixture until it cools down to approximately 40°C. Once it cools down to 40°C, carefully pour inside the experiment setup and leave it overnight to solidify. Store the phantom in a cool, dry place to maintain its consistency and properties.

The phantom for DMEM was fabricated by mixing distilled water and salt in the proportion recommended in Table 5.1.

In Figure 5.2, dielectric properties of the fabricated human muscle tissue phantom and the ANSYS human tissue numeric model is compared. The maximum deviation of the permittivity and the conductivity of the human muscle phantom is 4.62% and 27.9%, respectively, within the band of interest. The same comparison is done for the DMEM phantoms in Figure 5.3. The maximum deviation of the permittivity and the conductivity of the DMEM phantom is 4.13% and 7.91%, respectively.

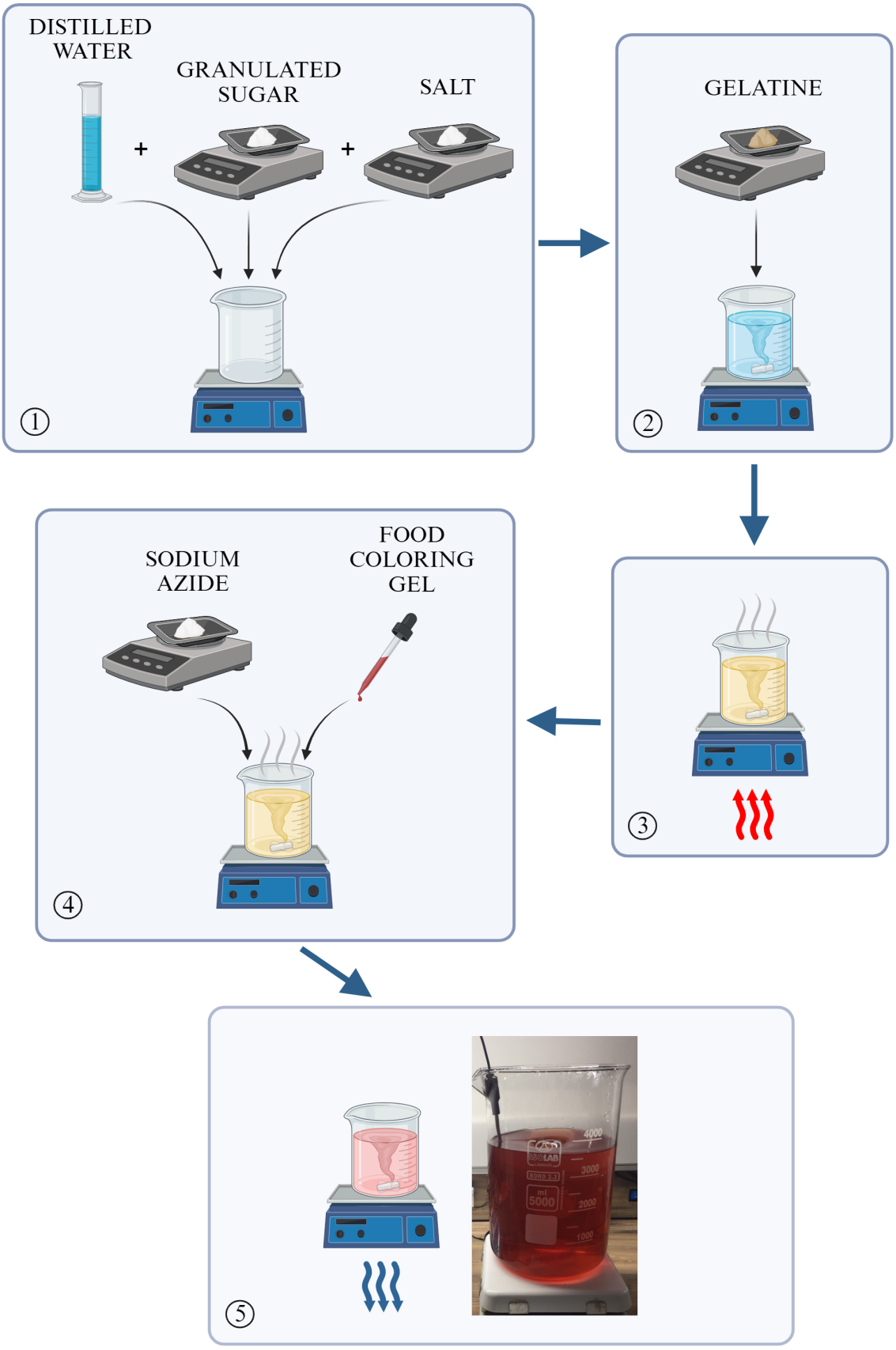

Figure 5.1. Human muscle tissue phantom fabrication steps.

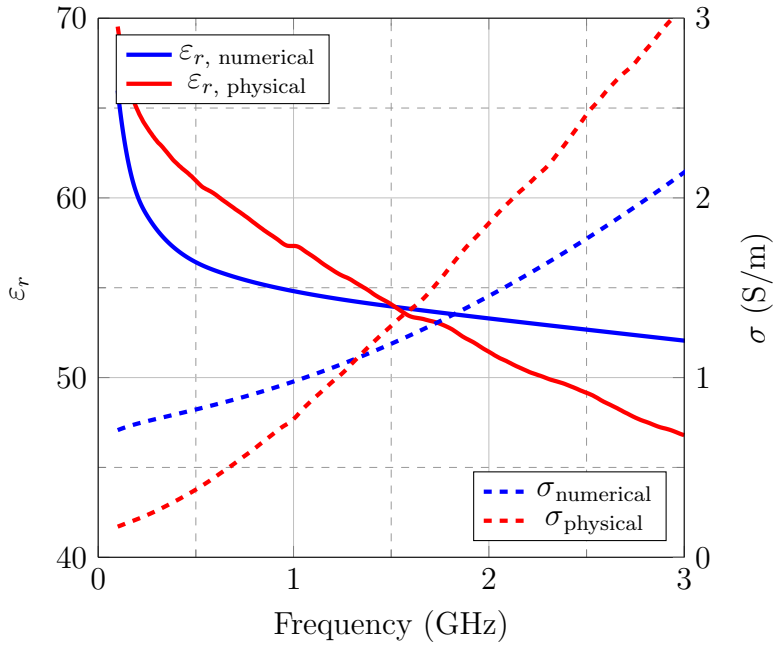

Figure 5.2. ε_r and σ of the numerical and physical human muscle tissue phantoms versus frequency.

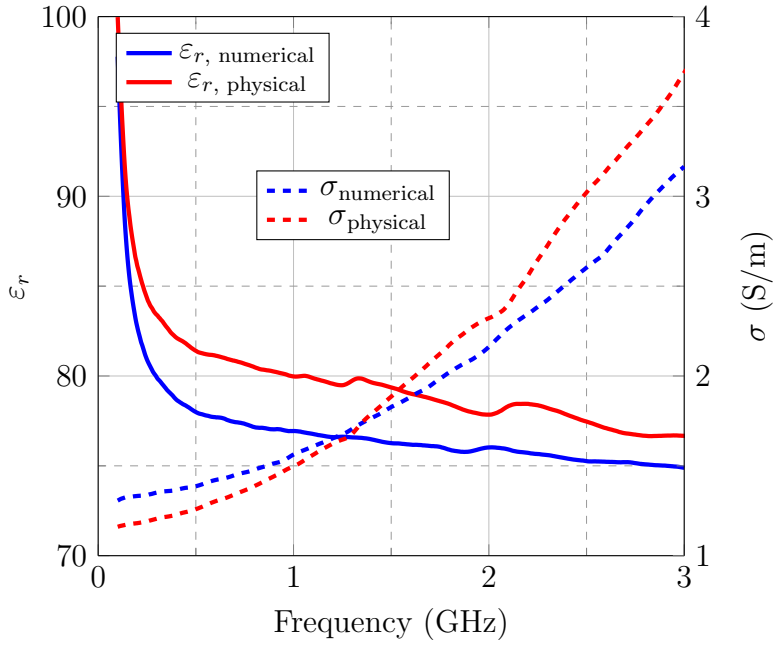

Figure 5.3. ε_r and σ of the numerical and physical DMEM phantoms versus frequency.

5.2. Measurement Setup and Results

The measurement setup is fabricated as a replica of the numerical electromagnetic simulation setup that is detailed in Section 4.2 to validate the electromagnetic simulations. While building the setup, the custom built plexiglass container was purchased from a vendor and the height-controlling fixers, the insert and the cup was 3D printed with Anycubic M3 Max printer using Anycubic clear resin at the BOUNTENNA laboratory. The isometric view of the measurement setup is shown in Figure 5.4. The top and the bottom views are shown in Figure 5.5(a) and Figure 5.5(b), respectively.

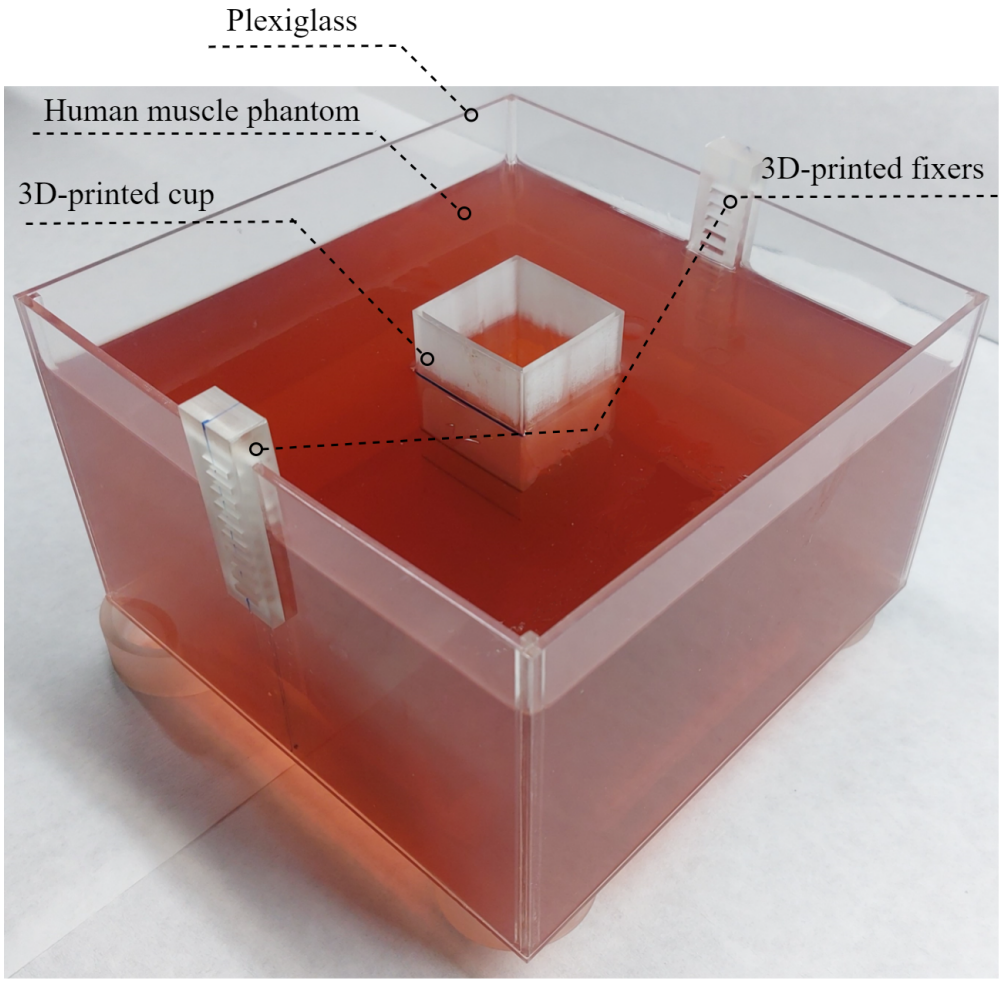

Figure 5.4. Isometric view of the measurement setup.

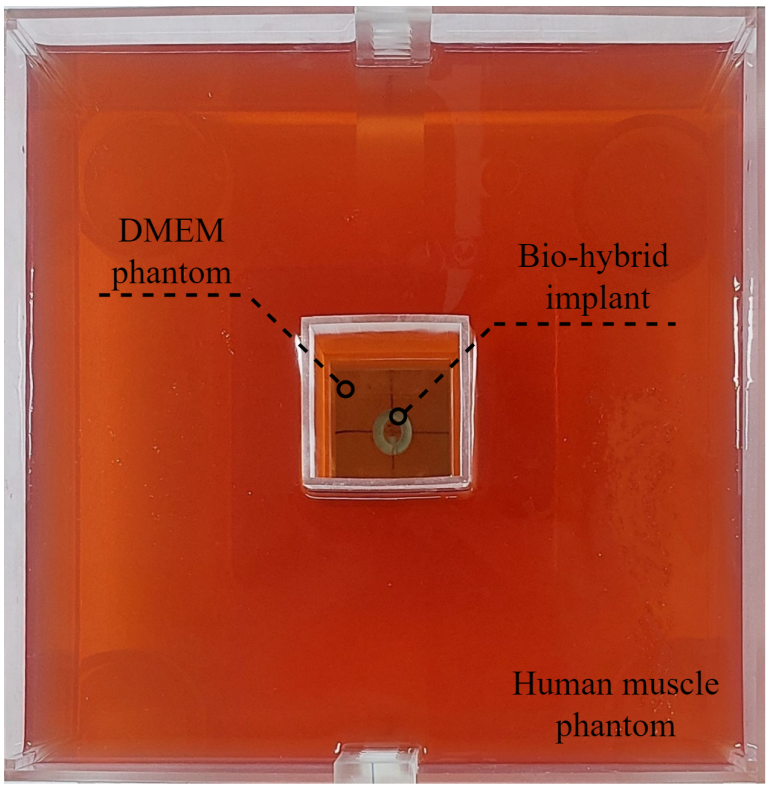

(a)

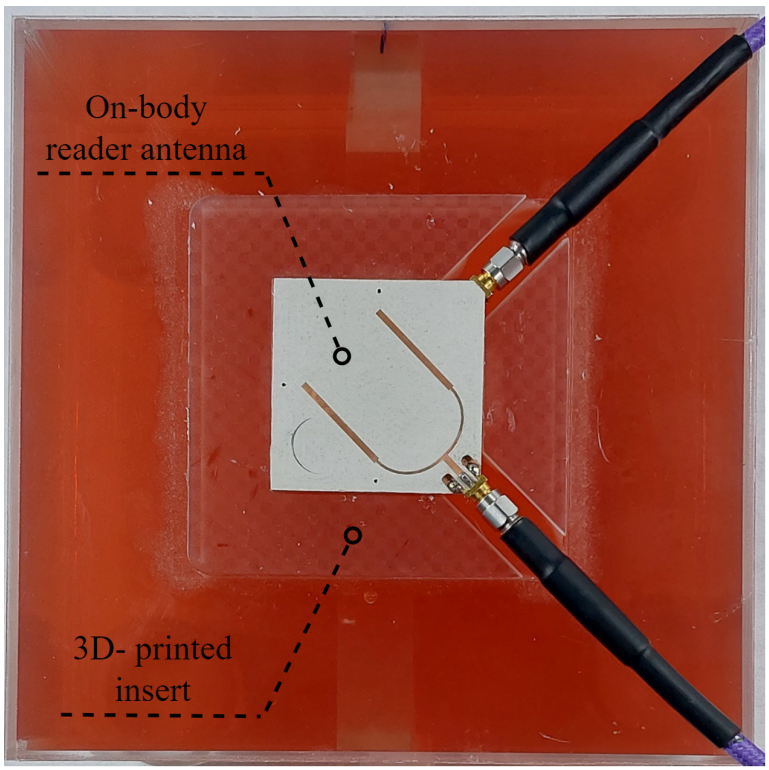

(b)

Figure 5.5. Fabricated measurement setup (a) top view. (b) bottom view.

Since the fabricated skeletal tissues were not able to produce sufficient force to deflect the pillars and cause implant antenna reconfigurations, mock deflected implants were fabricated to electromagnetically validate the reading system. For this, the outputs of the mechanical simulations were fabricated in Formlabs 3B+ printer. After curing the printed flexible scaffolds for the recommended duration, the conductive ink is carefully applied to the four versions of the scaffold that represent different degrees of deflection. The ink application is again conducted manually under a non-inverted microscope. The four versions of the fabricated prototypes are shown in Figure 5.6. During the measurements, the prototype versions were placed inside the DMEM phantom one by one. The measurements were taken with Rohde & Schwarz ZNLE6 model vector network analyzer (VNA).

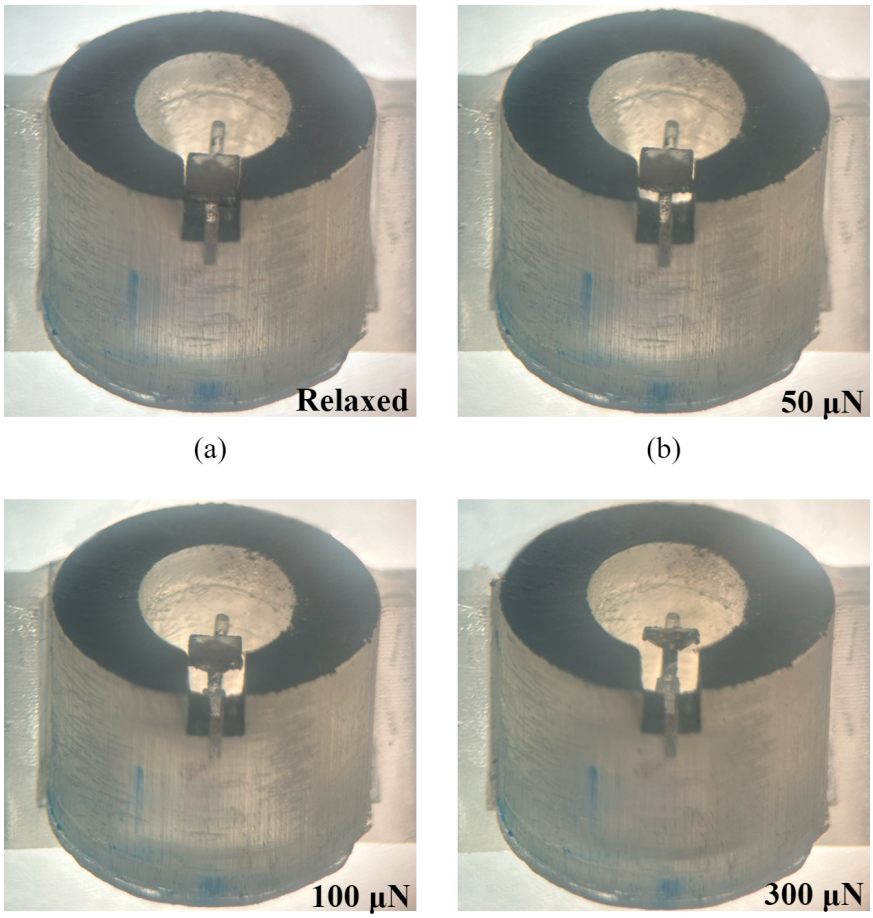

Figure 5.6. Bio-hybrid implant mock prototypes for (a) relaxed case. (b) 50 μN (c) 100 μN (d) 300 μN.

The $|S_{11}|$ and $|S_{22}|$ performance of the on body antenna located on the measurement setup is given in Figure 5.7. The fabricated antenna continues to reliably operate in the expected frequency interval. The transmission coefficient between the ports of the on-body antenna is measured to assess implant antenna resonance behavior across four different degree of deflection. Figure 5.8 illustrates the change in magnitude $|S_{21}|$ that is associated with the increase in force generated by the muscles. In relaxed case, $|S_{21}|$ of the on-body antenna is stable between -30 dB and -32 dB for the frequency interval of interest. When the hypothetical contraction forces subsequently increase to 50 µN a dip begins to appear at around 1.89 GHz. As the force increases to 100 µN, the dip shifts 1.94 GHz and when the force reaches to 300 µN, the dip no longer shifts but the magnitude of it lowers down to -33 dB. Although, the expected progressive frequency shift in the $|S_{21}|$ does not happen after 100 μN, the reconfiguration of the implant antenna is still clear between the relaxed and three different deflected cases. However, the expected progressive shift is observed in the $|S_{21}|$ phase, as given in Figure 5.9.

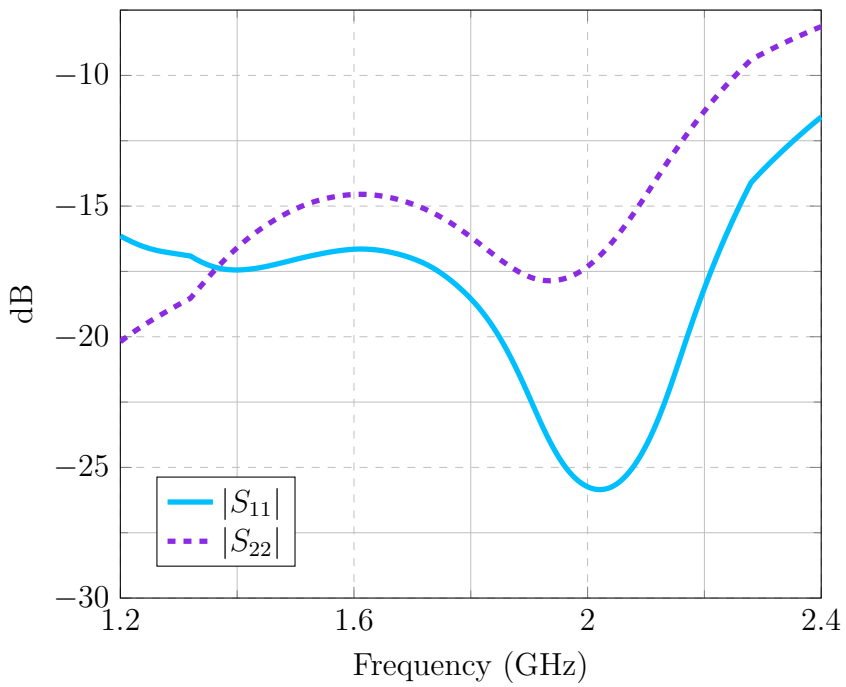

Figure 5.7. dB versus frequency graph for the $|S_{11}|$ and $|S_{22}|$ of the fabricated antenna located on the measurement setup.

During the reconfiguration of the implant antenna, as the force increases, the capacitance between the conductive bridge and the implantable antenna decreases since the bridge moves away from the antenna. The amplification of the $|S_{21}|$ resonance frequency is observed to correspond with the decrease in capacitance, as shown in Figure 5.8.

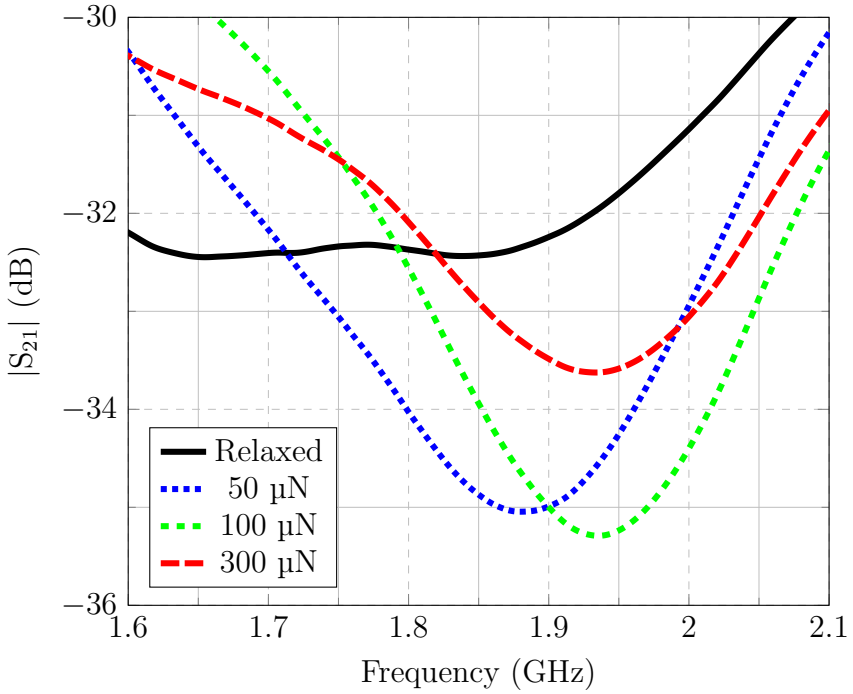

Figure 5.8. Electromagnetic measurement results for the change in $|S_{21}|$ magnitude against implant antennas mimicking reconfiguration under gradual muscle contraction.

It is important to emphasize that maintaining precise alignment between the reader antenna and the implant is essential. Previous research has shown that misalignment can greatly compromise the accuracy of sensing [8]. In the future, our plan is to incorporate time-domain techniques in order to address and overcome this challenge. Furthermore, the unresolved issue of addressing stabilization against parasitic effects within the body necessitates further investigation.

It is worth noting that the simulation results show frequency dips occurring in a lower frequency range of 1.5 to 1.6 GHz. However, the measured results show these

dips at a higher frequency range of 1.8 to 1.9 GHz. This disparity could be explained by differences in the composition of the phantom and imperfections in the bio-hybrid implant prototype. It is also important to acknowledge the potential inaccuracies that may occur when using the SPEAG DAK dielectric assessment kit to measure the dielectric properties of materials incorporated into numerical electromagnetic models. Although the SPEAG DAK probe is highly effective at accurately measuring the dielectric properties of liquids, it may face difficulties when it comes to precisely measuring the dielectric properties of solid materials. The main reason for this difference is the presence of air layers that get trapped between the assessment kit probe and the material being examined.

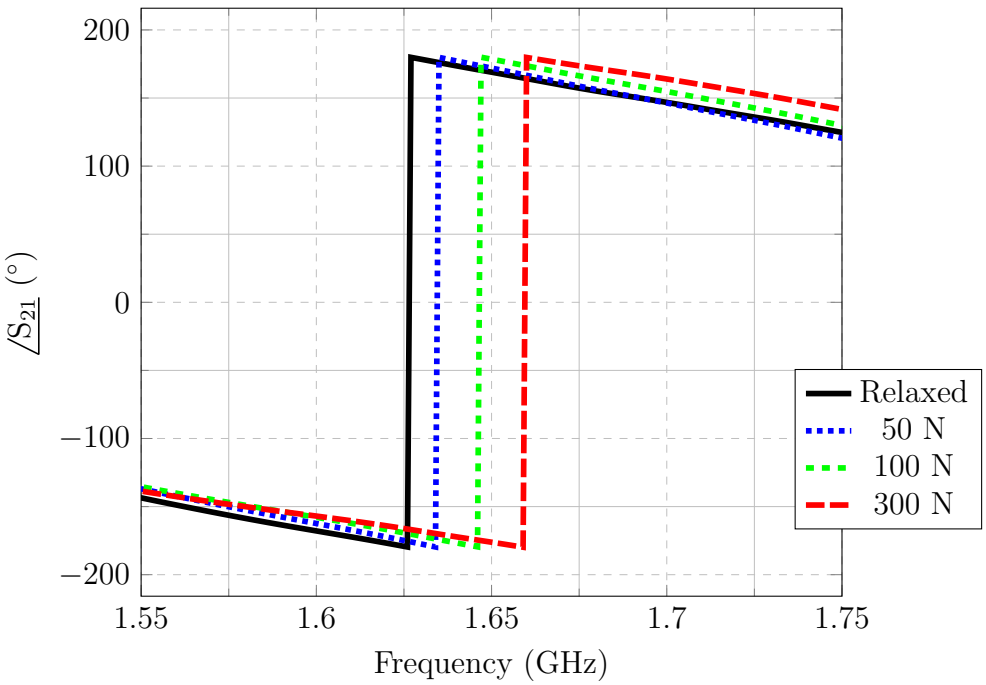

Figure 5.9. Electromagnetic measurement results for the change in $|S_{21}|$ phase against implant antennas mimicking reconfiguration under gradual muscle contraction.

The assessment process can be significantly affected by the presence of intermediary air layers. This is because air, which has a relative permittivity of 1, has very different dielectric properties compared to the solid materials being tested. As a result, there may be differences in dielectric properties between the numerical electromagnetic setup and the measurement setup due to the imprecise measurement outputs generated

by the dielectric assessment kit.

The lack of consistency observed between the expected frequencies in the measurement and simulation results can be associated with differences caused by the complexities involved in accurately measuring the dielectric properties of solid materials. When comparing the actual data with the simulated results, it is important to carefully consider and address any inaccuracies that may arise from measuring dielectric properties. However, the measurements taken consistently showed that the implantable antenna reconfiguration while crossing from relaxed case to deflected cases was successfully detected, even when there were variations in the resonant frequency.

6. CONCLUSION

The field of synthetic biology has the potential to revolutionize sensor technologies, specifically by enabling the programming of living cells to selectively respond to specific molecules. This advancement offers a special opportunity to achieve molecular-level sensing within a living organism. However, it is crucial to effectively address the challenge of establishing a seamless communication link between the genetically modified cells and the external environment of the host body. We propose an innovative wireless communication platform that serves as a channel between the molecular networks within living cells and the electromagnetic links outside the biological system. This platform enables seamless transmission between these two systems.

The novel communication framework introduced in this work represents a significant breakthrough that marks the merging of antenna design and synthetic biology. This convergence opens up new possibilities for interdisciplinary research, promising transformative advancements in the field. An example that clearly demonstrates this innovative idea is seen in the development of a bio-hybrid implant. This implant consists of engineered skeletal muscle combined with a reconfigurable implantable antenna. The implant's antenna acts as a passive reflector and is reconfigured when the skeletal muscle contracts in response to specific target molecules. This reconfiguration allows for molecular-level sensing capabilities.

This research is particularly noteworthy because it is the first instance where engineered muscle tissue has successfully achieved sensing functionalities. The contraction of the skeletal muscle is induced by integrating the trigger molecule. This contraction leads to the reconfiguration of the implantable antenna. As a result, there is a noticeable change in the transmission coefficient between the ports of a dual-port on-body antenna. Simulation studies have shown that the reconfiguration process can be triggered by a minimal force of 50 μN, which is generated by the skeletal muscle during mechanical stimulation.

Furthermore, the feasibility of tracking this reconfiguration process at a depth of 1 cm has been confirmed by both simulated experiments and phantom measurements. In the future, the main focus will be on integrating the entire system. This includes synchronizing wireless tracking of the reconfiguration process and enabling the engineered skeletal muscle to contract in three dimensions. We will achieve this by introducing the trigger molecule into the DMEM medium. The integrated approach mentioned here has the potential to push the boundaries of wireless communication and synthetic biology and could lead to a new era of advanced research and technological innovation.

REFERENCES

1. Koydemir, H. C. and A. Ozcan, "Wearable and Implantable Sensors for Biomedical Applications", *Annual Review of Analytical Chemistry*, Vol. 11, No. 1, pp. 127–146, 2018.

2. Soliman, M. M., M. E. H. Chowdhury, A. Khandakar, M. T. Islam, Y. Qiblawey, F. Musharavati and E. Zal Nezhad, "Review on Medical Implantable Antenna Technology and Imminent Research Challenges", *Sensors*, Vol. 21, No. 9, p. 3163, 2021.

3. Nelson, B. D., S. S. Karipott, Y. Wang and K. G. Ong, "Wireless Technologies for Implantable Devices", *Sensors*, Vol. 20, No. 16, p. 4604, 2020.

4. Bonora, M., S. Patergnani, A. Rimessi, E. De Marchi, J. M. Suski, A. Bononi, C. Giorgi, S. Marchi, S. Missiroli, F. Poletti, M. R. Wieckowski and P. Pinton, "ATP Synthesis and Storage", *Purinergic Signalling*, Vol. 8, No. 3, pp. 343–357, 2012.

5. Saltepe, B., E. Kehribar, S. S. Su Yirmibeşoğlu and U. Şafak Şeker, "Cellular Biosensors with Engineered Genetic Circuits", *ACS Sensors*, Vol. 3, No. 1, pp. 13–26, 2018.

6. Ismailov, A. D. and L. E. Aleskerova, "Photobiosensors Containing Luminescent Bacteria", *Biochemistry (Moscow)*, Vol. 80, No. 6, pp. 733–744, 2015.

7. Karabulut, C., A. Bilir, M. E. Lacin, A. Deniz Yalcinkaya and S. Dumanli, "Skeletal Muscle-Actuated Bio-Hybrid Implant and Wearable Reader Antenna System", *2022 3rd URSI Atlantic and Asia Pacific Radio Science Meeting (AT-AP-RASC)*, pp. 1–4, IEEE, Gran Canaria, Spain, 2022.

8. Karabulut, C., A. Bilir, M. E. Lacin and S. Dumanli, "Implant Antenna Reconfig-

ured by Engineered Skeletal Muscle Tissue", *2023 17th European Conference on Antennas and Propagation (EuCAP)*, pp. 1–5, IEEE, Florence, Italy, 2023.

9. Karabulut, C., A. Bilir, M. E. Lacin and S. Dumanli, "3D Enigneered Muscle Tissue as a Wireless Sensor: Antennalive", *IEEE Antennas Propagation Magazine*, Vol. 65, No. 6, pp. 28–36, 2023.

10. Chan, V., K. Park, M. B. Collens, H. Kong, T. A. Saif and R. Bashir, "Development of Miniaturized Walking Biological Machines", *Scientific Reports*, Vol. 2, No. 1, p. 857, 2012.

11. Ricotti, L., B. Trimmer, A. W. Feinberg, R. Raman, K. K. Parker, R. Bashir, M. Sitti, S. Martel, P. Dario and A. Menciassi, "Biohybrid Actuators for Robotics: A Review of Devices Actuated by Living Cells", *Science Robotics*, Vol. 2, No. 12, pp. 29–40, 2017.

12. Gao, L., M. U. Akhtar, F. Yang, S. Ahmad, J. He, Q. Lian, W. Cheng, J. Zhang and D. Li, "Recent Progress in Engineering Functional Biohybrid Robots Actuated by Living Cells", *Acta Biomaterialia*, Vol. 121, pp. 29–40, 2021.

13. Lin, Z., T. Jiang and J. Shang, "The Emerging Technology of Biohybrid Micro-Robots: A Review", *Bio-Design and Manufacturing*, Vol. 5, No. 1, pp. 107–132, 2022.

14. Panda, S., S. Hajra, P. M. Rajaitha and H. J. Kim, "Stimuli-responsive Polymer-Based Bioinspired Soft Robots", *Micro and Nano Systems Letters*, Vol. 11, No. 1, p. 2, 2023.

15. Schmalbruch, H., *Skeletal Muscle*, Springer Berlin, Heidelberg, 2011.

16. Xi, J., J. J. Schmidt and C. D. Montemagno, "Self-Assembled Microdevices Driven by Muscle", *Nature Materials*, Vol. 4, No. 2, pp. 180–184, 2005.

17. Nawroth, J. C., H. Lee, A. W. Feinberg, C. M. Ripplinger, M. L. McCain, A. Grosberg, J. O. Dabiri and K. K. Parker, "A Tissue-Engineered Jellyfish with Biomimetic Propulsion", *Nature Biotechnology*, Vol. 30, No. 8, pp. 792–797, 2012.

18. Shin, S. R., C. Shin, A. Memic, S. Shadmehr, M. Miscuglio, H. Y. Jung, S. M. Jung, H. Bae, A. Khademhosseini, X. S. Tang and M. R. Dokmeci, "Aligned Carbon Nanotube-Based Flexible Gel Substrates for Engineering Biohybrid Tissue Actuators", *Advanced Functional Materials*, Vol. 25, No. 28, pp. 4486–4495, 2015.

19. Holley, M. T., N. Nagarajan, C. Danielson, P. Zorlutuna and K. Park, "Development and Characterization of Muscle-Based Actuators for Self-stabilizing Swimming Biorobots", *Lab on a Chip*, Vol. 16, No. 18, pp. 3473–3484, 2016.

20. Park, S.-J., M. Gazzola, K. S. Park, S. Park, V. Di Santo, E. L. Blevins, J. U. Lind, P. H. Campbell, S. Dauth, A. K. Capulli, F. S. Pasqualini, S. Ahn, A. Cho, H. Yuan, B. M. Maoz, R. Vijaykumar, J.-W. Choi, K. Deisseroth, G. V. Lauder, L. Mahadevan and K. K. Parker, "Phototactic Guidance of a Tissue-Engineered Soft-robotic Ray", *Science*, Vol. 353, No. 6295, pp. 158–162, 2016.

21. Shin, S. R., B. Migliori, B. Miccoli, Y. Li, P. Mostafalu, J. Seo, S. Mandla, A. Enrico, S. Antona, R. Sabarish, T. Zheng, L. Pirrami, K. Zhang, Y. S. Zhang, K. Wan, D. Demarchi, M. R. Dokmeci and A. Khademhosseini, "Electrically Driven Microengineered Bioinspired Soft Robots", *Advanced Materials*, Vol. 30, No. 10, p. 1704189, 2018.

22. Sakar, M. S., D. Neal, T. Boudou, M. A. Borochin, Y. Li, R. Weiss, R. D. Kamm, C. S. Chen and H. H. Asada, "Formation and Optogenetic Control of Engineered 3D Skeletal Muscle Bioactuators", *Lab on a Chip*, Vol. 12, No. 23, p. 4976, 2012.

23. Boontheekul, T., E. E. Hill, H.-J. Kong and D. J. Mooney, "Regulating Myoblast Phenotype Through Controlled Gel Stiffness and Degradation", *Tissue Engineering*, Vol. 13, No. 7, pp. 1431–1442, 2007.

24. Cvetkovic, C., R. Raman, V. Chan, B. J. Williams, M. Tolish, P. Bajaj, M. S. Sakar, H. H. Asada, M. T. A. Saif and R. Bashir, "Three-dimensionally Printed Biological Machines Powered by Skeletal Muscle", *Proceedings of the National Academy of Sciences*, Vol. 111, No. 28, pp. 10125–10130, 2014.

25. Raman, R., C. Cvetkovic, S. G. M. Uzel, R. J. Platt, P. Sengupta, R. D. Kamm and R. Bashir, "Optogenetic Skeletal Muscle-Powered Adaptive Biological Machines", *Proceedings of the National Academy of Sciences*, Vol. 113, No. 13, pp. 3497–3502, 2016.

26. Morimoto, Y., H. Onoe and S. Takeuchi, "Biohybrid Robot Powered by an Antagonistic Pair of Skeletal Muscle Tissues", *Science Robotics*, Vol. 3, No. 18, p. eaat4440, 2018.

27. Liu, L., C. Zhang, W. Wang, N. Xi and Y. Wang, "Regulation of C2C12 Differentiation and Control of the Beating Dynamics of Contractile Cells for a Muscle-Driven Biosyncretic Crawler by Electrical Stimulation", *Soft Robotics*, Vol. 5, No. 6, pp. 748–760, 2018.

28. Li, Z., Y. Seo, O. Aydin, M. Elhebeary, R. D. Kamm, H. Kong and M. T. A. Saif, "Biohybrid Valveless Pump-Bot Powered by Engineered Skeletal Muscle", *Proceedings of the National Academy of Sciences*, Vol. 116, No. 5, pp. 1543–1548, 2019.

29. Hasebe, A., Y. Suematsu, S. Takeoka, T. Mazzocchi, L. Vannozzi, L. Ricotti and T. Fujie, "Biohybrid Actuators Based on Skeletal Muscle-Powered Microgrooved Ultrathin Films Consisting of Poly(styrene- *block* -butadiene- *block* -styrene)", *ACS Biomaterials Science & Engineering*, Vol. 5, No. 11, pp. 5734–5743, 2019.

30. Morimoto, Y., H. Onoe and S. Takeuchi, "Biohybrid Robot with Skeletal Muscle Tissue Covered with a Collagen Structure for Moving in Air", *APL Bioengineering*, Vol. 4, No. 2, p. 026101, 2020.

31. Joung, Y.-H., "Development of Implantable Medical Devices: From an Engineering Perspective", *International Neurourology Journal*, Vol. 17, No. 3, p. 98, 2013.

32. Mond, H. G. and A. Proclemer, "The 11th World Survey of Cardiac Pacing and Implantable Cardioverter-Defibrillators: Calendar Year 2009-A World Society of Arrhythmia's Project: 2009 Survey Cardiac Pacemakers and ICDS", *Pacing and Clinical Electrophysiology*, Vol. 34, No. 8, pp. 1013–1027, 2011.

33. Mulpuru, S. K., M. Madhavan, C. J. McLeod, Y.-M. Cha and P. A. Friedman, "Cardiac Pacemakers: Function, Troubleshooting, and Management", *Journal of the American College of Cardiology*, Vol. 69, No. 2, pp. 189–210, 2017.

34. Hale, M. F., "Capsule Endoscopy: Current Practice and Future Directions", *World Journal of Gastroenterology*, Vol. 20, No. 24, p. 7752, 2014.

35. Hashemi Noshahr, F., M. Nabavi and M. Sawan, "Multi-Channel Neural Recording Implants: A Review", *Sensors*, Vol. 20, No. 3, p. 904, 2020.

36. Lozano, A. M., N. Lipsman, H. Bergman, P. Brown, S. Chabardes, J. W. Chang, K. Matthews, C. C. McIntyre, T. E. Schlaepfer, M. Schulder, Y. Temel, J. Volkmann and J. K. Krauss, "Deep Brain Stimulation: Current Challenges and Future Directions", *Nature Reviews Neurology*, Vol. 15, No. 3, pp. 148–160, 2019.

37. Ledet, E. H., B. Liddle, K. Kradinova and S. Harper, "Smart Implants in Orthopedic Surgery, Improving Patient Outcomes: A Review", *Innovation and Entrepreneurship in Health*, Vol. Volume 5, pp. 41–51, 2018.

38. Burton, A. R., P. Sun and J. P. Lynch, "Bio-Compatible Wireless Inductive Thin-Film Strain Sensor for Monitoring the Growth and Strain Response of Bone in Osseointegrated Prostheses", *Structural Health Monitoring*, Vol. 20, No. 3, pp. 749–767, 2021.

39. Pande, S. and P. Dhatrak, "Recent Developments and Advancements in Knee

Implants Materials, Manufacturing: A Review", *Materials Today: Proceedings*, Vol. 46, pp. 756–762, 2021.

40. Damm, P., F. Graichen, A. Rohlmann, A. Bender and G. Bergmann, "Total Hip Joint Prosthesis for In Vivo Measurement of Forces and Moments", *Medical Engineering & Physics*, Vol. 32, No. 1, pp. 95–100, 2010.

41. Capozza, M. A., S. Triarico, S. Mastrangelo, G. Attinà, P. Maurizi and A. Ruggiero, "Narrative Review of Intrathecal Drug Delivery (IDD): Indications, Devices and Potential Complications", *Annals of Translational Medicine*, Vol. 9, No. 2, pp. 186–186, 2021.

42. Thevenot, D. R., K. Toth, R. A. Durst and G. S. Wilson, "Electrochemical Biosensors: Recommended Definitions and Classification", *Biosensors and Bioelectronics*, Vol. 16, No. 1-2,, pp. 121–131, 2001.

43. Maccaferri, N., K. E. Gregorczyk, T. V. A. G. De Oliveira, M. Kataja, S. Van Dijken, Z. Pirzadeh, A. Dmitriev, J. Åkerman, M. Knez and P. Vavassori, "Ultrasensitive and Label-Free Molecular-Level Detection Enabled by Light Phase Control in Magnetoplasmonic Nanoantennas", *Nature Communications*, Vol. 6, No. 1, p. 6150, 2015.

44. Hammond, P., D. Ali and D. Cumming, "A System-on-Chip Digital pH Meter for Use in a Wireless Diagnostic Capsule", *IEEE Transactions on Biomedical Engineering*, Vol. 52, No. 4, pp. 687–694, 2005.

45. Cash, K. J., F. Ricci and K. W. Plaxco, "An Electrochemical Sensor for the Detection of ProteinSmall Molecule Interactions Directly in Serum and Other Complex Matrices", *Journal of the American Chemical Society*, Vol. 131, No. 20, pp. 6955–6957, 2009.

46. Erickson, D., S. Mandal, A. H. J. Yang and B. Cordovez, "Nanobiosensors:

Optofluidic, Electrical and Mechanical Approaches to Biomolecular Detection at the Nanoscale", *Microfluidics and Nanofluidics*, Vol. 4, No. 1-2, pp. 33–52, 2008.

47. Gonzalez-Guillaumin, J., D. Sadowski, K. Kaler and M. Mintchev, "Ingestible Capsule for Impedance and pH Monitoring in the Esophagus", *IEEE Transactions on Biomedical Engineering*, Vol. 54, No. 12, pp. 2231–2236, 2007.

48. Lucisano, J. Y., T. L. Routh, J. T. Lin and D. A. Gough, "Glucose Monitoring in Individuals With Diabetes Using a Long-Term Implanted Sensor/Telemetry System and Model", *IEEE Transactions on Biomedical Engineering*, Vol. 64, No. 9, pp. 1982–1993, 2017.

49. Villena Gonzales, W., A. Mobashsher and A. Abbosh, "The Progress of Glucose Monitoring—A Review of Invasive to Minimally and Non-Invasive Techniques, Devices and Sensors", *Sensors*, Vol. 19, No. 4, p. 800, 2019.

50. Malik, J., S. Kim, J. M. Seo, Y. M. Cho and F. Bien, "Minimally Invasive Implant Type Electromagnetic Biosensor for Continuous Glucose Monitoring System: In Vivo Evaluation", *IEEE Transactions on Biomedical Engineering*, Vol. 70, No. 3, pp. 1000–1011, 2023.

51. Hanna, J., M. Bteich, Y. Tawk, A. H. Ramadan, B. Dia, F. A. Asadallah, A. Eid, R. Kanj, J. Costantine and A. A. Eid, "Noninvasive, Wearable, and Tunable Electromagnetic Multisensing System for Continuous Glucose Monitoring, Mimicking Vasculature Anatomy", *Science Advances*, Vol. 6, No. 24, p. eaba5320, 2020.

52. Liu, L. W. Y., A. Kandwal, A. Kogut, Z. E. Eremenko, E. Kogut, M. T. Islam, R. Dolia, S. Nosatiuk and S. T. Nguyen, "In-Vivo and Ex-Vivo Measurements of Blood Glucose Using Whispering Gallery Modes", *Sensors*, Vol. 20, No. 3, p. 830, 2020.

53. Saha, S., H. Cano-Garcia, I. Sotiriou, O. Lipscombe, I. Gouzouasis, M. Koutsoupi-

dou, G. Palikaras, R. Mackenzie, T. Reeve, P. Kosmas and E. Kallos, "A Glucose Sensing System Based on Transmission Measurements at Millimetre Waves using Micro strip Patch Antennas", *Scientific Reports*, Vol. 7, No. 1, p. 6855, 2017.

54. Kim, S., J. Malik, J. M. Seo, Y. M. Cho and F. Bien, "Subcutaneously Implantable Electromagnetic Biosensor System for Continuous Glucose Monitoring", *Scientific Reports*, Vol. 12, No. 1, p. 17395, 2022.

55. Gupta, N., V. Renugopalakrishnan, D. Liepmann, R. Paulmurugan and B. D. Malhotra, "Cell-Based Biosensors: Recent Trends, Challenges and Future Perspectives", *Biosensors and Bioelectronics*, Vol. 141, p. 111435, 2019.

56. Hicks, M., T. T. Bachmann and B. Wang, "Synthetic Biology Enables Programmable Cell-Based Biosensors", *ChemPhysChem*, Vol. 21, No. 2, pp. 132–144, 2020.

57. Wang, B., M. Barahona and M. Buck, "A Modular Cell-Based Biosensor Using Engineered Genetic Logic Circuits to Detect and Integrate Multiple Environmental Signals", *Biosensors and Bioelectronics*, Vol. 40, No. 1, pp. 368–376, 2013.

58. Archer, E. J., A. B. Robinson and G. M. Süel, "Engineered E. coli That Detect and Respond to Gut Inflammation through Nitric Oxide Sensing", *ACS Synthetic Biology*, Vol. 1, No. 10, pp. 451–457, 2012.

59. Mimee, M., A. Tucker, C. Voigt and T. Lu, "Programming a Human Commensal Bacterium, Bacteroides thetaiotaomicron, to Sense and Respond to Stimuli in the Murine Gut Microbiota", *Cell Systems*, Vol. 1, No. 1, pp. 62–71, 2015.

60. Barra, M., T. Danino and D. Garrido, "Engineered Probiotics for Detection and Treatment of Inflammatory Intestinal Diseases", *Frontiers in Bioengineering and Biotechnology*, Vol. 8, p. 265, 2020.

61. Caluori, G., J. Pribyl, M. Pesl, S. Jelinkova, V. Rotrekl, P. Skladal and R. Raiteri,

"Non-Invasive Electromechanical Cell-Based Biosensors for Improved Investigation of 3D Cardiac Models", *Biosensors and Bioelectronics*, Vol. 124-125, pp. 129–135, 2019.

62. Mimee, M., P. Nadeau, A. Hayward, S. Carim, S. Flanagan, L. Jerger, J. Collins, S. McDonnell, R. Swartwout, R. J. Citorik, V. Bulović, R. Langer, G. Traverso, A. P. Chandrakasan and T. K. Lu, "An Ingestible Bacterial-Electronic System to Monitor Gastrointestinal Health", *Science*, Vol. 360, No. 6391, pp. 915–918, 2018.

63. Sezgen, O. F., O. Altan, A. Bilir, M. G. Durmaz, N. Haciosmanoglu, B. Camli, Z. C. C. Ozdil, A. E. Pusane, A. D. Yalcinkaya, U. O. S. Seker, T. Tugcu and S. Dumanli, "A Multiscale Communications System Based on Engineered Bacteria", *IEEE Communications Magazine*, Vol. 59, No. 5, pp. 62–67, 2021.

64. Saldin, L., M. C. Cramer, S. S. Velankar, L. J. White and S. F. Badylak, "Extracellular Matrix Hydrogels from Decellularized Tissues: Structure and Function", *Acta Biomaterialia*, Vol. 49, pp. 1–15, 2017.

65. Lutolf, M. P. and J. A. Hubbell, "Synthetic Biomaterials as Instructive Extracellular Microenvironments for Morphogenesis in Tissue Engineering", *Nature Biotechnology*, Vol. 23, No. 1, pp. 47–55, 2005.

66. Capel, A. J., R. P. Rimington, J. W. Fleming, D. J. Player, L. A. Baker, J. M. Turner, M. C.and Jones, N. R. W. Martin, V. C. Ferguson, R. A.and Mudera and M. P. Lewis, "Scalable 3D Printed Molds for Human Tissue Engineered Skeletal Muscle", *Frontiers in Bioengineering and Biotechnology*, Vol. 7, p. 20, 2019.

67. Kuo, I. Y. and B. E. Ehrlich, "Signaling in Muscle Contraction", *Cold Spring Harbor Perspectives in Biology*, Vol. 7, No. 2, p. a006023, 2015.

68. Szent-Györgyi, A., "Calcium Regulation of Muscle Contraction", *Biophysical Journal*, Vol. 15, No. 7, pp. 707–723, 1975.

69. Schindelin, J., I. Arganda-Carreras, E. Frise, V. Kaynig, M. Longair, T. Pietzsch, S. Preibisch, C. Rueden, S. Saalfeld, B. Schmid, J.-Y. Tinevez, D. J. White, V. Hartenstein, K. Eliceiri, P. Tomancak and A. Cardona, "Fiji: An Open-Source Platform for Biological-Image Analysis", *Nature Methods*, Vol. 9, No. 7, pp. 676–682, 2012.

70. Nikolayev, D., A. K. Skrivervik, J. S. Ho, M. Zhadobov and R. Sauleau, "Reconfigurable Dual-Band Capsule-Conformal Antenna Array for In-Body Bioelectronics", *IEEE Transactions on Antennas and Propagation*, Vol. 70, No. 5, pp. 3749–3761, 2022.

71. Bao, Z., Y.-X. Guo and R. Mittra, "Conformal Capsule Antenna With Reconfigurable Radiation Pattern for Robust Communications", *IEEE Transactions on Antennas and Propagation*, Vol. 66, No. 7, pp. 3354–3365, 2018.

72. Yang, X.-T., H. Wong and J. Xiang, "Polarization Reconfigurable Planar Inverted-F Antenna for Implantable Telemetry Applications", *IEEE Access*, Vol. 7, pp. 141900–141909, 2019.

73. Khaleghi, A., A. Hasanvand and I. Balasingham, "Radio Frequency Backscatter Communication for High Data Rate Deep Implants", *IEEE Transactions on Microwave Theory and Techniques*, Vol. 67, No. 3, pp. 1093–1106, 2019.

74. Dumanli, S., "Challenges of Wearable Antenna Design", *2016 46th European Microwave Conference (EuMC)*, pp. 1350–1352, IEEE, London, United Kingdom, 2016.

75. Skrivervik, A. K., M. Bosiljevac, J. Trajkovikj, B. Fuchs and Z. Sipus, "Design Considerations for Wearable Antennas", *2016 URSI International Symposium on Electromagnetic Theory (EMTS)*, pp. 524–527, IEEE, Espoo, Finland, 2016.

76. Merli, F., B. Fuchs, J. R. Mosig and A. K. Skrivervik, "The Effect of Insulat-

ing Layers on the Performance of Implanted Antennas", *IEEE Transactions on Antennas and Propagation*, Vol. 59, No. 1, pp. 21–31, 2011.

77. Sangster, A. J., *Evolution of Compact Slot Antennas*, Springer International Publishing, 2019.

78. Bilir, A. and S. Dumanli, "Wide-band Dual Port Cross Slot Wearable Antenna for In-body Communications", *2023 17th European Conference on Antennas and Propagation (EuCAP)*, pp. 1–5, IEEE, Florence, Italy, 2023.

79. Balanis, C. A., *Antenna Theory: Analysis and Design, Second Edition*, John Wiley Sons, New Jersey, 1997.

80. Formlabs, "IBT Resin", *https://dental-media.formlabs.com/datasheets/2102519-TDS-ENUS-0.pdf*, accessed on June 23, 2023.

81. Akiyama, Y., A. Nakayama, S. Nakano, R. Amiya and J. Hirose, "An Electrical Stimulation Culture System for Daily Maintenance-Free Muscle Tissue Production", *Cyborg and Bionic Systems*, Vol. 2021, p. 2021/9820505, 2021.

82. McGarry, C. K., L. J. Grattan, A. M. Ivory, F. Leek, G. P. Liney, Y. Liu, P. Miloro, R. Rai, A. Robinson, A. J. Shih, B. Zeqiri and C. H. Clark, "Tissue Mimicking Materials for Imaging and Therapy Phantoms: A Review", *Physics in Medicine & Biology*, 2020.